VILNIUS UNIVERSITY
CENTER FOR PHYSICAL SCIENCES AND TECHNOLOGY

Modestas
VAINORIS

Co-based, Fe and Cu electrodeposited foams with large specific areas suitable for catalytic, sensing, and electrowinning applications

DOCTORAL DISSERTATION

Natural sciences,
Chemistry (N 003)

VILNIUS 2021

Academic supervisor:
Prof. dr. Henrikas Cesiulis (Vilnius University, Natural sciences, Chemistry – N 003).
Scientific consultant:
Assoc. Prof., dr. Natalia Tintaru (Tsyntsaru) (Vilnius University, and Institute of Applied Physics, Natural sciences, Chemistry – N 003).

This doctoral dissertation will be defended in a public meeting of the Dissertation Defense Panel:

Chairman – **Prof. habil. Dr. Albertas Malinauskas** (Center for Physical Sciences and Technologies, Natural Sciences, Chemistry – N 003).

Members:
Dr. Asta Grigucevičienė (Center for Physical Sciences and Technologies, Natural Sciences, Chemistry – N 003).
Doc. Dr. Lina Mikoliūnaitė. (Vilnius University, Natural Sciences, Chemistry – N 003).
Prof. Dr. Rimantas Raudonis (Vilnius University, Natural Sciences, Chemistry – N 003).
Prof. Habil. Dr. Wojciech J. Stępniowski (Institute of Materials Science & Engineering, Department of Functional Materials & Hydrogen Technologies, Poland, Natural Sciences, Chemistry, N 003)

The dissertation shall be defended at a public meeting of the Dissertation Defence Panel at 2 p.m. on the 24th of September 2021 at the Kazio Daukšo auditorium at the Faculty of Chemistry and Geosciences of Vilnius University. Address: Naugarduko str. 24, LT-03225, Vilnius, Lithuania, tel. (8 5) 219 3108; e-mail: info@chgf.vu.lt

The text of this dissertation can be accessed at the Library of Vilnius University and at the Library of FTMC, as well as on the website of Vilnius University: *www.vu.lt/lt/naujienos/ivykiu-kalendorius*

VILNIAUS UNIVERSITETAS
FIZINIŲ IR TECHNOLOGIJOS MOKSLŲ CENTRAS

Modestas
VAINORIS

Electrochemiškai nusodintos Co pagrindo, Cu ir Fe metalų putos, turinčios didelį specifinį paviršiaus plotą, skirtos panaudojimui jutiklių, katalizės ir elektroekstrakcijos tikslams

DAKTARO DISERTACIJA

Gamtos mokslai,
Chemija (N 003)

VILNIUS 2021

Mokslinis vadovas:
Prof. dr. Henrikas Cesiulis (Vilniaus universitetas, Gamtos mokslai, chemija – N 003).

Mokslinis konsultantas:
Prof. Dr. Natalia Tsyntsaru (Vilniaus universitetas, IFA Taikomosios fizikos institutas, Gamtos mokslai, chemija – N 003).

Gynimo taryba:
Pirmininkas – **Prof. habil. dr. Albertas Malinauskas,** (Fizinių ir technologijos mokslų centras, Gamtos mokslai, chemija – N 003).

Nariai:
Dr. Asta Grigucevičienė (Fizinių ir technologijos mokslų centras, Gamtos mokslai, chemija – N 003),
Doc. dr. Lina Mikoliūnaitė (Vilniaus universitetas, Gamtos mokslai, chemija – N 003),
Prof. dr. Rimantas Raudonis (Vilniaus universitetas, Gamtos mokslai, chemija – N 003),
Prof. habil. dr. Wojciech J. Stępniowski (Medžiagotyros ir inžinerijos institutas, Funkcinių medžiagų ir vandenilio technologijų institutas, Lenkija, Gamtos mokslai, chemija – N 003)

Disertacija ginama viešame Gynimo tarybos posėdyje 2021 m. rugsėjo mėn. 24 d. 14:00 val. Vilniaus universiteto Chemijos ir geomokslų fakulteto Kazio Daukšos auditorijoje. Adresas: Naugarduko g. 24, LT- 03225, Vilnius, Lietuva, tel. (8 5) 219 3108; el. paštas: info@chgf.vu.lt

Disertaciją galima peržiūrėti Vilniaus universiteto ir FTMC Chemijos instituto bibliotekose ir VU interneto svetainėje adresu:
https://www.vu.lt/naujienos/ivykiu-kalendorius

ABSTRACT

Metal foams offer a substantial specific surface area and a sturdy frame, which makes them great candidates for various applications such as catalysts, sensors, heat sinks, etc. Cobalt and its various compounds are being considered as an inexpensive alternative for precious and rare metal catalysts (like Pt and Ir and their oxides). Forming high surface area, porous and textured compounds, where their physical (density, pore diameter, and thickness of the coating) properties, as well as chemical (composition) properties, can be easily controlled via electrochemical deposition. Obtained porous/textured surfaces can be easily modified using numerous electrochemical techniques, further enhancing their applicability in various fields.

Various porous and textured Co and Co-Pt metallic foams have been electrochemically deposited using a dynamic hydrogen bubbles template (DHBT). Influence of deposition conditions on porosity and morphology overall have been investigated (current density, potential, pH, solution composition). A comprehensive study of obtained metallic foams, as well as commercially available copper foam, has been done, estimating their true surface area as well as electrochemically active surface area. Obtained porous materials have been tested in their electrochemical catalytic activities in alkaline media – hydrogen evolution reaction (HER) as well as oxygen evolution reaction (OER), and also modified and applied as sensors for free chlorine in water detection. The commercial copper foam properties have been investigated, and their potential applications as cathode for copper electrowinning tested. Later copper foam with electrodeposited Fe layer has been tested as a catalyst for Fenton reaction in methyl orange (MO) dye aqueous solution organic decomposition. Small amounts of Pt (2-3 at. %) Co-Pt metallic foams have been electrochemically deposited with expectations for higher HER and OER activity in alkaline media.

Morphology and various other properties of the obtained materials have been investigated using different techniques. For morphology investigations scanning electron microscopy (SEM) coupled with energy dispersive spectroscopy (EDS) have been used. Crystalline structures have been investigated using X-ray diffraction spectroscopy (XRD). For electrochemical properties as well as surface area estimations voltammetry and cyclic voltammetry (CV), electrochemical impedance spectroscopy (EIS) have been used.

It was found that ammonium sulfate allows to electrochemically deposit Co foams with a much larger electrochemically active surface area per gram

of deposit. The increase of electrochemically active surface area, when compared to that of a substrate, was around a hundredfold. The Co foams showed great activity for HER in alkaline solution and seemed to be a two-stage process. The overpotential required to reach 10 mA current was only 220 mV. The whole process had two distinct slopes, namely – 22 to 44 mV/dec, and the second one - 244 to 325 mV/dec. Upon addition of a small amount of Pt during deposition, the foam with $Co_{97}Pt_3$ has been obtained. The overpotential for HER to reach 10 mA current decreased by approx. 100 mV. However the slope became worse - 269 to 313 mV/dec. The Co foams were tested as catalysts for OER in alkaline media as well, but the results were poor. Overpotential required to reach 10 mA current was ~330 mV and the slope around 130mV/dec. The obtained Co foams were modified using the CV technique, forming cobalt hexacyanoferrate. The modified foams were tested for free chlorine detection in water. The calculated limit of blank (LOB = 1.65σ) was 3.06 ppb, the obtained limit of detection (LOD = 3σ) was 5.57 ppb and the limit of quantification (LOQ = 10σ) was 18.86 ppb.

Commercial Cu foams have been investigated, and judging from EIS data, was established that the true surface area of the foam was established to be 7-14 times larger than its geometrical area. The foam was tested as a cathode for copper deposition and showed lower charge transfer resistance, as well as better diffusion qualities than the flat surface copper counterpart. Furthermore, the commercial Cu foam was modified by electrochemically depositing Fe. The modified Fe/Cu foams were tested as catalysts for Fentons reaction, where 70 mg/L methyl orange (MO) solution was discolored in 2.2 minutes, and approx. 1/3 of all organic matter was mineralized in 10 min at 40°C.

LIST OF PUBLICATIONS

This thesis is based on these articles included in the Web of Science database

I.   **M. Vainoris**, N. Tsyntsaru, H. Cesiulis, Cobalt Foam Coatings as Sensors for Detection of Free Chlorine in water, *Coatings*, **2019**, *9*, 306. https://doi.org/10.3390/coatings9050306

II.   **M. Vainoris**, H. Cesiulis, N. Tsyntsaru. Metal Foam Electrode as a Cathode for Copper Electrowinning. *Coatings* 2020, *10*, 822. https://doi.org/10.3390/coatings10090822

III. K. Mažeika, J. Reklaitis, A. Nicolenco**, M. Vainoris**, N. Tsyntsaru, H. Cesiulis, Magnetic state instability of disordered electrodeposited nanogranular Fe films. *Journal of Magnetism and Magnetic Materials*. 2021, 168433. Accepted for publication in this journal. https://doi.org/10.1016/j.jmmm.2021.168433

AUTHORS CONTRIBUTION TO THE ARTICLES

I.   The author carried out the electrochemical deposition of Co foams and investigated their true surface area from EIS data calculated DL capacitance. Investigated morphology and structural properties of obtained films. Modified obtained Co foams and has done the measurements of free chlorine in the water. The obtained data were analyzed with co-authors and later published as an article.

II.   The author has carried out the electrochemical measurements of commercial copper foams. Investigated the deposition mechanism of copper onto copper foams, and estimated the true surface area of the foams. Has done the morphological analysis as well as EIS data analysis. The results were discussed and analyzed with the co-authors and published in an article.

III. The author investigated Fe deposition onto Si wafer and studied the influence of deposition conditions on morphology, crystalline structure, as well as overall properties of the coatings.

TABLE OF CONTENTS

LIST OF ABBREVIATIONS

AAO	Anodized aluminum oxide
AC	Alternating current
BET	Brunauer–Emmett–Teller
CE	Current efficiency
CPE	Constant phase element
CV	Cyclic voltammetry
DHBT	Dynamic hydrogen bubbles template
DI	Deionized water
DL	Double layer
DPD	N,N-diethyl-p-phenylenediamine
EEC	Equivalent electric circuit
EIS	Electrochemical impedance spectroscopy
HCF	Hexacyanoferrate complex
HER	Hydrogen evolution reaction
IPA	Isopropyl alcohol
MO	Methyl orange
NW	Nanowire
OER	Oxygen evolution reaction
PC	Polycarbonate
PPD	Potentiostatic pulse deposition
RPM	Rotations per minute
SEM	Scanning electron microscope
TEM	Transmission electron microscopy
UV	Ultraviolet radiation
WE	Working electrode
XRD	X-ray diffraction

INTRODUCTION

This Ph.D. thesis is devoted to the electrochemical synthesis of porous Co and Co-Pt materials, as well as the investigation of obtained and commercial metal foams, their modification, and application capabilities. Cobalt has drawn great attention because of its great catalytic properties in electrochemical water splitting, where it could act as an alternative for other expensive rare metal catalysts such as Pt or Ir [1-4]. Cobalt has other attractive chemical and physical properties, useful for potential applications such as catalysts, sensors, magnetic materials [1-6].

The increase of the surface area of catalyst or sensor is very desirable, because of many more active sites, where specific reactions take place [7,8]. In such way the reaction rate or sensitivity can be increased many folds, or even some unusual properties can be achieved (lightweight, fire resistance, magnetic properties, sound/vibration absorption, etc.) [8-10]. The increased activity of high surface area substrates allows the use of less expensive, lighter, smaller but usually less active materials for various applications [8-13].

There have been many attempts to form various porous or textured surfaces especially in recent years (metallic foams, nanowires, aerogels, etc.) [8-10, 14]. Most of these methods require very specific and costly equipment. But even these production methods usually are limited by material choice, the density of porous material, pore diameter, open/closed pore systems, etc. [10,14]. There are many ways to obtain metal foams, however, electrochemical deposition offers a simple, highly tunable, cost-effective way for the production of metal foam from all electrochemically possible to deposit materials [15-17]. There are two main ways to deposit metallic foams using electrochemical deposition – that is using a porous conductive template (usually made out of polymer or other metal) or use a dynamic hydrogen bubble template. In the latter case, the metal ions are being reduced between the hydrogen bubbles, forming a metal foam of tunable density and composition [10,14,15]. Using DHBT one can form a metallic foam on almost any conductive surface.

Electrochemically deposited copper foams are amongst the most popular ones, that have received a lot of research [15, 18, 19]. However, cobalt and various other metal foams have not received so much attention. Some quite recent works can be found investigating various metallic foams and structures, but unfortunately, most of them do not investigate the porosity dependence on deposition conditions. They mostly focus on using the foams as a scaffold for electrochemical catalysis/sensing formation but are not

investigating the electrochemically active surface area or even the reaction rates in more detail.

The porous surface makes it challenging to estimate the true surface area not only electrochemically but using other methods too [20,21]. Methods like Brunauer–Emmett–Teller (BET) allow estimating the true surface area of the whole sample. However, this can give very skewed results, when trying to estimate the activity of a catalyst that will be immersed in an aqueous solution. Since water permeability of the catalyst can differ a lot when compared to gas molecules [22]. So electrochemical techniques allow estimating the true surface area, electrochemically active surface area, and even the amount of active sites. [23,24] They also allow modification and even various applications of these porous materials as catalysts and sensors, making such production methods a very time and cost-effective way to synthesize such materials.

Metallic foams that are flow-through type (open cells at both sides of the foam) are very attractive scaffolds to be used for highly active catalysts, sensors, or even membranes [3,25,26]. Such metal foams can be easily modified and applied for various purposes, like a Fe-based catalyst for Fenton's reactions in wastewater treatment. There have been already various attempts to use high surface area catalysts for Fentons reaction [27-30]. However, most of these methods have serious drawbacks (agglomeration, poor activity, etc.) and catalyst reusability issues.

The aim of this work was to electrodeposit Co-based, Cu, and Fe materials and to investigate the influence of deposition conditions (current density, solution composition, etc.) on their specific surface area in the view of targeted application as catalysis, sensing, and electrowinning.

The objectives of the study:

1. To electrodeposit Co and Co-Pt foams by using dynamic hydrogen bubbles template as electrocatalysts for water splitting (HER and OER).

2. To assess Co foam modified with cobalt hexacyanoferrate for sensing of free chlorine in the water.

3. To assess Cu electrodes (plates and 3D foam) as an advanced cathode for copper electrowinning;

4. To electrodeposit Fe on Cu foam from eco-friendly electrolyte as an effective Fenton catalyst for methyl orange decomposition.

SCIENTIFIC NOVELTY

The high surface area and textured conducting surfaces have been gaining interest in recent years including electrochemically formed metallic foams especially using dynamic hydrogen bubble templates. During this study, the high surface area deposits with tunable composition, porosity, and pore size were obtained. The estimation of the electrochemically active surface area allows to predict and compare the behavior of various catalysts and sensors more adequately than BET measurements. The obtained metallic foams having a high surface area offer lower charge transfer resistance, facilitates the mass transfer from the bulk to the electrode. To the best of our knowledge, none of the discussed foams has been deposited from solutions used in this work, as well did not describe in detail. This work assesses possibilities to synthesize novel materials and then use them in "green" chemistry applications (HER, OER, sensors for free chlorine in water, Fenton catalyst for dye degradation).

Statements to be defended:

1. Electrodeposited 3D foams of Co and Co-Pt with large specific areas can act as effective catalysts for electrochemical water splitting.

2. Electrodeposited Co foams can be modified by forming cobalt hexacyanoferrate on the surface. The modified foams can be used as a reliable sensor for the detection of free chlorine in the water.

3. 3D copper foams can possess lower charge transfer resistance and have better mass transfer properties, which result in a more efficient cathode for electrowinning.

4. Electrodeposition of Fe from the eco-friendly electrolyte onto the Cu foam, forms an electrode that can be used as a catalyst for an effective heterogeneous Fenton reaction catalysis for methyl orange decomposition.

1. LITERATURE REVIEW

1.1. Synthesis of metal foams

Porous metal foams have received great interest due to their compelling physical and chemical properties, such as high porosity, low density, good electrical, magnetic, and mechanical properties, and make an appealing material for a wide area of applications/devices: catalysis [31–37], fuel cells [38], sensors [39], batteries [40,41] and heat exchangers [42,43]. Recent studies regarding foams based on iron group metals usually focused on an increase in the surface area of a foam (high surface area catalysts) for hydrogen [33,34,37] or oxygen [35–37] evolution reactions. Commonly, to achieve these aims modified foams are employed. The modified foams have proven to be an attractive alternative for expensive catalysts such as platinum and ruthenium dioxide, where very active asymmetric electrodes cell for water splitting can be synthesized [37].

Metal foams can be manufactured using different methods including electrochemical ones: either using hard (polymeric or metallic template) or dynamic hydrogen bubble template [32,34,44–46]. Dynamic hydrogen bubble template is based on the use of high current densities, and hydrogen bubbles forming on the substrate surface prevent the deposition of metal, then the metal ions are reduced only in the gaps between gas bubbles, thus leading to the development of the metal foam structure [47].
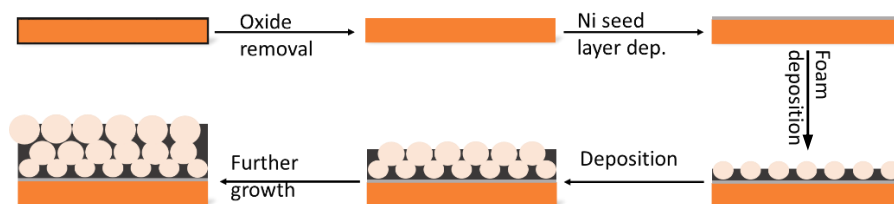
Fig. 1. *Schematic representation of metal foam growth during electrochemical deposition using dynamic hydrogen bubble template*

This method of metal foams production has received much attention, because of the ability to control pore size, deposits density, crystallite size, and morphology. Numerous metallic foams have been deposited, however, to the best of our knowledge, no pure cobalt foams have been deposited using a dynamic hydrogen bubble template-assisted electrodeposition. Also, papers focusing on the effects on porosity, mechanical stability, and overall

surface area of various organic and inorganic additives, especially using high current density ($j > 1A/cm^2$).

Usually, galvanostatic, potentiostatic, or pulse deposition techniques are used for metal foams production. When the pulse electrodeposition technique is used, one can still form a metallic foam, which offers both micro and nanoscale morphological templating [41,48]. Organic additives and different ions (ammonium ions, BTA, etc.) during metal foams depositions also help to control the porosity and mechanical stability [49–51]. Ligands, which can form weak complexes with cobalt ions and produce hydrogen bubbles during the cathodic reaction, can increase the porosity and mechanical stability of cobalt foams [49]. Organic additives such as polyethylene glycol, and 3-mercapto-1-propane sulfonic acid are also commonly used in copper foams electrodeposition and act as a suppressor and an accelerator respectively. [50] These additives have been shown to produce superconformal filling of trenches in the chip interconnections [51, 52]. Effect on the morphology of these additives using them during electrochemical deposition of copper foams with DHBT at high current densities has been also investigated [50]. And it has been shown that particularly 3-mercapto-1-propane sulfonic acid helps to form interconnected 3D pores and increases the mechanical stability of copper foams [50].

Controlling the size of hydrogen bubbles during deposition is also very important since it allows to control the size of pores, and also to get better reproducibility and mechanical strength of the metal foams. The size of hydrogen bubbles can be controlled by adding various salts to the deposition solutions [53, 54]. The effect of the bubbles coalescence prevention agent is related to the surface tension, and the entropy of hydration of the ions used. Strongly hydrated ions such as Cr^{3+}, it also can be seen that dissolved gas concentration as well plays an important role in the coalescence of bubbles in aqueous solutions. Also, the Gibbs-Marangoni effect and surface elasticity strongly affect the coalescence [54].

1.2. Advantages of surface area estimations using EIS

It is evident that any solid metal surface which acts as a substrate for electrochemical reactions possesses a certain roughness that in different ways affects the values of the limiting diffusion current and the exchange current density [55]. It has been shown that when the metal deposition is controlled by diffusion (particularly silver) that the surface with the highest surface roughness had a lower number of active sites, however higher

deposition efficiency and higher efficiency of charge transfer [56]. The dependence between surface roughness and deposition efficiency is non-linear, the surface roughness needs to be significant to affect the deposition efficiency [56,57]. It was proven, that when the deposition reaction is controlled by diffusion, the geometry of the electrode has no significant influence on the reaction [58]. Using very porous or surfaces with high roughness, one can eliminate activation and diffusion overpotentials, making the reaction process controlled by Ohmic effects, so making the reaction much faster [55,56]. All these effects make porous metal electrodes, with pore diameter higher than 50 μm, great cathodes for deposition reactions under diffusion control.

The estimation of the active surface area of highly porous conducting materials is also very important and various techniques can be used to do it in situ or ex-situ. In situ techniques are preferred, since drying the sample can cause changes in the surface area and/or oxidation of the surface, changing surfaces characteristic. Depending on the material and its porosity one can use techniques for double electric layer estimations (cyclic voltammetry, initial charge up dependencies, Electrochemical Impedance Spectroscopy (EIS)), or adapt various adsorption/redox reactions occurring on the surface (underpotential depositions, adsorption measurements, reduction of various dyes, etc.). [59-65] The classical techniques for surface area estimation – liquid permeability, gas adsorption (BET technique) in some cases can also be used. [60,61,64]. However, these techniques require higher amounts of materials and can have quite large error margins, depending on the geometry of the pores and the sample itself. For porous materials that are quite level, and with ordered pores, more sophisticated techniques could be used for porosity estimation like Atomic Force Microscopy (AFM) or spectroscopic ellipsometry, the latter requiring complex models [66-68].

EIS is a very powerful and versatile in situ technique, which allows not only to estimate the true surface area of conducting materials but also to investigate the surface and the processes happening at the surface [59,69-71]. Using the EIS technique one can investigate both Faradaic and non-Faradaic processes on the surface. [59-61,72,73] Even the size and distribution of the pores can be characterized by employing the EIS technique. [74,75] The EIS technique has already been used to characterize various porous materials surfaces, and Faradaic and non-Faradaic processes. [59,60,61,72-76] However the surface area determined by EIS or any other electrochemical method is not the full true surface area, but the electrochemically active surface area, which can be much more useful when

trying to determine porous materials activity in HER or of some electrochemical reaction. [65-68,72-76] Nevertheless, when investigating porous surfaces each case is different, because of the material being investigated, pores size and shape and surface porosity, chosen potential, and the solution used for investigation.

Some of the authors whilst trying to characterize the surface using EIS use transmission line models [74]. Such models sometimes can even reflect the form (oval, pear-shaped, etc.), however, usually using them with real data is quite complicated. This is especially true using thicker foams, with some Faradaic reaction going on in the background. The pore size distribution and their length (depth of the foam) are examples where the geometry of the electrode affects the response of the EIS and can be seen to affect the double-layer capacitance. In such cases, the diffusion path is longer than the pore length, especially so if pores are smaller than 10 μ, [74]. Characterization of such surfaces is even further complicated by possible corrosion of very active high surface area electrodes. So al in all characterization of porous electrodes with ongoing Faradaic reactions is complex and obtained equivalent circuits are highly dependent on the porosity, length of the pores, and materials that the electrode is made of. Making modeling of such surfaces case by case scenario, where using the same model for whin and thick foams may not work.

1.3. Applications for Co and Co-Pt porous foams

The porous materials with their large surface area and many active sites can be applied for a very wide variety of applications. The ever-increasing need for electronics, especially, handheld and portable electronics, and the need to reduce its size and increase efficiency, generates a lot of various electronics waste all over the globe. [77-79] There are many ways to reclaim used metals in electronic waste, however, electrowinning is a very efficient and quite selective process allowing to recover high amounts of various pure metals [80-82]. Metallic foams and porous electrodes have outstanding a great potential to be used as a cathode to collect deposited metals because of combined material properties with functionality resulting from their specific morphology.

The Co and its various compounds are known to be a good catalyst in alkaline media for both water splitting reactions – HER and OER. In an ideal case, both porous cobalt electrodes could be used in a symmetrical cell manner, in order to obtain clean hydrogen and oxygen in a fuel cell [82,83]

The high activity in both water splitting reactions – HER and OER, can be seen from the volcano plots for alkaline media seen in **Fig. 2,3,** and **4** [85,86].
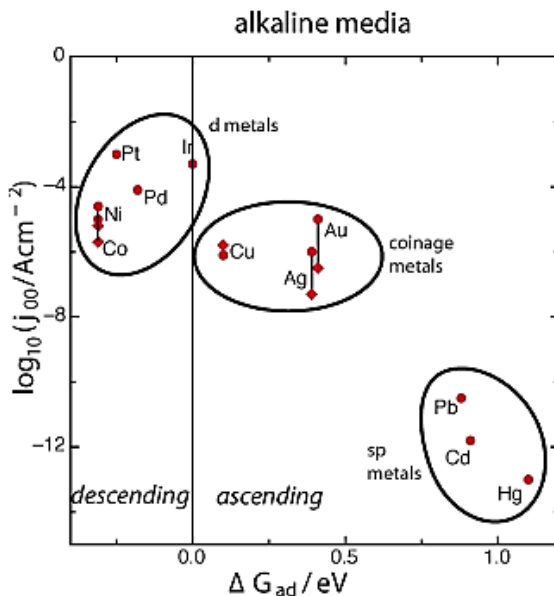

Fig. 2 *Volcano plot for hydrogen evolution in alkaline aqueous solutions. [85]*
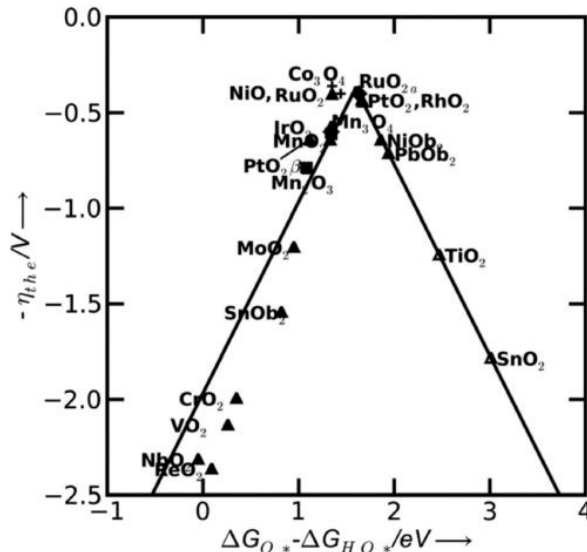

Fig. 3. *Theoretical overpotential for oxygen evolution vs. the difference between the standard free energy of two subsequent intermediates ($\Delta G^0_{O*} - \Delta G^0_{HO}$) for various binary oxides.[85]*

Cobalts oxides activity in OER is also at the top of the volcano plot **Fig. 3** and **4** [85, 86]. Cobalts hydroxides and oxyhydroxides also display great activity. This is very fortunate since these hydroxides can be formed *in*-situ during the testing or using additional electrochemical modification.
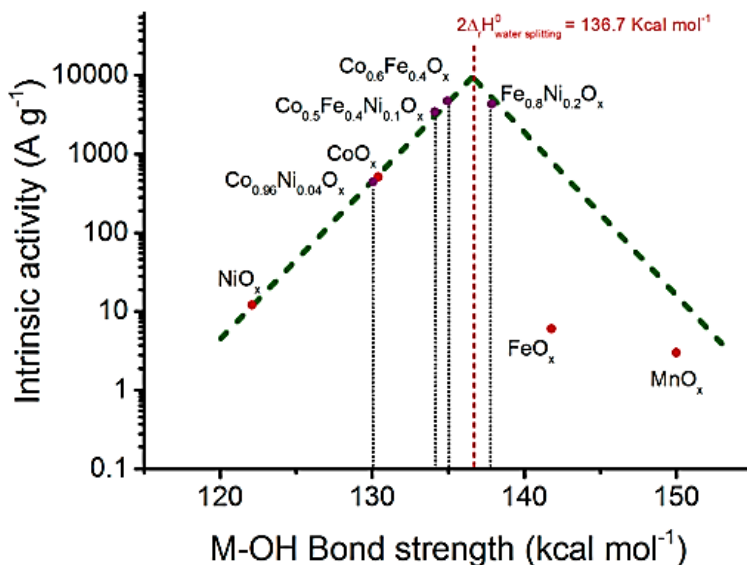

Fig. 4 *Volcano plot of the intrinsic activities of transition metal (oxy)hydroxides vs M−OH bond strength. The green dotted lines indicate a hypothetical, perfect volcano [86]*

It has been noticed that Fe and Ni have great intrinsic activity towards OER, especially when mixed, but recently it was noticed that creating an alloy where Co and Fe are in almost parts, and forming their ohydyroxides, can have even higher activity towards OER in alkaline media [86]. As mentioned earlier bot (Co and Fe) hydroxides and oxyhydroxides can be formed electrochemically in-situ in alkaline media.

Another way to enhance the activity of the catalyst and even the longevity is to alloy transition metals (Co, Ni, Fe, etc.) with platinum [87]. It has been proven that the Pt introduced into transition metal, modified the electronic structure of Pt resulting in ensemble and ligand effect, in turn increasing electrocatalytic activity [88,89]. Amongst Pt-based alloys, Co-Pt is considered a front-runner as an alternative with its exceptional activity towards ORR and good long-term stability, which is great for various fuel cells [90,91].

Cobalt being an iron group metal can easily form complexes, the high surface area, and sturdy Co foams could be applied directly or modified creating a Prussian blue $Fe_4[Fe(CN)_6]_3$ like complex on the surface of the

foam. Prussian blue and other derivatives with transition metals such as cobalt, nickel, copper, etc., have been extensively investigated for many years [92-99]. Its applications vary from the detection of new molecules [88], ascorbic acid [96], morphine [98], free chlorine in water [92,93], or even used as photoanodes [97].

1.4. High surface area Fe catalyst for Fenton's reaction catalysis

With the constantly increasing population and industrial and agricultural growth, water pollution has become an acute problem worldwide [100]. The textile industry is one of the main sources of water pollution since wastewater after dyeing can contain up to 15% of the original dye concentration, and such wastewater can be released into the environment [101]. Such effluents can cause serious harm to the ecosystem because of their toxicity and complex biodegradability. This is especially the case with widely used azo dyes, which can be used not only for textile dyeing but also in the cosmetic, paper-making, and printing industries [101,102]. The azo dyes (containing -N=N- bond) account for around 60-70% of dye groups and are quite stable [103]. There is a lot of different azo dyes, which can contain multiple double bonds, making them very stable. Such dyes can be very harmful to the environment and can have carcinogenic and even mutagenic effects on various organisms [103,104]. Over the years various physical (coagulation, adsorption, reverse osmosis), chemical (ozonation and chlorination), and anaerobic biodegradation techniques have been developed to remove such pollutants [105,106]. Usually, these techniques require costly equipment, don't fully mineralize all the pollutants, but rather convert them into other compounds, and the process itself may cause undesirable effects (chlorine gas evolution and chlorination of compounds) [107,108].

Advanced oxidation processes (AOPs) were first proposed for potable water treatment in the 1980s, which was earlier defined as the oxidation processes involving the generation of hydroxyl radicals (OH •) in sufficient quantity to affect water purification [109]. The use of hydrogen peroxide and iron salts for the oxidation of tartaric acid was first discovered by H.J.H Fenton in 1894 [110]. It involves the use of catalytic degradation of hydrogen peroxide initiated by Fe(II) ions into hydroxyl radicals. Although the Fenton reagent has been known for more than a century, the mechanism of the Fenton reaction is still under intense discussion [111, 112]. Two main pathways have been proposed – the Hauber – Weiss mechanism (which involves the participation of free radicals in the reaction mechanism) and the

Kremer – Stein mechanism (ionic mechanism involving species like FeO^{2+} or use of Fe(IV) ions) [113, 114]. It is possible that both hydroxyl radicals and ferryl ions can coexist in Fenton chemistry (Fenton and Fenton-like reactions) and depending on the environmental conditions or operating parameters, one of them will dominate [115]. Following one of the possible mechanisms, it involves the generation of highly oxidizing hydroxyl radicals, bringing sustainability and environmentally-friendly aspects to the process. The reaction takes place at ambient conditions, is not selective, and using hydrogen peroxide as oxidizing agent makes it more environmentally friendly. Using a homogenous Fenton reaction produces large amounts of iron sludge, that has to be removed, making the overall pollutant removal process costly The heterogeneous Fenton process allows to circumvent this problem, since the hydroxyl radicals are generated near or on the solid surface, minimizing the corrosion, granting the reusability of the catalyst. Also according to Karthikeyan et al. heterogeneous Fenton reaction has lower activation energy than the homogenous one [116]. The heterogeneous reaction may as well show a higher removal efficiency due to a large number of surface-active sites where the generation of OH• radicals takes place [117].

Lately, there have been developed a lot of various AOP's for wastewater treatment, that can be divided into four categories (**Fig. 5**). They are of various efficiency and energy requirements, however, electro-Fenton is still the most simplistic one. However lately the progress in AOPs shows strong potential for full mineralization of various organic pollutants in water. [101,102,108,119]. Traditionally Fenton reaction uses iron (II) ions for the catalytic degradation of hydrogen peroxide, nevertheless, several alternative transition metals, e.g., Cu^+, Cr^{3+}, Co^{2+}, Ti^{3+}, etc., can catalyze similar reactions [120]. AOPs usually combine Fentons (or Fenton-like) reaction with either UV illumination, ultra-sound generation, micro-waves, and other various techniques to increase the efficiency of organic material degradation[101,102,118, 119, 111, 120-127]. Some of these techniques (micro-cavitation and electrochemical catalysis) can help to produce hydrogen peroxide *in-situ*. Even though these techniques can increase pollutants removal efficiency, they require costly equipment and can increase the basic cost of operation by 50-60% [128]. A much more energy-efficient way is to use surface texturization - to increase the surface area that is in contact with wastewater, sometimes even achieving higher efficiency in organics mineralization when compared to homogenous Fenton reaction [129]. Thus, highly efficient heterogeneous textured catalysts can be

prepared by immobilizing/depositing iron species into porous templates (zeolites, activated carbon, etc.) or using various nanoparticles [111, 120, 129, 130]. However, such templates are not active in the reaction and nanoparticles tend to clump up forming larger clusters. In this case, the active surface area (where species participating in the reaction can adsorb) is limited and the activity/efficiency of the whole Fenton reaction decreases. [125]. Therefore, templates that can be reused and actively participate in the Fenton reaction are desirable [101, 121, 125]. One of such – copper, an efficient catalyst for Fenton-like reactions, and can be used for a homogenous reaction but also for heterogeneous in various forms – nanoparticles, modified carbon particles, etc. [102, 131-133].
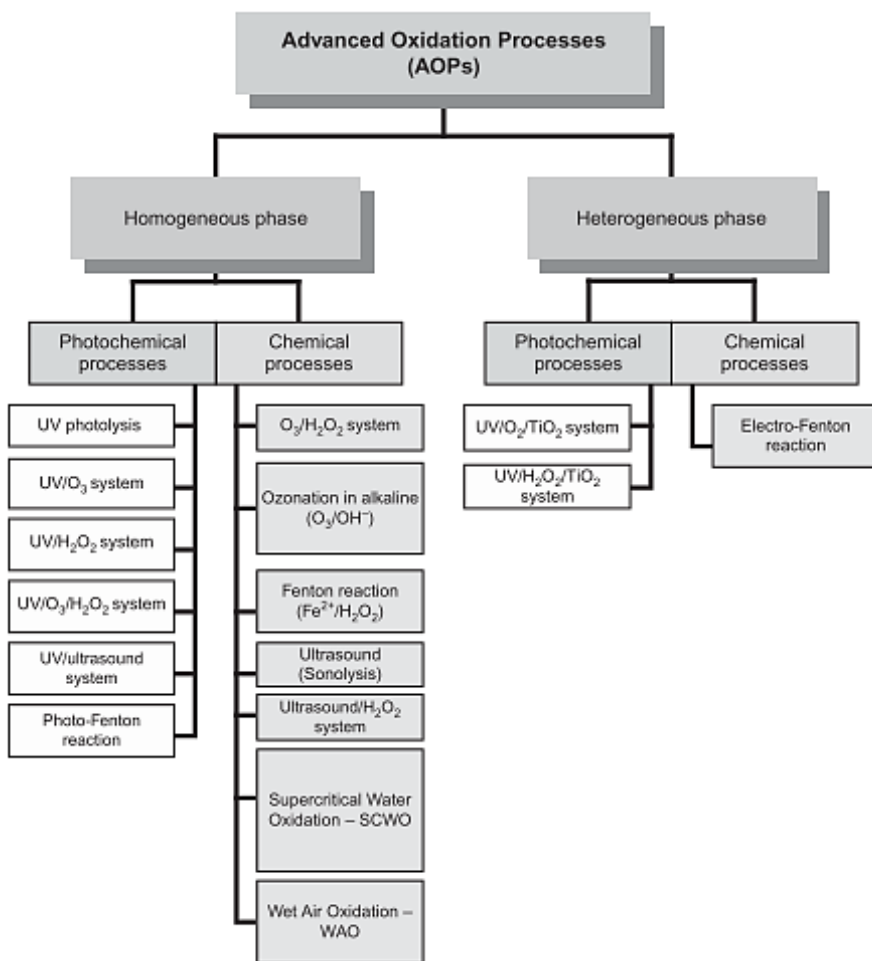

Fig. 5. *List of major types of AOP's [118]*

Nevertheless, Fe(II) ions still show the best activity towards the catalytic degradation of hydrogen peroxide into ·OH·radicals. The heterogeneous textured catalysts, where the constant supply of Fe (II) ions can be ensured, show a better overall activity. According to A. Rossi et al., the activity of the catalyst towards the Fenton reaction can be further enhanced by combining Cu and Fe, where Cu can help to restore Fe(II) ions. [134]. In turn, some of the best Fenton-like reaction catalysts are Fe and Cu mixed-species heterogeneous catalysts, which display great activity at various concentrations of organic matter as well as stability with multiples uses [125, 134-135].

To make the whole process even more environmentally friendly, the synthesis method for catalysts should be considered. Electrodeposition is one of the simplest and cost-efficient ways to synthesize an iron-based catalyst. Such a catalyst can be electrodeposited using Fe (II) citrate or citrate-ammonia baths, however, such baths can suffer from stability issues and are less environmentally friendly [136,137]. Therefore, by using Fe(III) based citrate-glycolate electrolytes, that display great stability over long periods, good control of magnetic and mechanical properties, with good electrochemical deposition rates [136-138]. The catalyst obtained from this bath, combined with copper foam substrate, should show a good activity towards a Fenton-like reaction. The addition of metals possessing multiple oxidation degrees can also increase the efficiency of catalysis [139]. One of such metals could be tungsten which already has been proven to have great activity towards Fenton-like reaction [140]. The addition of tungsten to the iron and copper foam combination could also help to control the iron corrosion rate, and in turn, increase the stability and longevity of the heterogeneous Fenton-like catalyst.

2. MATERIALS AND METHODS

2.1. Reagents

All of the reagents were of analytical grade and have been used as purchased without further purification. Most of the reagents have been purchased from Carl Roth. All of the metal substrates (plates, wires, and foams) have been purchased from Alfa Aesar.

2.2. Co and Co-Pt metal foams

The compositions of electrolytes for cobalt foams deposition are presented in **Table 1**. All of the solutions were prepared using deionized water (DI). Electrodeposition of Co foams was performed at room temperature.

Table 1. *The chemical compositions of solutions used for Co foam depositions, pH 2.*

Solution No	$CoCl_2$, M	NH_4Cl, M	$CoSO_4$, M	$(NH_4)_2SO_4$, M	Isopropyl alcohol, M
1	0.2	2	–	–	–
2	0.2	2	–	–	2
3	–	–	0.2	1	–
4	–	–	0.2	1	2

Cobalt foams were electrodeposited using a dynamic hydrogen bubble template method on a copper substrate, which was used as a working electrode. The geometrical area of copper foil sheets was 0.8 cm². Prior to the electrodeposition, the Cu substrate was mechanically polished, degreased in acetone, and then cleaned with DI water in the ultrasonic bath. Before deposition, the native copper oxide layer was removed by dipping the substrate into a 2 M H_2SO_4 solution. To improve the adhesion of the deposits to the substrate, a Ni seed layer (~10 nm) was deposited from the solution containing 1 M $NiCl_2$ and 2.2 M HCl under galvanostatic mode (j = −12.5 mA/cm²) for 1 min.

Two electrode cells were used for the deposition of the cobalt foams, where a circular platinized titanium mesh was used as the counter electrode. The distance between electrodes was fixed at 2.5 cm. The cobalt foams were deposited under galvanostatic or pulse deposition mode. The influence of Cl^- and SO_4^{2-} based electrolytes, on the cathodic current density (0.6–2.5 A/cm²), of the deposition time (20–300 s) on porosity, structure, and morphology of cobalt foams were evaluated.

As-deposited cobalt foams were thoroughly rinsed with DI water, then were immediately transferred into a beaker with ethanol, to minimize contact with the atmosphere and thus avoid oxidation of a highly active surface area of cobalt foams.

The electrodeposition of Co foams and Co-Pt foams was performed in the 0.1 M $CoSO_4$ and 0.5 M $(NH_4)_2SO_4$ solution (for Co) or 0.015 M $PtCl_4$, 0.1 M $CoSO_4$ and 0.5 M $(NH_4)_2SO_4$ (for Co-Pt). The influence of current, electric charge, and orientation of sample to the counter electrode on the porosity of foams and their true surface area have been investigated. Activities of water splitting (OER and HER) in alkaline media (1M KOH solution) have been tested. All electrochemical measurements were performed at room temperature.

The other electrochemical measurements (CV, EIS) were carried out in the 3-electrode cell. A circular platinized titanium mesh was used as the counter electrode, and the saturated Ag/AgCl electrode was used as a reference electrode. The scans of EIS at different potentials were recorded at four decades of frequencies (f = 10^3–0.1 Hz). Cyclic and linear voltammetry has been also employed trying to estimate the activity and efficiency of obtained foams as catalysts in water electrolysis using in 0.1 M Na_2SO_4 solution.

2.2.1. Modification of Cobalt foams

Cobalt hexacyanoferrate was formed using cyclic voltammetry (**CV**) in the 3-electrodes cell. Cobalt foams were immersed into 0.05 M ammonium acetate buffer solution with 0.1 M KNO_3 and 1.5 mM of $K_3[Fe(CN)_6]$; the pH of the chosen buffer solution was fixed at 5.5, adjustments were made using acetic acid. All solutions were freshly prepared. CV measurements were performed at room temperature. To find the best conditions for foams modification (i.e., enhanced sensitivity and longevity of a free chlorine sensor), the influence of different cycling speeds (25, 50, 100 mV/s) and count of cycles was investigated.

Chronoamperometric measurements were performed to determine the amount of free chlorine in the water. $Ca(OCl)_2$ was used as a source of chlorine. Various amounts of $Ca(OCl)_2$ were dissolved in 0.05 M ammonium acetate buffer, containing 0.1 M KNO_3 as a background electrolyte. All the solutions used for chlorine detection were prepared just prior to chronoamperometric measurements. A standard three-electrode system was used during chronoamperometric measurement, with a modified cobalt foam

as the working electrode. All of the measurements were performed at room temperature.

2.3. Copper foam investigation

Solution compositions used for electrochemical experiments are shown in **Table 2**. The pH of solutions was adjusted using sulfuric acid and controlled by a benchtop pH-meter ProLine Plus (Prosence B.V.). Cu plates and Cu foam electrodes served as working electrodes. The Cu foam sheets used to fabricate electrodes were purchased from Alfa Aesar. To characterize commercially available copper foams, we have done some experiments trying to determine the basic characteristics of this foam. Foam density has been determined as gravimetrically being equal to 0.748 g/cm^3, making the porosity of the foam to be around 90.5%. The copper foam has a 3D interconnected porous structure. The pore size varies from 1 to 0.1 mm. The surface of the foam is very uneven, making the true surface area of the already porous copper foam even larger

Table 2. Composition of solutions used for electrochemical measurements.

C(CuSO$_4$), M	C(Na$_2$SO$_4$), M	pH
0.01	0.49	3.6
0.05	0.45	3.6
0.1	0.4	3.7
0.2	0.3	4.1

Working electrodes (copper plates and copper foams) have been washed and degreased using acetone, ethanol, and water in succession and in combination with an ultrasonic bath. The geometrical size of both flat and porous samples was 1 cm × 1 cm, and both sides were conducting. To ensure that the working surface was that of the desired size, other parts of the samples were isolated using insulating plastic spray (PRF 202). Just before measurements, the native copper oxide layer has been removed by dipping copper samples into 2 M H_2SO_4 solution for 2 s and afterward rinsing with DI water.

2.4. Iron deposition onto copper foam

Cu wires and Cu foam electrodes served as working electrodes. Working electrodes have been washed and degreased using acetone, isopropanol, and water in succession and in combination with an ultrasonic bath. The

electrodes were 1 cm × 1 cm in geometrical size with both sides conducting. To ensure that the working surface was that of the desired size, other parts of the samples were isolated using insulating plastic spray (Plastik 70 Super). Just before measurements, the native copper oxide layer has been removed by dipping copper samples into 2 M H_2SO_4 solution for 2 s and afterward rinsed with DI water.

Solution compositions used for electrochemical deposition of iron was performed using a solution with 0.1 M. $Fe_2(SO_4)_3$, 0.3 M citric acid, and 1 M glycolic acid, pH 6.5 at 60°C temperature under constant stirring using magnetic stirring bar rotating at 600 RPM. The pH of solutions was adjusted using sulfuric acid and/or sodium hydroxide and measured using a benchtop pH-meter ProLine Plus. Depositions have been performed using a standard three-electrode system, where Cu foam or wire served as a working electrode, circular platinized titanium mesh (Alfa Aesar) was used as a counter electrode, and $Ag/AgCl/KCl_{sat}$ (Sigma-Aldrich) was used as a reference electrode. The distance between the counter and working electrode was fixed at 2.5 cm, and the distance between working and reference electrodes was fixed at 1.5 cm.

Electrochemical depositions have been performed using programmable potentiostat/galvanostat AUTOLAB PGSTAT 128N (Metrohm, Utrecht, The Netherlands) with a 10 Amps booster. The software used for controlling the hardware was Nova 1.11.2. Three distinct potentials have been chosen for deposition (-1.5, -1.7, and -1.9 V vs Ag/AgCl) and the desired amount of charge was used for iron electrochemical deposition. Five distinct values have been chosen – 150, 300, 450, 900, and 1350 C.

2.5. Catalytic testing of modified copper foams in Fentons reaction

To evaluate the catalytic activity of our modified foams we used a model nitro dye (MO) aqueous solution. Typical test solution contained 40, 70, or 100 mg/L MO and 20 g/L Na_2SO_4 at pH 3 (± 0.1), adjusted using H_2SO_4. The solution's temperature was kept at desired value (30, 40, or 50°C) and constant stirring using a magnetic stirring bar at 600 RPMs. All the experiments with MO solutions were carried out using 100 mL of the chosen solution. The hydrogen peroxide was added to the beaker with MO solution 30 s before the experiment, allowing it to fully homogenize. The modified copper foams were immersed in the solution for 10 minutes unless stated otherwise.

The discoloration of the solution was tracked every minute by extracting 2 mL of solution and measuring the light adsorption in 320-620 nm range (scan step 2 nm) using a Spectrophotometer (T60 UV-Visible Spectrophotometer, PG Instruments Limited). After the measurement, the aliquot was poured back into the beaker. The modified copper foams mass has been tracked carefully before deposition, after the deposition of Fe, and after the catalysis to evaluate electrochemical deposition efficiency and also the amount of iron that has corroded away during the organic degradation.

The total organic content (TOC) and total nitrogen (TN) were determined using the TOC-VCSN Shimadzu analyzer (with TNM-1 block for nitrogen determination). The analysis was carried out after removing iron from the test solution by increasing pH to around 9.8 by adding 7M NaOH solution. The formed iron oxides and hydroxides have been removed via centrifuge, and the supernatant was used for TOC and TN analysis.

3. RESULTS AND DISCUSSION

3.1. Electrochemical deposition of Co foams

3.1.1. The influence of electrolyte composition

Electrochemical deposition of metal foams using dynamic hydrogen bubbles template requires the use of very high current densities (usually $j \geq 0.6$ A/cm²). At such high current densities, the deposition typically is controlled by diffusion. The current efficiencies during such deposition are quite low because most of the current is used for HER.

The composition of electrolyte allows to control the size of the pores (diameter), the overall porosity of the foam, the thickness of the layer, and also mechanical durability.

As it was shown by DoHwan Nam et al. [141] the ammonium ions played an important role in copper foams formation, whilst using a dynamic hydrogen bubble template method. The ammonium ions in aqueous solutions are in equilibrium with NH_3:

$$NH_3 + H^+ \Leftrightarrow NH_4^+ \qquad (1)$$
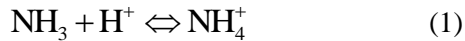
In the current case, the solution used for depositions was acidic (pH 2), thus the equilibrium is shifted towards the formation of NH_4^+. Ammonia can act as a ligand, forming complexes with cobalt ions, while ammonium ions may adsorb onto the surface of a substrate during deposition. Reduction of the adsorbed ammonium ions on the cathode leads to a decrease of the cathodic current efficiency, but also acts as an additional hydrogen source (Eq. (2)), which in turn influences the porosity of the obtained coatings [142]:

$$NH_4^+ + e^- \rightarrow 0.5H_2 + NH_3 \qquad (2)$$

To reveal the role of ammonium ions, whilst depositing cobalt foams coatings, the ammonium-free electrolytes contained 0.2 M $CoCl_2$ or 0.2 M $CoSO_4$ were used. The galvanostatic deposition at various cathodic current densities (0.6–4.8 A/cm²) and deposition times (10–180 s) were studied, but foam-like deposits were not obtained (**Fig. 6**). The coatings were extremely uneven using both sulfate and chloride electrolytes, and the jet of formed hydrogen bubbles removed most of the reduced metal from the substrate surface. Nevertheless, as it is depicted in SEM images the coatings obtained from chloride electrolyte had a better coverage (**Fig. 6a**) than coatings obtained from the sulfate bath (**Fig. 6b**) which were uneven and had micro-

agglomerates on the surface. Both time and current density did not positively affect the formation of cobalt foams from the electrolytic baths.
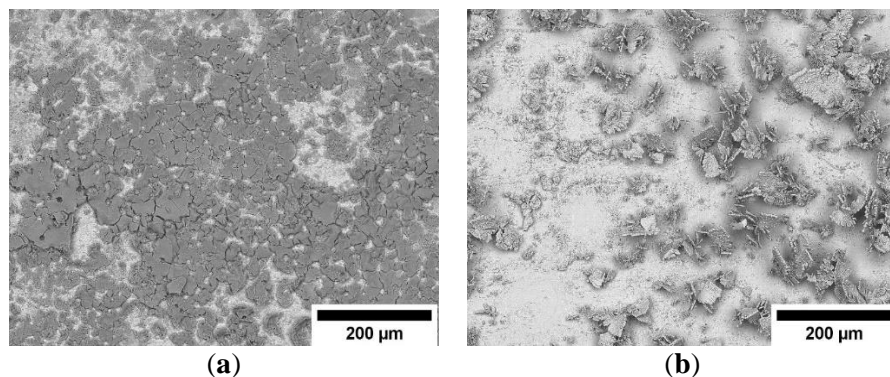

(**a**)   (**b**)

*Fig. 6. SEM images of Co coatings deposited under galvanostatic conditions, at cathodic current density j = 2.5 A/cm², deposition time t = 60 s. The composition of solutions: (**a**) 0.2 M CoCl₂; (**b**) 0.2 M CoSO₄.*

The addition of ammonium ions (**Fig. 7**) to the solutions resulted in the deposition of Co coatings riddled with cylindrically shaped pores of various sizes, but often displaying numerous defects, caused by hydrogen evolution. Coatings electrodeposited from the chloride-based solution (**Table 1 solution 1**) had larger and irregular pores (diameter of pores varied from 5 to 100 μm). In comparison to the sulfate-based solution, where pores size were much more uniform (diameter 5–20 μm **solution 3**). This fact can be explained by the higher capacity of the ammonium sulfate in the suppression of hydrogen bubble coalescence compared to the ammonium chloride solutions [53,54].

The influence of the cathodic current density on the foam's formation revealed the following findings: From the chloride-based solution, the foam-like structure was obtained only at cathodic current densities >1.8 A/cm² (**Fig. 7 a–c**). The porosity of these coatings obtained from solution 1 varied dependently on the cathodic current density ($q = 360$ C), namely: 19% at 1 A/cm², 23.3% at 1.8 A/cm², and 21.7% at 2.5 A/cm², respectively. The increase in porosity of foams obtained from the chloride-based solution at higher cathodic current densities could be explained by the HER rate increase. As it was mentioned above, the ammonium sulfate was approximately three times better at suppressing hydrogen bubbles coalescence thus, the diameter of pores usually does not exceed 15 μm for foams obtained from a sulfate-based solution. Hence, the overall porosity of

such foams is much lower than the ones obtained from a chloride-based solution: at 2.5 A/cm² porosity is ca 8.2%.
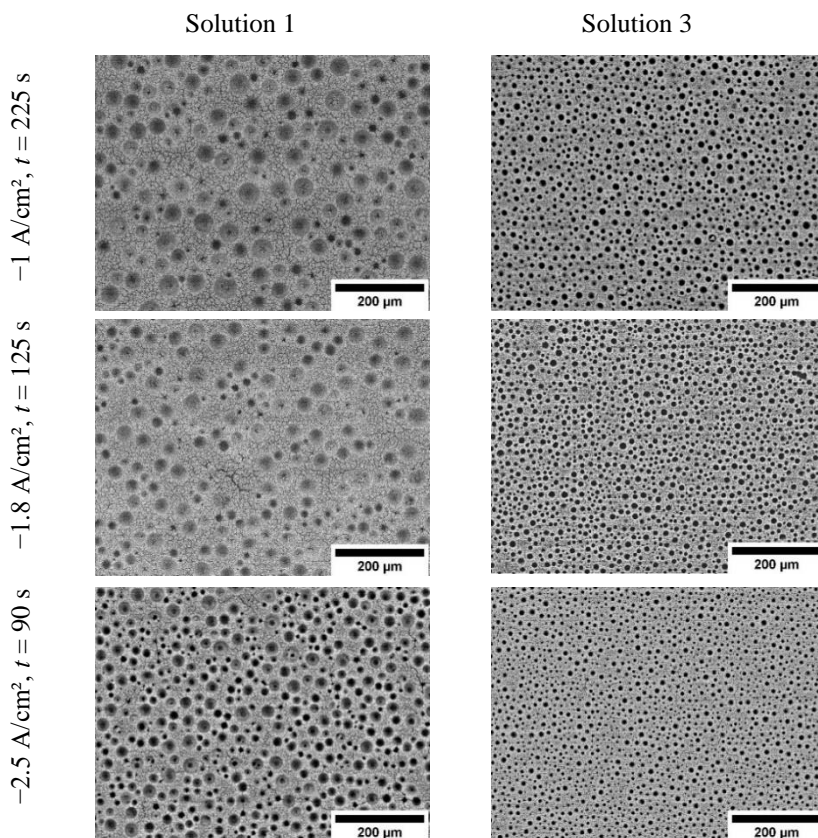

Fig. 7. SEM images of Co coatings were obtained under a galvanostatic mode at various deposition conditions, but constant charge passed (q = 180 C). Solution 1 - 0.2 M CoCl$_2$ and 2 M NH$_4$Cl, Solution 3 - 0.2 M CoSO$_4$ and 1 M (NH$_4$)$_2$SO$_4$

In order to evaluate the role of a surfactant on the formation of Co foams, the isopropyl alcohol was added (**solutions 2 and 4**), and the porosity and morphology of the growing coatings were evaluated. Isopropanol was chosen as an efficient agent to reduce the surface tension. With the reduced surface tension, the hydrogen bubbles formed during deposition are able to detach easier from the surface. Making the surface much more porous as can be seen from the SEM pictures (**Fig. 8**). The porosity of the deposits increased considerably even at comparatively low cathodic current densities of 1 A/cm². However, the radius of pores did not change due to the reduction of the solution's surface tension. This could be linked to the fact, that the influence of ammonium ions on hydrogen bubbles is much higher than that of isopropyl alcohol on the reduction of surface tension. The porosity of the

foams obtained from the sulfate-based solutions also increased substantially with the addition of isopropyl alcohol. Thus, at a cathodic current density of 2.5 A/cm², the development of a tridimensional cobalt foam structure can be noticed, and it is formed from interconnected cylindrical pores (**Fig. 8**). In this case, the estimation of the porosity using SEM images was rather difficult due to many interconnected pores.
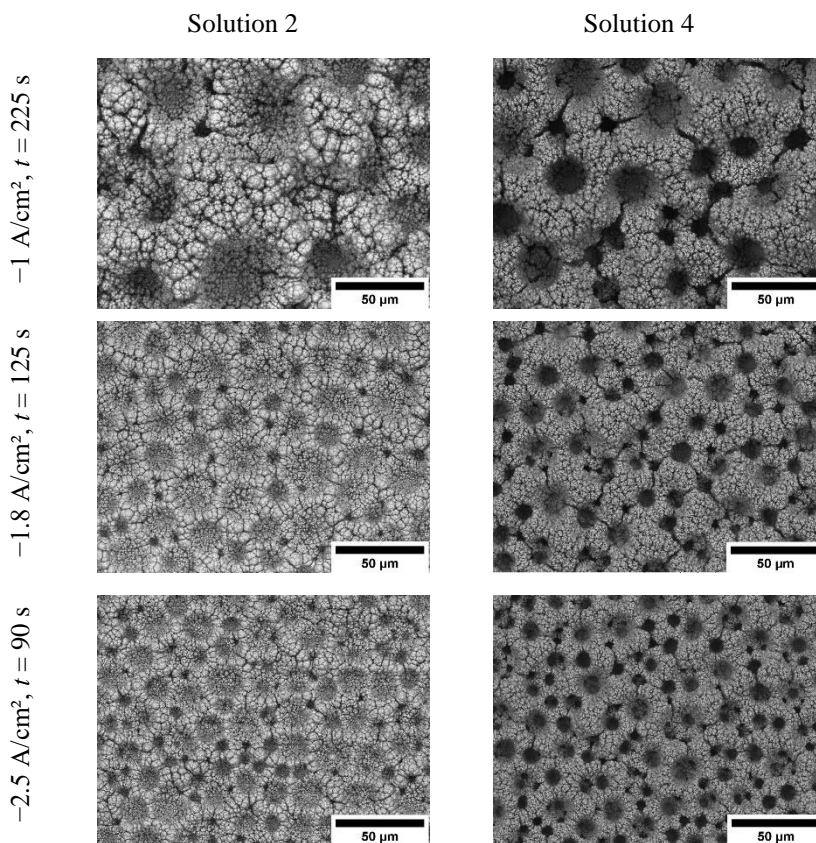

Fig. 8. SEM images of cobalt coatings obtained under galvanostatic deposition conditions at three different charge densities, with the same amount of charge passed (q = 180 C), from solutions containing isopropyl alcohol. Solution 2 - 0.2 M CoCl₂, 2 M NH₄Cl and 2 M isopropyl alcohol, Solution 4 - 0.2 M CoSO₄, 1 M (NH₄)2SO₄, 2 M isopropyl alcohol.

The two main reactions occurring during depositions using such high current densities were reduction of cobalt ions and reduction of water. The use of a DHBT template takes advantage of HER, forcing the metal ions to be reduced only in-between the hydrogen bubbles. With the use of high

current densities both reactions occur at a very high rate, however, the HER is dominant at all tested current densities. Cobalt by itself is a very good catalyst for the HER, and during the deposition further increases the HER rate, especially so with increased surface area as foam formation occurs. The decrease in surface tension, caused by isopropanol, allows easier detachment of formed bubbles resulting in an increase in the area for metal ions reduction. Also, the addition of isopropanol makes the water reduction reaction the dominant reaction by a huge margin. All these effects are evident from CE data (**Fig. 9**), which was calculated using Faraday's law. The hollow figures display solutions with isopropanol.
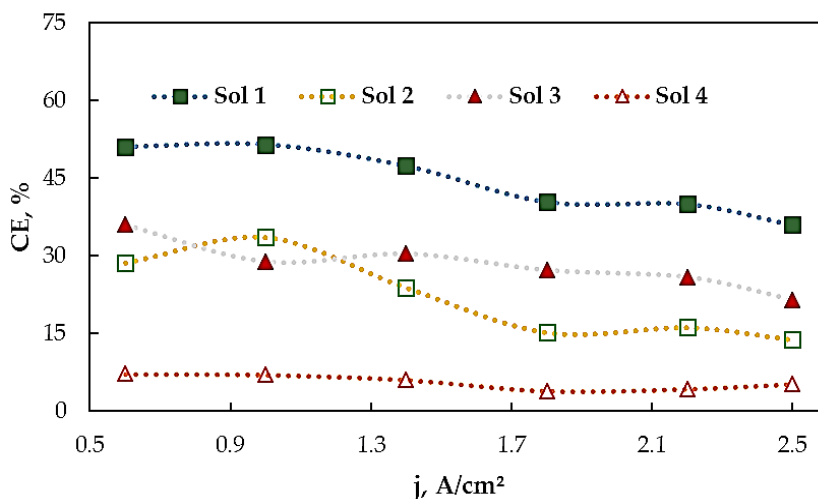

Fig. 9. Influence of the cathodic current density on the current efficiency (CE) of Co coatings obtained under a galvanostatic mode and q = 180 C. Formulation of solutions are provided in Table 1 (p. 24)

There were three clear trends for CE dependence on applied current density: (1) Increasing cathodic current density decreased the amount of deposited metal on the substrate; (2) the use of sulfate-based electrolytes (solutions 2 and 4, Table 1, p. 24) led to less deposited metal compared to chloride-based electrolytes (solutions 1 and 3); (3) the isopropyl alcohol significantly lowers CE.

The first phenomenon can be explained by an increased overpotential, which in turn increased the rates of both reactions (Co and hydrogen evolution). The cobalt ions reduction was controlled by the diffusion rate, which affected the quantity of deposited metal with increased current density. The second trend can be explained by the significantly different capabilities of hydrogen bubble coalescence suppression. Using the sulfates caused the formation of smaller bubbles, that cover the surface, encumbering

the diffusion of cobalt ions around them, and in turn, significantly reduces the CE. The third phenomenon is caused by a significant reduction of surface tension when using isopropyl alcohol. When the surface tension is reduced, hydrogen bubbles detach faster, and since the reduction reaction is diffusion controlled, the amount of current used for HER increases further, hence the increase in porosity and the formation of highly porous cobalt foams.

The use of such high current densities could also affect the preferred crystallographic orientation of Co. XRD spectra (**Fig. 10**) recorded for cobalt foams electrodeposited from solution 4 by applying various current densities showed a clear face-centered cubic (fcc) structure. Usually, for electrodeposited cobalt coatings, the hexagonal close-packed (hcp) structure is observed [143]. The fcc structure of Co with the two most intensive XRD peaks corresponding of (1 1 1) and (2 0 0) planes are commonly obtained using other synthesis methods [144]. Nevertheless, electrodeposited Co foams formed crystalline deposits with most preferred plains (2 0 0) and (2 2 0), while the intensity of (1 1 1) was comparable to that of the (3 1 1) plane. Increasing the current density caused to form more stable (2 0 0), (2 2 0) and (3 1 1) planes. That outcome could be linked to the distortion created by the evolution of hydrogen bubbles.
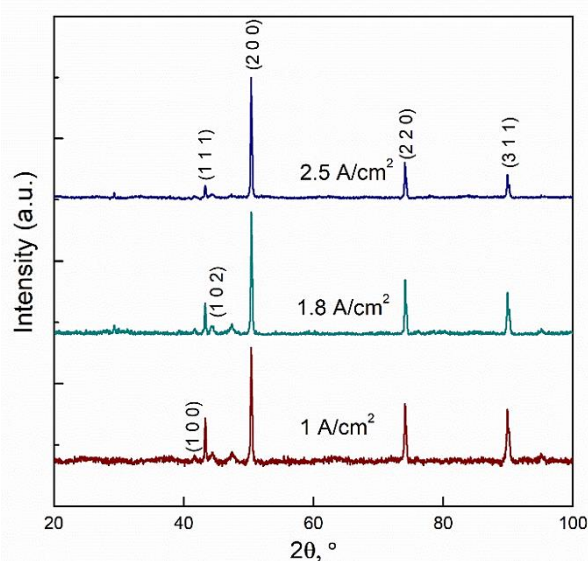

Fig. 10. *XRD pattern of Co foams electrodeposited from solution 4. Peaks were analyzed according to JCPDS cards No. 01-071-4238 and 01-077-7453.*

3.1.2. The mechanism of Co foams deposition and estimation of a true surface area

As it was mentioned above, using the DHBT at high current densities the deposition of Co occurred in-between hydrogen bubbles, whilst being diffusion controlled. SEM images of top-view (**Fig. 8**) and cross-sections (**Fig. 11**) cobalt foams, coupled with EDS data of the surface, revealed that after the initial formation of crystallization centers, intensive growth of fern-like cobalt agglomerates occurred. In such a way synthesized cobalt foam had cylindrically shaped pores. During the growth of the Co layer, the radius (size) of the pores increased. Such an increase can be explained by the rise of the HER rate, caused by the exposed high surface area of the cobalt - a good catalyst for the HER reaction [145-147].
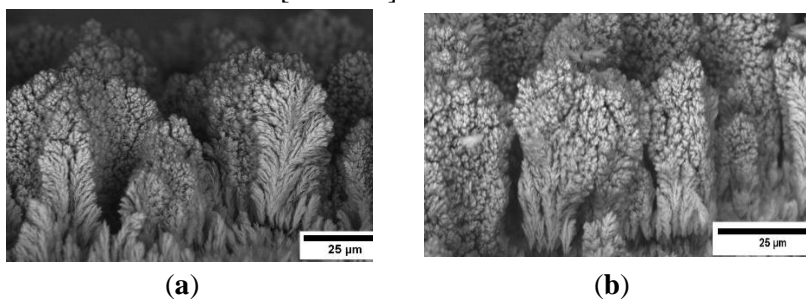

<p style="text-align:center">(a)   (b)</p>

Fig. 11. SEM images of cobalt foams cross-sections. Co foams deposited under galvanostatic conditions, from solution 4: (a) j = 1 A/cm², t = 225 s; (b) j = 2.5 A/cm², t = 90 s.

With huge differences in porosity and CE, the true surface area was estimated by EIS under the assumption that the capacitance of the DL of the same metal depended on the real surface area. This assumption is based on the fact, that thickness of DL is very small in comparison with the roughness, therefore the shape of formed DL "repeats" the surface.

The EIS measurements were performed across a wide range of frequencies (10 kHz to 0.1 Hz), at selected cathodic potentials of −0.8, −1, and −1.2 V (vs Ag/AgCl). An example of EIS spectra is presented in **Fig. 12** recorded using cobalt foams obtained from Solution 4 at different current densities. Fitting of the impedance spectra was performed using an equivalent electric circuit containing two pairs of constant phase elements in parallel with resistances (inset in **Fig. 12**). We could see only one clear capacitive behavior. However since the electrodes were very porous and EIS was measured during HER, in order to render the physical meaning, two capacitors were used in EEC In our case, the EEC presented in **Fig. 12**

showed the best fit for the obtained EIS spectra (minimal Chi-squared and elements values errors). First capacitance could be attributed to (1) porosity of the electrode, (2) double layer formation, or (3) diffusion limitations. According to Mulder et al., at highly contorted surfaces (3D) one can expect, to obtain n values of CPE at around 0.5 [148]. Also, it has been shown that when the first (high frequency) semicircle radius was potential independent, it was related to the porosity and the shape of pores [149,150]. However, in our case the high-frequency semicircle capacitance changed, hence it could not be linked to porosity. Also, during the measurement, evolving hydrogen bubbles could have blocked up some of the pores and restricted further hydrogen evolution. In this case, a diffusion limitation would be seen in the impedance spectra

Moreover, Łosiewicz et al. [151] showed that charge-up of the DL of the porous electrodes usually occurs unevenly (there is a frequency dependence). Hence the second semicircle (low frequency) could then represent the charge transfer resistance process and differential charge-up of the DL. It was also shown that DL capacitance becomes smaller with an increase in the overpotential in HER [151]. Similar behavior was observed with the low-frequency semicircle values in our case. Nevertheless, the first semicircle probably was related to the combination of the DL partial charge-up process, and the porosity of the electrode. There could be some effect of the diffusion processes, but the separation of these processes in our case was quite difficult.

The second semicircle, located in the low frequencies region that also changed with potential was attributed to DL partial charge-up capacitance and adsorption of hydrogen on the surface of cobalt foams. Both of these processes are potential dependent. Unfortunately, efforts to separate the two processes were fruitless.

Further calculations and comparisons were made from the data obtained at −1.0 V vs Ag/AgCl. The EEC model (**Fig. 12**) represented our best efforts, as it can be seen that it fit quite well the measured data. The Chi-squared values were usually in the range from 10^{-4} to 10^{-5}, which was acceptable for porous electrodes. Some examples are shown in **Table 3**. The second constant phase element value was recalculated into true capacitance values using Mansfeld's procedure. The calculated capacitances were much higher than the ones obtained for flat metallic cobalt, which did not exceed 100–200 μF/cm^2. It indicated that the obtained porous electrodes had **100–300** times larger electrochemically active **surface area** than the flat Co wire surface.
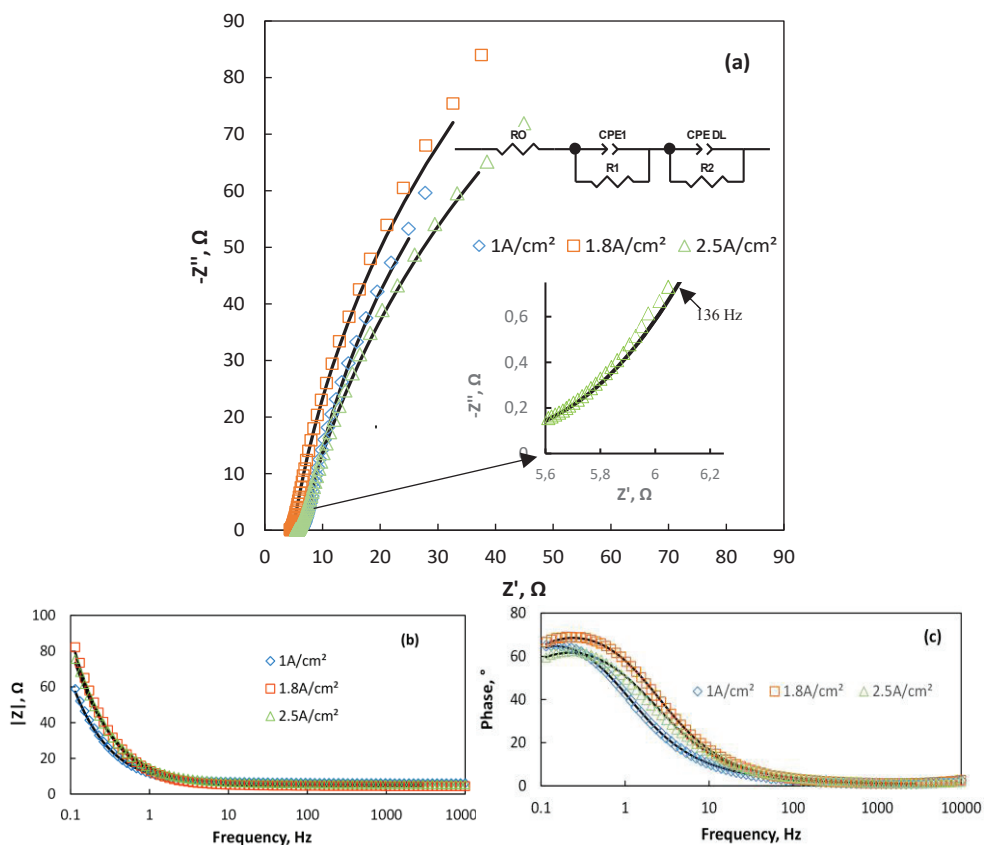
Fig. 12. *EIS data measured in 0.1 M Na$_2$SO$_4$ at −1.0 V on Co foams, deposited from solution 4, q = 180 C, EIS data represented in : (a) Nyquist's coordinates, (b) Bode modulus, and (c) Bode phase modulus coordinates. The EEC used for fitting is presented in the insert; points–experimental data, solid lines–results of the fitting.*

As it might seem, the second CPE element values (double layer and hydrogen adsorption capacitance), obtained using chloride-based solutions got the highest DLcapacitance, thus the highest electrochemically active surface area of cobalt foam. Nevertheless, after recalculations of CPE to true capacitance and further calculations of capacitance per gram of cobalt foam (**Fig. 13**), the results changed completely–the highest surface area to mass ratio was obtained for foam electrodeposited from solution 4. This could be explained by the higher efficiency of ammonium sulfate in hydrogen coalescence suppression and lowered surface tension using isopropyl alcohol. These factors allowed the growing coating to form a tridimensional porous structure, with interconnected pores. All of the other foams were

quite similar in a surface area exposed per unit of mass; however, the ones obtained from solution 4, were three or more times superior.

Table 3. *Values of elements of the EEC fitted for EIS data obtained in 0.1 M Na_2SO_4 at $-1.0V$ on Co foams deposited at $j = 2.5$ A/cm², $t = 90$ s.*

Sol. No	R_0, Ω	CPE_1, Fs^{n-1}	n	R_1, Ω	CPE_{DL}, Fs^{n-1}	n	R_2, Ω
1	3.67± 0.50%	0.113± 1.7%		0.732± 3.5%	0.034± 0.91%	0.93± 0.54%	133.7± 5.5%
2	4.08± 0.27%	0.050± 1.6%		0.765± 1.4%	0.011± 0.37%	0.88± 0.17%	349.7± 1.8%
3	4.87± 0.43%	0.047± 1.9%	0.5	0.878± 2.1%	0.028± 0.82%	0.83± 0.48%	508.8± 10.7%
4	5.42± 0.53%	0.047± 2.9%		0.809± 2.3%	0.017± 0.94%	0.85± 0.45%	311.9± 9.1%
Co	8.44± 0.17%	–	–	–	0.00018± 0.402%	0.91± 0.0868%	1458± 0.79%

Cobalt foams obtained using pulse deposition, showed better CEs across the board, sometimes reaching up to 50% in efficiency, hence the obtained foams were thicker. EIS analysis of these foams showed that the surface area to mass ratio was in all cases lower than the one obtained using galvanostatic deposition conditions.
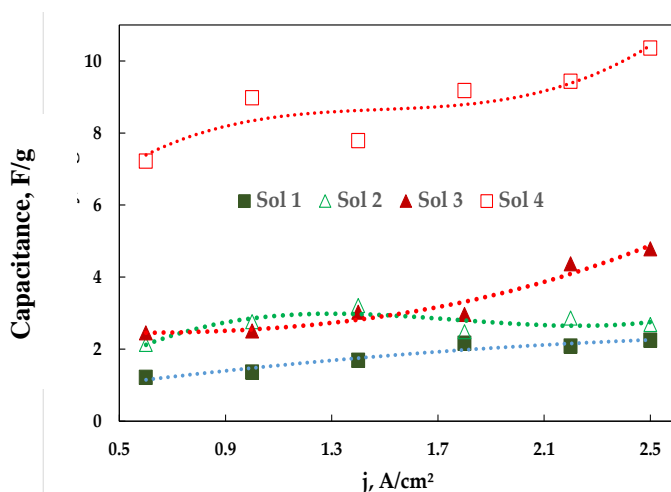

Fig. 13. *Influence of cathodic current density on the recalculated capacitance (from CPE$_{DL}$) per gram of cobalt foams in the investigated solutions.*

3.1.3. Effect of the deposition angle the Co foams catalytic activity

We chose to further examine the deposition of Co foams and the effect of the WE positioning (more specifically the angle) in regards to counter electrode and the effect it has on the porosity of the Co foam. It was decided to examine three angles of the WE – 0, 45, and 90°. The 0° means that the WE is perpendicular to the counter electrode. Since it was already found that Solution 4 works best to give the highest surface area per gram of material, it was used for further investigations. As it can be seen from SEM images (**Fig. 14** a and b) even at low current densities ($j = 0.2$ A/cm²), a foam-like structure can be formed on the bottom side of the WE when the electrode is angled at 90° compared to the counter electrode.
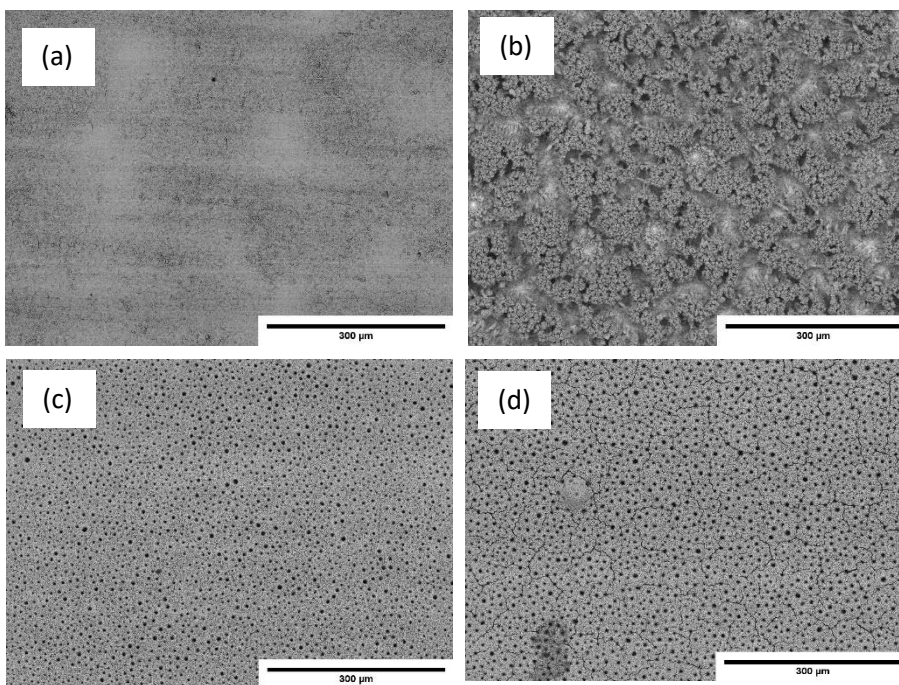
Fig. 14. *SEM images of Co coatings obtained different angles of the working electrode to the counter electrode: 90° angle j = 0.2 A/cm² q=100 C (a) top and (b) bottom sides, j = 2.5A/cm² 45° angle (c) top and (d) bottom sides.*

This is a much better result than what we obtained before, since a truly porous surface when the electrodes are in a perpendicular position, was obtained only at 1.4 A/cm². This allows to reduce the energy requirements, increase the efficiency and possibly even the porosity of the films. However with increasing the current density (**Fig. 14** c and d) the differences between the sides of the electrode disappears, especially so at a 45° angle. At 90°

angle, the difference is more apparent, because the bubbles trapped underneath the WE and the pores diameter increase. No interdependencies from the deposition angle and the preferred crystallographic orientation have been observed from the XRD measurements. The same face-centered cubic (fcc) has been observed.

The effects of the current density, the angle between the electrodes, and the surfactant (IPA) on the CE were also investigated (**Fig. 15**). As we can see even without the IPA the CE is quite a bit lower when compared with perpendicular electrodes (**Fig. 9** Sol 2). This is caused by the angle of the electrode, which allows easier detachment of the hydrogen bubbles from the surface of the electrodes. As we can see the efficiency is 1-4 % lower at 90° angle. The cause for this is likely the trapped bubbles on the underside of the sample (the one facing the bottom of the beaker). In there most of the surface is blocked by the bubbles so, therefore, blocking the solutions access. Also at a 90° angle, the detachment of the bubbles is even faster.With the addition of the IPA, the efficiency drops even further to only around 3-10 %. This is expected since the reduction of the surface tension and the beneficial angles add up. SEM images also indicated that the foams obtained with IPA had fern-like crystallite agglomerate structures, further increasing the surface area. Since the trapped bubbles on the bottom of the substrate create a more porous structure. Hence we decided to isolate the top-side and do the depositions only on the underside of the foam for further tests. These all points that obtained Co foams should be great high surface area catalysts.
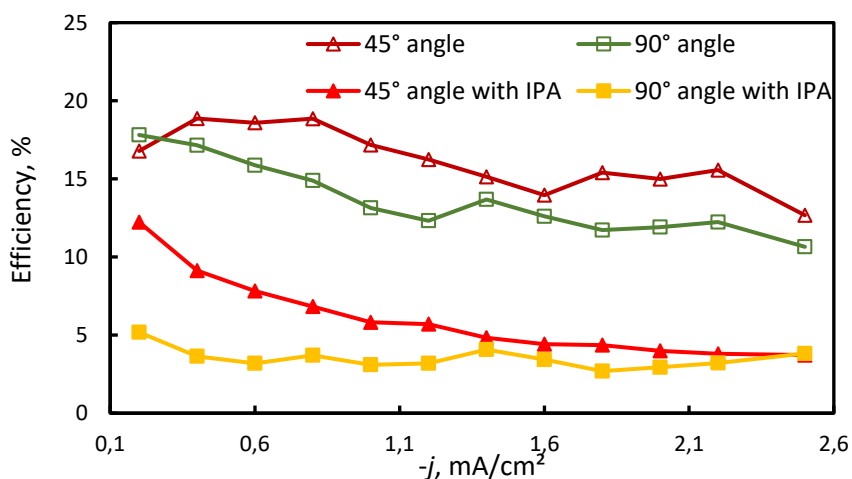

Fig. 15. *Influence of the cathodic current density and the angle between WE and counter electrode on the current efficiency of Co coatings obtained under a galvanostatic mode and q = 180 C.*

3.2. Electrochemical deposition of Co and Co-Pt foams and various applications

3.2.1. Catalytic activity of Co and Co-Pt foams as catalysts in electrochemical water splitting in alkaline media

Cobalt is considered to be a great alternative for pricier but more active and efficient Pt/Pd catalysts for HER reaction in alkaline media [79]. Cobalt is also very active in the neutral or acidic media, however, our attempts to use obtained foams as catalysts in such a manner proved that Co foams are too unstable, and dissolve too quickly. We have tried forming phosphates on the surface, but the whole surface was simply covered, blocking it. However in alkaline media Co foam work quite well. They require comparatively low overpotentials to start the HER (**Fig. 16**). The HER usually started after ~220 mV overpotential. The current density shown in the figures was calculated for the geometric area of the foam, not the true surface area. Also, two distinct HER stages can be seen, first quick but short (slope – 22 to 44 mV/dec) second - much slower (slope 244 to 325 mV/dec). The first stage probably is limited by either Heyrovsky or the Tafel step. Both are plausible since the pores could be clogged up with bubbles limiting solutions access. And the second must be controlled by the Volmer step.

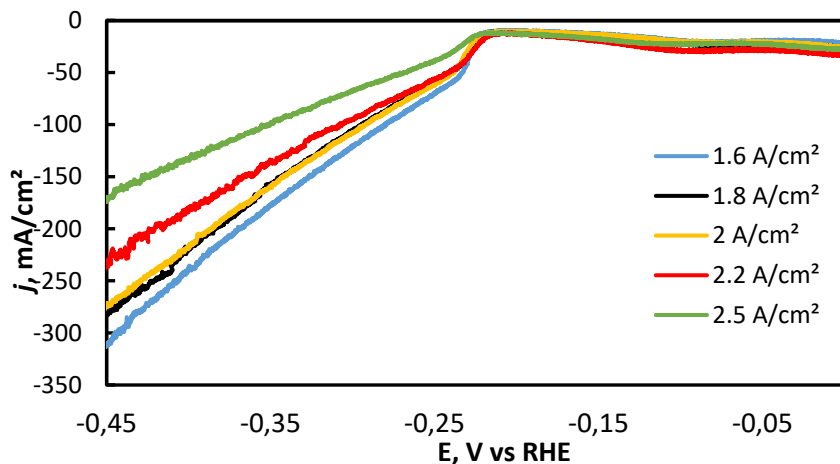|		
Volmer step	$H_2O + e^- \rightarrow H^* + OH^-$	$120 \ mV dec^{-1}$
Heyrovsky step	$H_2O + e^- + H^* \rightarrow H_2 + OH^-$	$40 \ mV dec^{-1}$
Tafel step	$H^* + H^* \rightarrow H_2$	$30 \ mV dec^{-1}$

Fig. 16. Voltammetry data for HER in 1 M KOH using Co foam as the catalyst which was deposited at different cathodic current densities (q= 180 C), potential sweep rate – 2mV/s.

What is interesting is that the higher the current density used for deposition the higher the slopes are. The samples after deposition were washed and kept in ethanol to prevent oxidation, however, some of it still occurred during the transfer and beginning of the measurement. Hence some reduction peaks can be seen at -0.1 V vs RHE. This could also somewhat impact the activity of the catalyst. The high activity and later drop-off could be explained by either destruction of the foam, lowering of its surface area. Or by the clog-up of the pores with hydrogen bubbles in this case hindering the diffusion, and in turn, lowering the activity. Nevertheless, the longevity of the catalyst was very poor, we could not run a second test using the same samples. Such poor stability has proven to be detrimental in trying to obtain a good alternative catalyst for Pt for HER reaction.

Cobalt oxides and also hydroxides/oxyhydroxides are at the top of the OER reaction volcano plots in alkaline media. [85,86]. So we also decided to test Co foams in this catalytic reaction, and the dependence of deposition conditions it might have on the activity of the reaction (**Fig. 17**). It was decided not to oxidize the foams in a furnace, but rather electrochemically, by forming cobalt hydroxides and oxyhydroxides. As can be seen, the overpotential required to reach 10 mA current with ongoing OER was quite high ~330 mV. And the slopes did not depend much on the deposition conditions are were fairly poor, the best one around 130mV/dec. Such subpar results prompted us to try and improve on the foams by creating Co-Pt alloy foams.
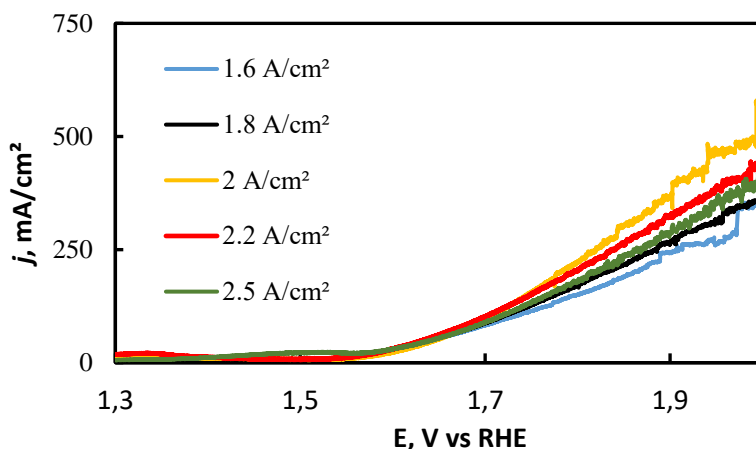

Fig. 17. *Voltammetry data for OER in 1 M KOH, using Co foam as a catalyst, which was deposited at different cathodic current densities (q= 180C). Potential sweep rate 2mV/s. The current densities applied for foam electrodepositions are shown in the legend.*

The Co-Pt foams were deposited just as the Co foams, using a 90° angle between the electrodes with IPA in the solution. It has been attempted to make Co-rich alloys by adding a small amount of Pt to the solution trying to form $Co_{85}Pt_{15}$. However, the obtained alloy according to EDS analysis showed that we obtained $Co_{97}Pt_3$ alloy. Such a big difference between the solution composition and that of the alloy is most likely related to the high deposition rate. The Pt-formed complexes with amines have a lower diffusion rate, hence the disparity between the two compositions. As can be seen from the SEM images the Co-Pt foams had similar porosity when compared to purely Co foams (**Fig. 18**).
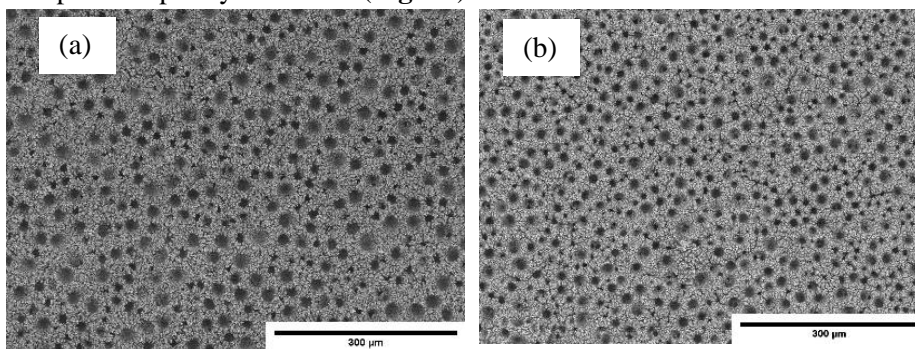

Fig. 18. *SEM images of CoPt foams (a) 45° angle j = 1.6 A/cm² q= 180 C, (b) 90° angle j= 2.5A/cm² q=180 C.*

Depositions at 90° angle have been done in order to obtain samples for HER catalysis tests. The one-step OER foam catalyst idea was scrapped because the hydroxides formed *in-situ* were not as active as previously expected. The two-stage Co foam HER catalysis looked very interesting. Similar results with the addition of Pt were expected only with lower overpotential to reach 10 mA current and overall better Taffel slope. As can be seen from the results shown in **Fig. 19**.

As can be seen from the voltammetry data as expected the overpotential required to start HER was reduced to around 120 mV which is around 100 mV lower than the result obtained using Co foam. Also, no additional reduction peaks have been observed during the voltammetry scan, which points that even a low Pt amount prevented the formation of oxides and hydroxides on the surface of the deposited CoPt foam.

Nevertheless, the overall activity of the CoPt foam was quite poor. The Tafel slope was 269 to 313 mV/dec. Which is similar to Co foams investigated previously. In this case, no initial high activity stage was observed, and the overall activity was quite low. Multiple measurements

were taken and further slopes were even worse. This points that the generated hydrogen gas bubbles destroy the surface of the foam. Also as it was seen from Co foams, the thickness of the foam has to be lower in order to fully utilize the full volume and surface area of the foams. Also, calcifications of the foams in an inert atmosphere have to be considered, to increase the longevity of the catalyst/ and or form the oxides on the foam's surface.
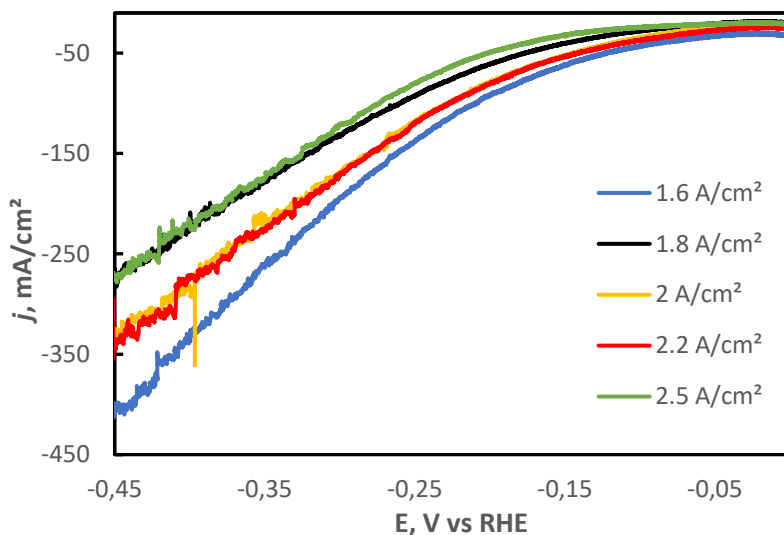
Fig. 19. *Voltammetry data for HER in 1 M KOH, using $Co_{97}Pt_3$ foams as a catalyst, which was deposited at different cathodic current densities (q= 180 C). Potential sweep rate 2 mV/s.*

3.2.2. Modification of Co foams and detection of free chlorine in the water

Modification of cobalt foams was done using ferrocyanide, utilizing cyclic voltammetry technique. The measurements were performed in an acetic acid buffer solution. Such a buffer was chosen because of highly active and substantial cobalt foams surface. Other buffer solutions such as phosphate or citrate were tested, however, either the foam reacted with the anions in the buffer solution (phosphate), or formed complexes at the surface (citrate case), diminishing the modification capabilities. The potassium nitrate was used as a background electrolyte has been shown to have second best ion permeability in various metal HCFs structures, ensuring good

conductivity and electrons exchange [92,99]. The chosen potential window for modification was –from 0 to -0.8 V vs Ag/AgCl.

The potential in CV was first scanned to the anodic side, to dissolve some of the foam near the surface, and afterward to cathodic, to form cobalt ferrocyanide complex on the surface of the foams. Comparatively, high scan rates were used to form cobalt ferrocyanide, trying to preserve the structure and the high surface area of cobalt foams. Additionally, no clear peaks could be seen on the voltammetric curve, since the scan speed used was high, the Co foams surface was very porous, and the response might have been too slow to be detected in such a system. A high scan rate was chosen to try to keep the highest possible surface area intact, but still covering the whole surface of foam with Co HCF complex. With no clear oxidation or reduction peaks obtained during CV scans, a formation of cobalt ferrocyanide on the surface of cobalt foams had to be done externally. For that reason, SEM and EDS measurements were performed to ensure the successful formation of the cobalt ferrocyanide complex (**Fig, 20**). The EDS picture represents a typically modified cobalt foam. It can be seen that the whole surface was quite uniformly covered with Fe and C compound, proving successful formation of Co HCF complex on the surface of the Co foam.
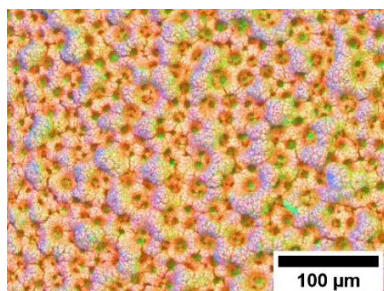
Fig. 20. SEM image of modified Co foam, using CV at 100 mV/s scan rate and after 100 cycles with overlaid EDS mapping. Red color represents cobalt, green– iron, blue–carbon.

Free chlorine concentration, which is a sum of dissolved chlorine gas, hypochlorous acid, and hypochlorite anion, was detected using acetic acid buffer solution whilst measuring the amperometric response of our system. Before the testing, the purity of $Ca(OCl)_2$, which was used as a source of free chlorine, has been checked using the standard DPD method. It was determined purity of calcium hypochlorite was 64%. The chosen pH value for chlorine detection measurements was −5.5 and was done so for two reasons: (1) Trying to simulate real tap water pH range, which was usually 5

< pH < 8, (2) all of the compounds of free chlorine exist in the solution at such pH values. However, most of the chlorine exists in the form of HClO, since the pK_a of reaction (3) was 7.48 at 25 °C.

$$HClO \rightarrow ClO^- + H^+ \qquad (3)$$

Hypochlorous acid reduction occurs in two steps (reactions 4 and 5), which according to Cheng et al. if the pH is above 3 is irreversible [152], making it possible to fully reduce and hydrolyze free chlorine in the water to chloride anions.

$$HClO + H^+ + e^- \rightarrow 0.5Cl_2 + H_2O \qquad (4)$$

$$Cl_2 + 0.5H_2O \rightarrow HClO + H^+ + Cl^- \qquad (5)$$
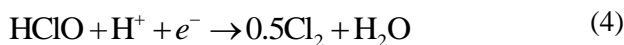
All of the free chlorine-containing compounds have been reduced electrochemically very easily. Trying to minimize the damage of high surface area modified cobalt foams, ensuring the longevity of the sensor, a plethora of potentials were tested. The best results were obtained using −0.45 V vs Ag/AgCl potential with the cobalt foams modified for 40 cycles at a 100 mV/s scan rate. A calibration curve and typical chronoamperometric measurements are shown in **Fig. 21**. The linearity of the curve was slightly distorted probably by oxygen reduction that was dissolved in testing solutions. Nevertheless, the increase of cathodic current with the addition of very small amounts of chlorine into the water proved very high sensitivity for our sensor. The standard deviation of the blank solution was calculated using data from 10 chronoamperometric measurements. The calculated limit of blank (**LOB** = 1.65σ) was **3.06 ppb**. The obtained limit of detection (**LOD** = 3σ) was **5.57 ppb** and the limit of quantification (**LOQ** = 10σ) was **18.86 ppb**. Such results were acceptable since the usual concentration of residual chlorine in tap water was somewhere between 0.2 and 1 ppm.
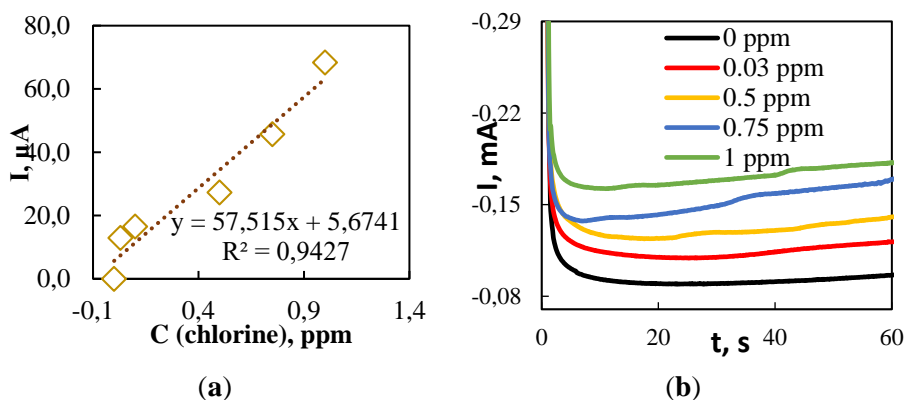

(a)   **(b)**

Fig. 21. *Calibration curve for sensors (**a**) and typical chronoamperometric curves for free chlorine detection in acetic acid buffer (**b**).*

Cobalt metal foams were successfully deposited using a DHBT template on the flat copper substrate. The true surface area of cobalt foams was estimated using the EIS technique. It was determined that the highest surface area cobalt foams were electrodeposited using a solution containing 0.2 M $CoSO_4$, 1 M $(NH_4)_2SO_4$, and 2 M isopropyl alcohol at a cathodic current density of 2.5 A/cm². In this case, there was a synergy between the ammonium sulfate bubble suppression effect, and solutions surface tensions reduction, which allowed for the formation of highly porous 3D structured cobalt foams. The cobalt foams surface was modified with Co hexacyanoferrate, and such modified foams have been tested as sensors for the detection of free chlorine in the water. A linear range from 5.6 ppb to 1 ppm was shown. It was demonstrated that such a sensor can be a good and a less expensive alternative to noble metal sensors currently used for the detection of the concentration of residual chlorine in the water.

3.3. Copper foam as a complex cathode

3.3.1. Characterization of copper foam

The copper foam has a 3D interconnected porous structure, which can be observed in SEM images (**Fig. 22**). The pore size varies from 1 to 0.1 mm. The surface of the foam is very uneven, making the true surface area of the already porous copper foam even larger. In order to determine how the behavior of copper foams differs from flat surfaces in solutions, voltammetry experiments with different copper (II) sulfate concentrations were carried out; the compositions of the solutions are shown in **Table 2**. The concentration of the sulfate anion was kept at 0.5 M to maintain the same buffering power in all of the solutions.
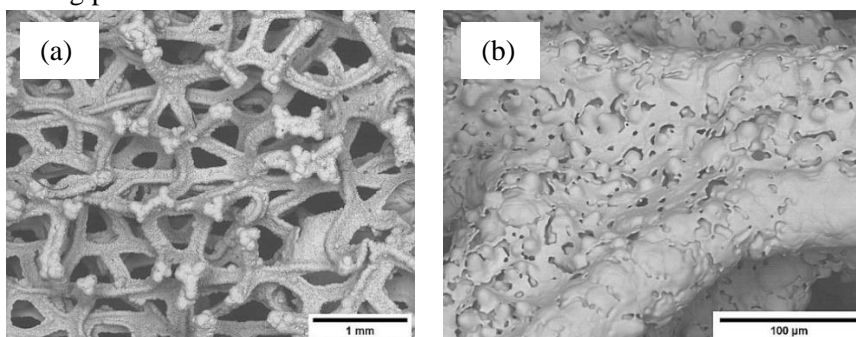

Fig. 22. *SEM images at low (a) and high (b) magnification of 3D copper foam.*

The obtained polarization curves for the plate and foam electrode are shown in **Fig. 23**, where the ordinate axis is displayed on a logarithmic scale because of a big difference in the current values between tested concentrations. To estimate the influence of porosity on the copper deposition, the geometrical sample size was the same for both Cu plates and Cu foams (1 cm × 1 cm). As can be seen from **Fig. 23,** Cu deposition starts somewhere around −0.075 V versus Ag/AgCl and did not depend on the substrate used. After the peak representing the Cu^{2+} reduction to Cu^0, the current on both surfaces and all the concentrations turns into an almost constant one. The reason for this could be the mass transport limitations because the leveling off of the current depends on the concentration of Cu(II) in the solution. This is also supported by the slight increase of the current with the rise of polarization at higher concentrations (50 mM to 0.2 M), showing that at higher potentials, the positive ions are attracted from further away, and the deposition rate increases.

In addition, voltammetry tests also showed that independently of the used substrate, the hydrogen evolution reaction (HER) started in the range of −1.0 to −1.1 V vs Ag/AgCl in the solutions containing 10 and 50 mM of $CuSO_4$. This fact could be attributed to the governing role of pH change in the near electrode layer during electrodeposition, and this change seems to be similar for both solutions. However, in the solution containing 0.2 M $CuSO_4$, the HER started around −0.75 V vs Ag/AgCl on both surfaces. This earlier HER start could be linked to the higher rate of copper electrodeposition, and in turn, the pH decrease near the working electrode. Additionally, one major difference between the two surfaces can be noted from voltammetry experiments: there was an approximately 3 times higher current on the foam substrate at all potentials in comparison to the flat surface. This difference can be explained by the better hydrodynamic conditions of copper foams substrate: the porous surface allows for faster mass transport and exchange.
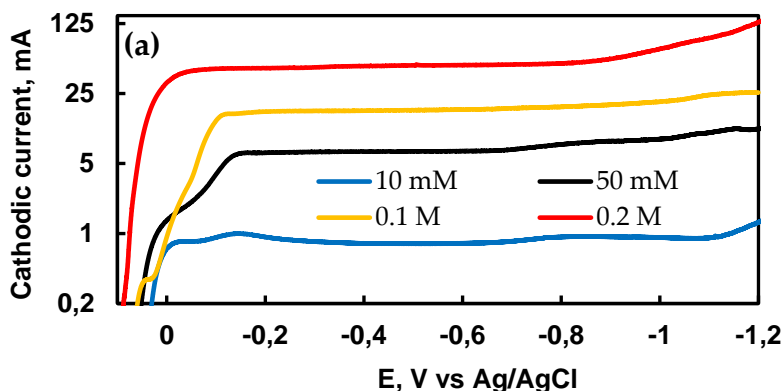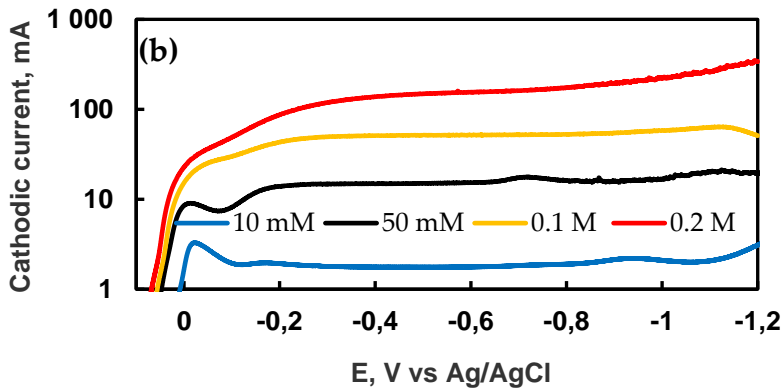
Fig. 23. *Cathodic voltammograms on Cu plate (a) and foam (b) were obtained in the electrolytes with various concentrations of CuSO₄ (the compositions of solutions are shown in Table 2), potential scan rate 2 mV/s.*

For further investigation, the solution containing a similar amount of Cu(II) as in solutions used for various metals recovery from the electronic waste was chosen. Regarding the influence of the surface type on the Cu electrochemical deposition, chronoamperometric measurements have been done in 0.1 M $CuSO_4$ and 0.4 M Na_2SO_4 solution at four fixed potentials: −0.1, −0.2, −0.4, and −0.6 V vs Ag/AgCl, and at a fixed amount of charge passed through the cell (30 C). The results have been summarized and are shown in **Table 4**.

Chronoamperometric measurements (**Table 4**) clearly show an approximately 3 times faster copper deposition rate on the foam at all tested potentials. In this case, there was no hydrogen evolution, and the deposition efficiency was almost 100% on both substrates.

Table 4. *Cu deposition rates on 2D and 3D electrodes in the solution containing 0.1 M CuSO₄ and 0.4 M Na₂SO₄. A fixed amount of charge was let through the electrochemical cell at each potential (q= 30C).*

Substrate	E, V vs Ag/AgCl	Deposition time, s	Deposition rate, mg/min
Cu plate	-0.1	1763	0.33
	-0.2	1681	0.35
	-0.4	1603	0.36
	-0.6	1571	0.37
Cu foam	-0.1	643	0.94
	-0.2	574	1.1
	-0.4	593	1.0
	-0.6	518	1.2

A considerably higher deposition rate on the cooper foam substrate supports the idea that the deposition is controlled by diffusion to the electrode surface - the one having a higher specific surface area. In addition, a higher metal deposition rate on the foam electrodes makes them an attractive substrate for the electrowinning of metals compared to other materials having a similar geometric area. The morphology of deposits is influenced by the potential and type of substrate, as is shown in the SEM images in **Fig. 24**.

The copper deposits have globular shapes on the flat electrodes, and the morphology did not differ at these two potentials. This is related to the very similar electrochemical deposition rates at these potentials, and as can be seen from the voltammetry data (**Fig. 23**) and efficiency of deposition, there were no side reactions, and the current was similar at these two potentials. Another case is the deposition on the porous substrate. At −0.2 V versus Ag/AgCl, copper forms cauliflower-like crystalline agglomerates with well-defined edges. At higher potential, the copper forms smoother surfaces that are still cauliflower-like structures. The coverage of both surface geometries was good even without external agitation, even at low potentials

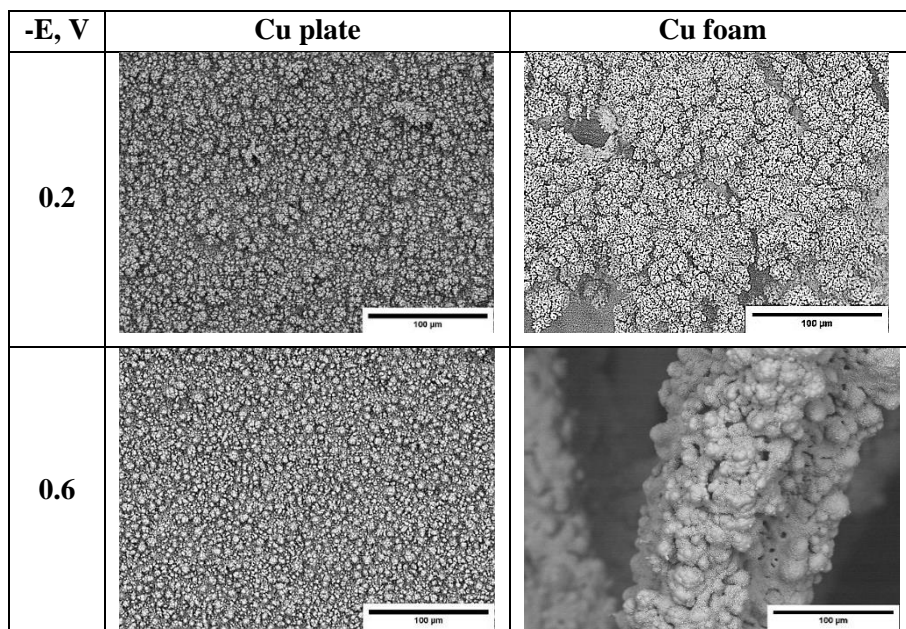| -E, V	Cu plate	Cu foam
0.2		
0.6		

Fig. 24. *SEM images of potentiostatically electrodeposited Cu coatings at different cathodic potentials on flat and foam copper substrates after 30 C passed charge. The bath was 0.1 M CuSO$_4$ and 0.4 M Na$_2$SO$_4$.*

3.3.2. Copper foam surface area and diffusion rate estimations

To characterize copper foams and estimate the active surface areas for charge and mass transfer processes that occur during the electrochemical deposition of copper, the EIS technique was utilized. EIS measurements have been done in all solutions listed in **Table 2**. EIS measurements were performed at cathodic potentials of -0.125, -0.15, -0.175, and -0.2 V vs Ag/AgCl on flat and porous copper substrates. These potentials were chosen based on chronoamperometric data. At comparatively low potentials, the change of surface morphology during deposition is still minimal and can be ignored in this case. Typical EIS scans on the copper plate at various potentials are shown in **Fig. 25**. From the EIS data plots, we can see that at investigated potentials the data plot can be divided into two zones – the high-frequency semicircle and the low frequency (starting around 75-100 Hz) 45° angle line. The high-frequency semicircle can be attributed to the charge-up of the double layer and charge transfer to the copper ions, whilst the low-frequency line is attributed to the formation of the concentration gradient of the copper ions. To better evaluate ongoing processes EIS data were fitted to the equivalent electric circuit (EEC) that is shown as an **inset** in **Fig. 23** of the Nyquist plot (a).

The elements of applied EEC have the following physical meaning: R_0 is resistance at electrode/electrolyte interface, CPE(DL) is a double-layer capacitance modeled via constant phase element (CPE), R(CT) is a charge transfer resistance, CPE(W) stands for capacitance caused by the concentration gradient, R(Diff) is a resistance caused by the concentration gradient. The element CPE(W) is attributed to the diffusion because of the signature 45° angle seen in the Nyquist plots at low frequencies (**Fig. 25**), and the value n in this CPE element was very close to 0.5 in all the experiments. This constant phase element acting only in the low-frequency region) represents diffusion and it can be used as a Warburg element when $n = 0.5$ [153,154]. The values of constant phase element CPE(DL) have been recalculated into true capacitance using Hsu and Mansfeld equation [155]. All values of components of the fitted EEC are indicated in **Table 5**.
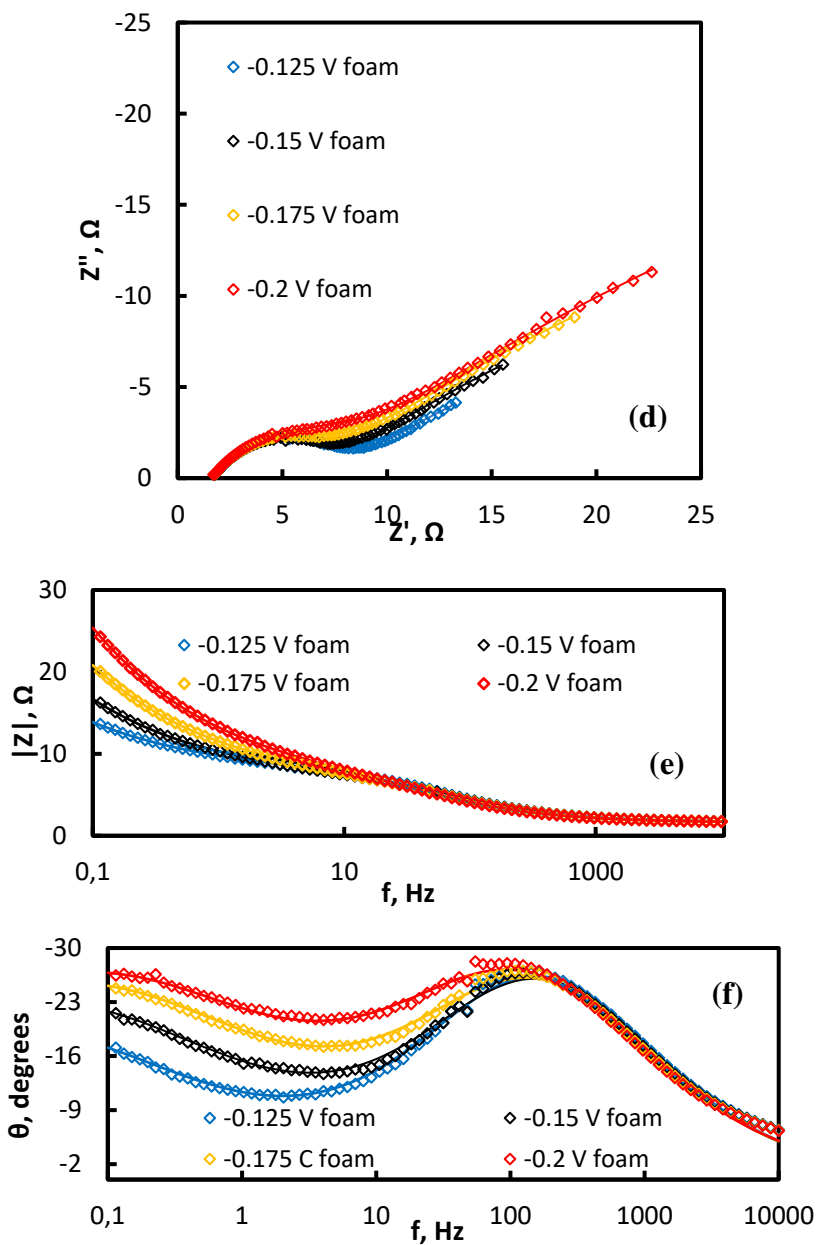
(a)

(b)

(c)
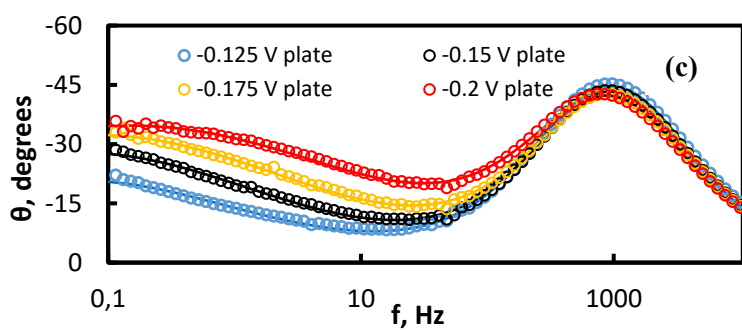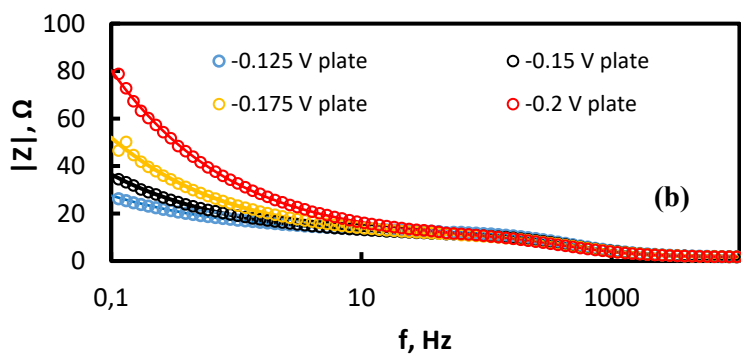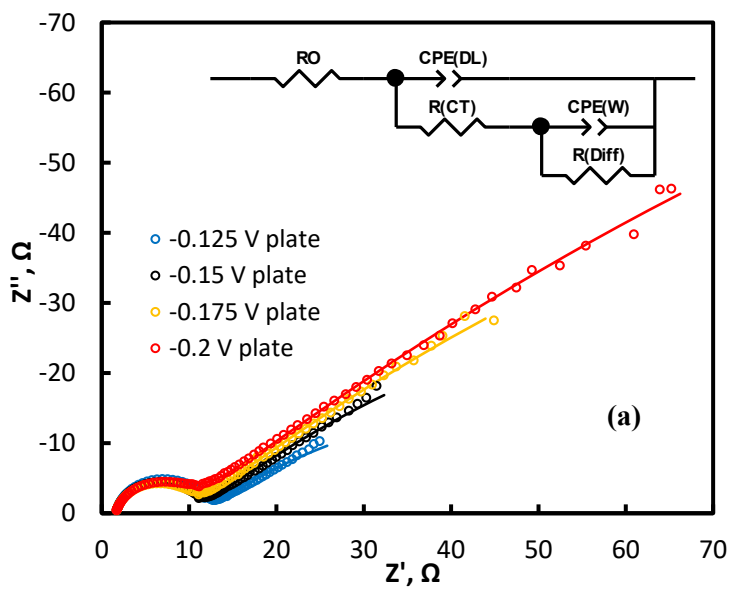
Fig. 25. Nyquist (a,d) and Bode plots (b-c,e-f) on Cu plate (a-c) and foam (d-f) registered at various potentials (indicated on graphs) in 0.1 M CuSO₄ + 0.4 M Na₂SO₄ solution at 20°C. Points – experimental data, solid lines – results of fitting to EEC shown in the inset (a).

Table 5. *Values of EIS parameters were obtained by fitting data obtained on copper foam and copper plates at -0.175 V vs Ag/AgCl at different copper concentrations. EEC used for modeling is shown in* **Fig. 25 inset.**

Electrolyte	Substrate	C(DL), µF	R(CT), Ω	CPE(W)	R(Diff), Ω
0.2 M $CuSO_4$ + 0.3 M Na_2SO_4	plate	40.5	2.98	0.0696	233.4
	foam	299.2	2.39	0.2033	14.9
0.1 M $CuSO_4$ + 0.4 M Na_2SO_4.	plate	49.3	8.76	0.0260	319.3
	foam	513.5	6.65	0.0748	74.9
0.05 M $CuSO_4$ + 0.45 M Na_2SO_4	plate	41.9	7.44	0.0285	199.6
	foam	456.6	6.74	0.0668	83.3
0.01 M $CuSO_4$ + 0.49 M Na_2SO_4	plate	56.4	54.66	0.00247	663.7
	foam	754.1	122.20	0.0039	1551.0

As can be seen, the proposed EEC describes well experimental EIS data on both substrates in a whole investigated potential range. The values of the capacitance of the DL on both substrates might be used to estimate differences in real areas between plate and foam electrodes, i.e. to estimate the roughness factor as a ratio of C(DL) on foam and plate of the same geometric area (1x1 cm). Notably, the double-layer capacitance (C(DL)) extracted from EIS data is 50 µF (see **Fig. 26**), and is in good agreement with the theoretical values assigned to 1 cm² of copper [143]. The capacitance of the DL of a commercial foam, that has the same geometric area as a plate, is 7 to 14 times higher in comparison with a plate electrode. The thickness of the DL is very small and is in tens of nanometers, therefore this layer replicates the surface morphology on the nano-level, and the ratio with the value obtained on the plate electrode can represent the roughness factor, and matches the ratio of C(DL) of both surfaces - 7-14. However, the increase of DL capacitances with the increase of applied cathodic potential on both flat and porous surfaces is different. On the porous electrode, the C(DL) increase is much higher when compared to the change in capacitances of the flat electrode. This increase is related to the much higher surface area, and the distribution of current on the surface of the foam – with higher potential the current distributes more evenly on the whole foam surface, and the edge effect is less apparent, this also influences the surface area estimations. (DL) [156, 157].

When looking at the effect the concentration of copper ions has on the EIS parameters (**Table 5**), we can divide the results into three sections high concentration (0.2 M), mid-level concentrations (0.1 and 0.05 M), and low

concentrations (0.01 M). The DL capacitance values do not differ that much with the change of the concentration on both surface geometries. However, when looking at charge transfer resistance, the differences between concentrations are significant. At low concentrations the charge transfer resistance is very high, this is caused by lack of copper ions, and this resistance at mid-level concentrations is around 6-9 Ω, it depends on the surface geometry as well as applied potential (**Fig. 26**). And at high concentrations (0.2 M and higher) the charge transfer resistance values decrease ~3 times on both surfaces, because of an abundance of conducting particles, nevertheless, this charge transfer resistance is lower at all investigated potentials and all concentrations on the foam electrode. This shows that reduction reaction occurs faster on the copper foams.
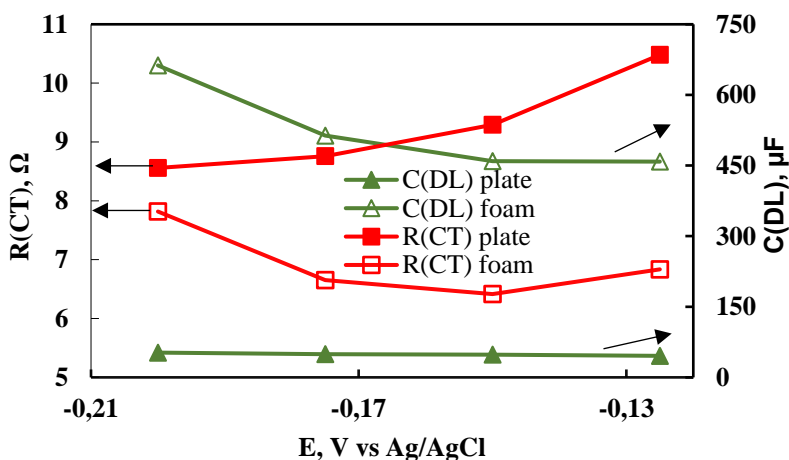
Fig. 26. Dependence of double-layer capacitance (ordinate at the right) and charge transfer resistance (ordinate at the left) on potential applied for Cu plate and foam electrodes in 0.1 M CuSO$_4$ + 0.4 M Na$_2$SO$_4$ solution.

When taking a look at the charge transfer resistance dependence on potential (**Fig. 26** and **Table 5**) with both types of electrodes, it's clear that the 3D electrode displays approx. 1.5-1.7 times lower charge transfer resistance than 2D electrode, agreeing with the results of voltammetry (see **Fig. 23**). The differences in charge transfer resistance on plate and foam electrodes are lower than differences in the capacitances of DL, because the reaction layer is thicker than DL, and in some areas of the foam electrode it overlaps. As it can be seen from **Fig. 26** the difference between 2D and 3D electrodes in charge transfer resistance is higher at low potentials, thus charge transfer reaction on the foam occurs easier, and partially explains the

higher Cu deposition rate (see **Table 4**). However, the lower charge transfer resistance, or in turn the increase of the rate of the charge transfer reaction by ~2 times does not result in increases in Cu deposition rate by around 3 times.

To further characterize the difference in copper deposition reactions on flat and porous copper surfaces the components of EEC related to diffusion have been investigated in detail (**Fig. 27**). The foam has lower charge transfer resistance, meaning faster reactions, and better hydrodynamic qualities, allowing for faster diffusion and in turn the much faster deposition, even with a larger surface and in turn – lower current density.
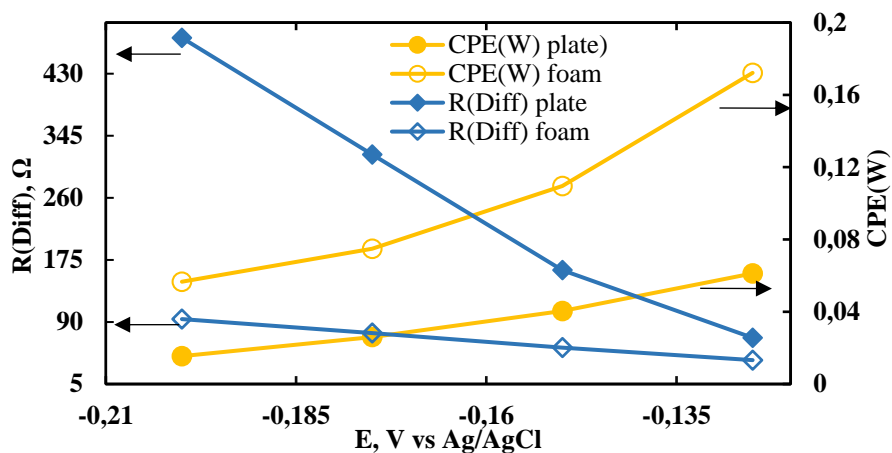
Fig. 27. *Dependence of diffusion-related elements of EEC on the potential applied. Measurements performed using a copper plate and copper foam as working electrodes in 0.1 M CuSO₄ + 0.4 M Na₂SO₄ solution.*

The parameter related to diffusion CPE(W) at low concentrations is almost equal on both surface geometries, showing that the diffusion effect is similar, but the resistance at low concentrations is about 2.5 times higher. It means that the diffusion layer is much thicker on the copper foams surface because of the porosity effect. Therefore, it causes a higher rate of copper electrodeposition. The overall trend in mid-level and high concentrations is that with the increase of Cu^{2+} concentration, the CPE(W) value increases, and the R(Diff) decreases. As it is seen from **Table 5**, the difference between R(Diff) values at 0.2 and 0.05 M concentrations on the flat surface is only around 14%, whereas, on the foam electrode, the values of R(Diff) are lower, but all values are sensitive to the concentration of Cu(II) in the solution. The highest value of R(Diff) is obtained on the foam electrode at a relatively low concentration of Cu(II), i.e., 0.01 M, which is probably due to

the faster depletion of copper ion concentration in the 3D diffusion layer and the necessity of longer time to supply Cu(II) ions into the pores. Since the deposition rate on the foam electrode at a higher concentration of Cu(II) is 3 times faster than on the flat electrode, this is mirrored by the behavior of CPE(W), showing that the diffusion occurs 3 times faster on the foam. The efficiency of charge transfer on the porous surfaces is higher as well, which is in good agreement with other studies of metal depositions on porous surfaces [56]. To even better understand the diffusion peculiarities on 2D and 3D electrodes, the diffusion impedance using extracted values from total impedance data (presented in **Table 5**) was calculated. As it is shown in **Fig. 25**, the copper deposition occurs under diffusion control at low frequencies (below 100 Hz) on both foam and plate electrodes, and diffusion is modeled by a parallel connection of CPE(W) and R(Diff) elements. In this case, diffusion impedance, Z_{diff}, as a function of frequency is calculated by the equation:

$$Z_{diff}(\omega) = \frac{R_{Diff}}{1 + (j\omega)^{\alpha} QR_{Diff}} \qquad (4)$$

where Q and α are parameters of CPE(W), R(Diff) is resistance caused by diffusion, and ω is the phase angle (ω=2πf). When α = 1 - Q is pure capacitance, in our case however α = 0.5 and the CPE represents diffusion [158].

The calculated diffusion impedance data are presented in **Fig. 28**. As it is seen, the diffusion impedance on the plate Cu electrode is 2–4 times higher than that on the foam Cu electrodes, which is dependent on the frequency and potential applied.

These results once again confirm the chronopotentiometry data obtained on both 2D and 3D Cu-electrodes. For chronopotentiometry experiments, current values have been chosen higher than the limiting current values seen in **Fig. 28**. In this case, the transition time, at which the concentration of metal ions on the electrode becomes equal to zero, is visual on the chronopotentiograms, and the effective diffusion coefficient can be calculated by the Sand equation:

$$i\sqrt{\tau} = \frac{nFAC_0\sqrt{\pi D_{eff}}}{2} \qquad (5)$$

where τ is a transition time (s), i is a current (A), C_o is the concentration of Cu(II) ions (mol/cm^3), D_{eff} is the effective diffusion coefficient (cm^2 s^{-1}), F is Faraday's constant, n is the number of electrons participating in electrochemical reaction; A is a geometrical surface area.
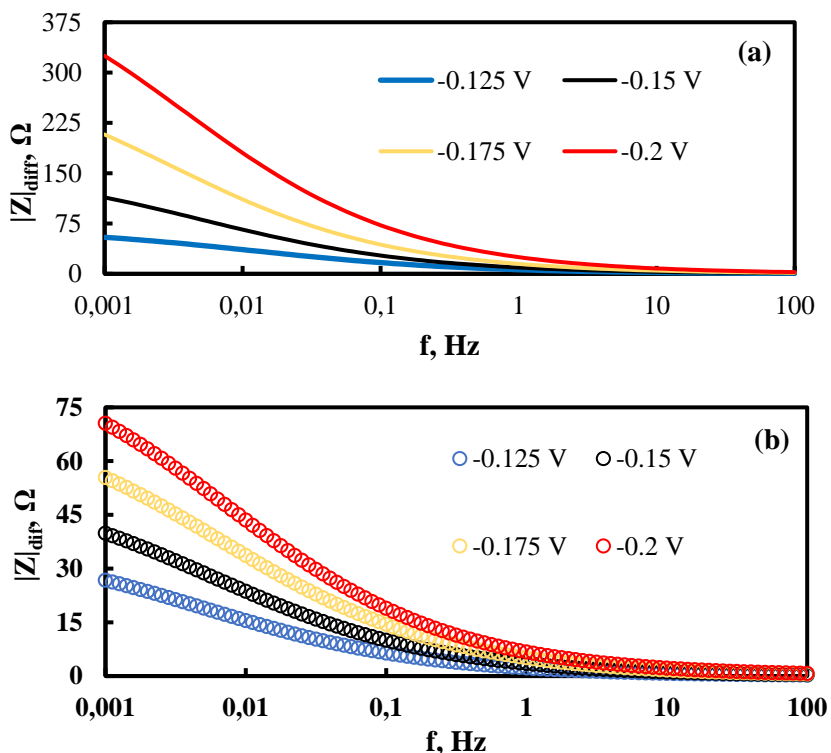
Fig. 28. *Bode plots of extracted diffusion impedance at various potentials on flat Cu substrate (a), and Cu-foam substrate (b).*

In our case $i\sqrt{\tau} \sim const$, so the maximal deposition rate is controlled by the mass transfer. The values of the effective diffusion coefficient of Cu^{2+} ions on both plate and foam Cu electrodes were calculated by Eq. (2) and the data are shown in **Table 6**. The effective diffusion coefficient on the plate electrode is almost three times lower than on the foam electrode, and it is in good agreement with EIS data.

So, copper foams are great substrates for reactions that are either limited by the mass transfer (electrochemical depositions, etc.) or the ones that are restricted by adsorption or activation (HER and similar), making them great candidates to reduce the size of electrodes, but not to lose out on efficiency and activity of electrodes.
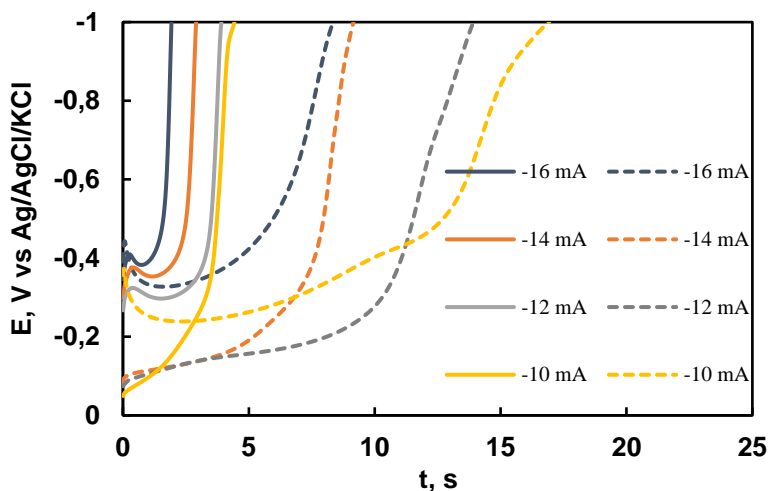
Fig. 29. *Chronopotentiograms on flat (continuous lines) and porous (dashed lines) electrodes at various current densities in 50 mM CuSO$_4$ and 0.45 M Na$_2$SO$_4$ solution. All the densities have been calculated for the geometrical area of the substrate of 1 cm².*

Table 6. *Effects of electrode geometry on effective Cu(II) ions diffusion coefficient.*

Applied current	Effective diffusion coefficient	
	Plate	Foam
I, mA	10^6 D, cm²s^{-1}	10^6 D, cm²s^{-1}
-10	6.79	18.06
-12	6.72	19.70
-14	6.73	20.16
-16	6.62	20.77
Average D$_{eff}$	**6.72**	**19.67**

Overall a comprehensive investigation of the electrochemical deposition of copper onto 2D (plate) and 3D (foam) Cu substrates has been done. Using various electrochemical methods, it was determined that the rate-determining step in a copper deposition is diffusion. The main processes occurring on the electrode are - the charge-up of double electric layer, charge transfer, and diffusion. The specific electrochemically active area of Cu foam was estimated from EIS data, and based on the values of the double electric layer, it was determined to be 7–14 times higher than that for the plate electrode. Based on the EIS data, it was determined that the charge transfer resistance on the Cu foam electrode is 1.5–1.7 times lower than that on the Cu plate

electrode, which results in an increase in a charge transfer rate of approximately 2 times. Based on the analysis of the diffusion impedance and chronopotentiometry data, it was found that Cu^{2+} mass transfer and the copper deposition rate is up to 3 times faster on the foam surface in comparison with a flat surface having the same geometric area in the same potential range. In addition, effective diffusion coefficients have been calculated from chronopotentiometry data using Sand's equation. Overall these findings make Cu foam an attractive material for metal electrowinning processes as well as for processes controlled by adsorption (e.g., hydrogen evolution reaction).

3.4. Electrochemical deposition of Fe. Testing their catalytic activity in Fentons reaction

3.4.1. Iron deposition

Using environmentally friendly electrolyte for Fe deposition, and trying to optimize the deposition conditions, Si wafers were used as substrates, while changing deposition conditions like temperature and deposition time. Depositions were done galvanostaticaly (j = 15 mA/cm²) without agitation. Two distinct temperatures were selected - room temperature and 65° C. Ar room temperature the current efficiency was only around 10 %. Low efficiency was caused by bulky ferrous complexes that were formed with citric and glycolic acids. Raising the temperature to 65°C the efficiency grew to around 50%. The surface morphology did not change drastically, however, from the cross-sections, huge differences between thicknesses in the middle and at the edges of the sample were noticed. The coatings exhibited body-centered cubic (bcc) structure, with the main difference is the preferred plane changes from (1 1 1) at room temperature to (2 1 1) at 65°C. Also, the coatings obtained at room temperature had very poor adhesion to the substrate, at higher temperatures the adhesion improved. So it was decided to perform deposition at 65°C for efficiency and coating adhesion stability.

Further investigation has been done using copper foams as substrates for Fe deposition. Depositions have been done under strict temperature control with constant stirring. The effects of potential and deposition length on the morphology of iron deposits have been investigated, and three potentials were chosen, for each one 5 distinct amounts of coulombs have been let through the electrochemical cell. The morphology of the iron deposits

slightly changes with the applied potentials (**Fig. 30**). At all chosen potentials for the deposition, the iron covers the whole copper foams surface.
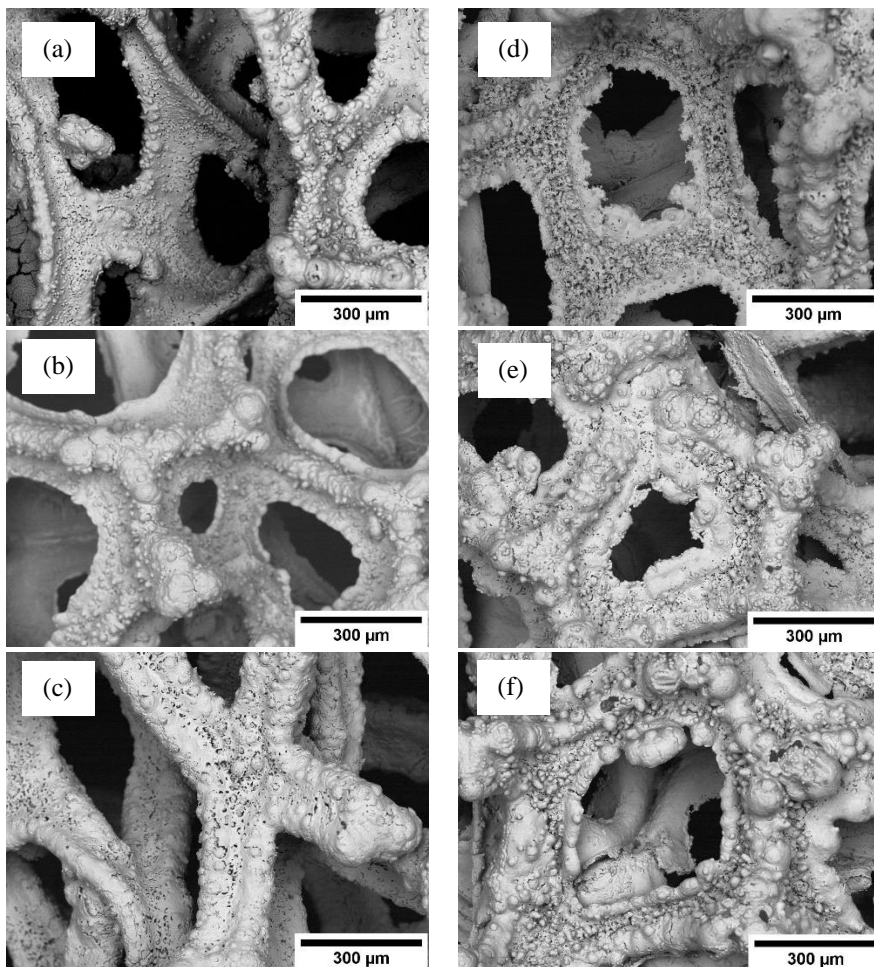
***Fig. 30**. SEM images of electrodeposited Fe under conditions: left column q = 450 C a) -1.5 V; b) -1.7 V; c) -1.9 V, right column: E = -1.9 V d) q = 150 C; e) q = 900 C ; f) q = 1350 C.*

With increasing the potential iron deposits on the surface of the substrate in dendrite-like structures. This can be seen in the (d) through (f) images where -1.9 V vs Ag/AgCl potential was applied for Fe deposition. Because of the high surface area of the copper foams at all the potentials edge effect (quicker growth and formation of almost foam-like structure) was observed. Even using quite vigorous stirring the even coverage could not be quite achieved even using the highest cathodic potential. Unevenly structured Fe deposits obtained using -1.9 V vs Ag/AgCl potential could provide even

more active sites for the Fenton reaction catalysis. With the increase of deposition time (amount of coulombs) the surface develops uneven bumps, which could even further increase the surface area, and in turn activity of the heterogeneous catalyst.

Current efficiency calculations have been made from the gravimetrical data and can be seen in **Fig. 31.** All the depositions have been repeated at least 8 times, and afterward, the current efficiency average was calculated and is shown in **Fig. 31**. As it was mentioned earlier the solution used for deposition contained Fe(III) ions as a precursor. Since these ions have higher stability, it also makes the efficiency calculations easier, under the assumption that the electrochemical deposition requires 3 electrons for the reduction of one iron ion. The overall efficiency of the deposition, regardless of the potential applied, did not exceed 30 %. The cause for this is probably adsorption of the organic matter on the working electrode, effectively blocking the surface of the electrode. According to Belevski et al. anode material also plays an important role in the efficiency of reaction, since it can facilitate the oxidation of citric and glycolic acids, which can later adsorb onto the working electrode [136, 137].
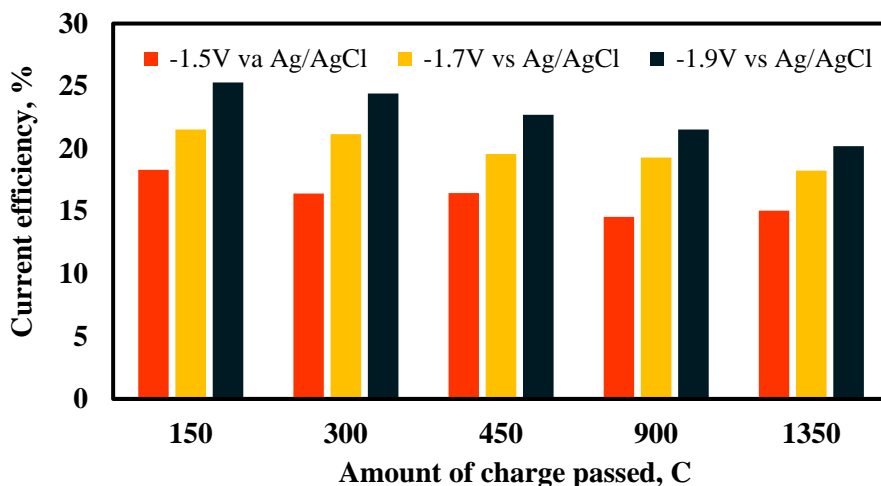
Fig. 31. *The efficiency of Fe (III) electrochemical deposition dependence on the applied potential and the amount of charge passed through the electrochemical cell.*

Nevertheless, the current efficiency is acceptable, since three electrons transfer is required for the iron deposition, and the use of a working electrode with complex geometry, makes the reduction bit more complex than with the simple Fe deposition. With the increase of applied potential, there is a noticeable increase in the current efficiency. At low potentials, the

current density is quite low, and the iron is heavily complexed (citrates and glycolates) hence the deposition is quite slow, and there is not enough energy to cover all of the foam's surface equally (can be seen from SEM images). With increased potential and vigorous mixing, the deeper levels of the foam get enough electrons to flow through them to reduce adsorbed iron species on their surface.

As the deposition time increases, the deposition efficiency drops regardless of the applied potential. The cause for this decrease probably is vigorous mixing. The flow of the solution breaks apart the dendrite-like structure. The drop in efficiency when comparing different deposition times at -1.5 V vs Ag/AgCl is quite small only around 3 %. Because of the low deposition rate, the surface iron forms are quite smooth, hence the efficiency loss is quite small. However, when the potential is increased, the current efficiency drop with longer depositions becomes significant. The morphology of iron deposits at -1.9 V vs Ag/AgCl becomes foam-like (foam formation on the copper foam), and the moving electrolyte solution inside of the copper foams' pores destroys this less mechanically stable structure. The drop of the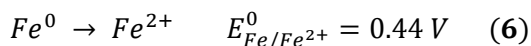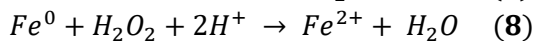 current efficiency, when comparing shortest and longest deposition times, becomes around 5 % and is significant since the overall deposition efficiency at max is approx. 25%.

3.4.2. Fenton reaction mechanism using heterogeneous catalysts

The typical Fenton reaction simply involves Fe(II) ions acting as catalysts in the degradation of hydrogen peroxide, forming the highly oxidizing OH• radicals. Since there are quite a few possible reactions taking place at the same time, the full Fenton reaction mechanism is still disputed to this day [111]. Two main pathways have been proposed – the Hauber – Weiss mechanism (which involves the participation of free radicals in the reaction mechanism) and the Kremer – Stein mechanism (ionic mechanism involving species like FeO^{2+} / Fe(IV) ions) [113, 114]. In this case, we chose to follow the Hauber – Weiss mechanism. Also since with involved heterogeneous surface, the possibility of other various heterogeneous and homogeneous reactions taking place are very high, making the overall mechanism very complex.

The first three reactions show the reactions that can occur on the iron surface and near-surface area in acidic solutions, and also in the presence of hydrogen peroxide:

$$Fe^0 \rightarrow Fe^{2+} \qquad E^0_{Fe/Fe^{2+}} = 0.44\,V \qquad (6)$$

$$Fe^0 + 2H^+ \rightarrow Fe^{2+} + H_2 \qquad (7)$$
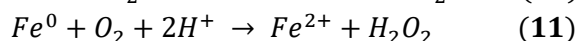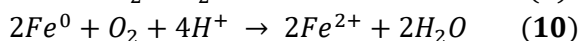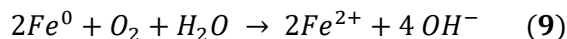$$Fe^0 + H_2O_2 + 2H^+ \rightarrow Fe^{2+} + H_2O \quad (8)$$
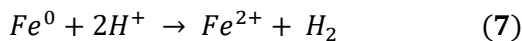
Iron corrosion occurs quickly and easily in acidic solutions. The high surface area copper foams covered with iron have a very large accessible surface area, hence in our case, the corrosion rate is very high.

The dissolved gasses (like CO_2 and O_2) in actual dyeing solutions are not removed by bubbling inert gas or using other methods. Since oxygen is dissolved in the aqueous solution few other corrosion reactions could also take place:

$$2Fe^0 + O_2 + H_2O \rightarrow 2Fe^{2+} + 4\,OH^- \qquad (9)$$
$$2Fe^0 + O_2 + 4H^+ \rightarrow 2Fe^{2+} + 2H_2O \qquad (10)$$
$$Fe^0 + O_2 + 2H^+ \rightarrow Fe^{2+} + H_2O_2 \qquad (11)$$

On the heterogeneous surface, the regeneration of the very active Fe^{2+} ions can also take place, where the hydrogen peroxide can directly oxidize the iron's surface:

$$Fe^{3+} + Fe^0 \rightarrow 2Fe^{2+} \quad \Delta E^0 = 0.77\,V \qquad (12)$$
$$Fe^0 + H_2O_2 \rightarrow Fe^{2+} + 2OH^- \qquad (13)$$
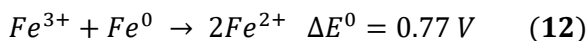
All the above-mentioned reactions are just a few possible sources of Fe(II) ions. As can be seen, there are quite a few pathways for Fe(II) to form in the solution when using heterogeneous surfaces and solutions with dissolved oxygen in them. The source of the Fe(II) ions is important, because the reaction producing highly active hydroxyl radicals, has a much higher reaction rate constant with the Fe(II) ions in homogenous Fentons reaction, than that of the Fe(III) ions [120]. There are several most important rate-determining reactions in organics breakdown:

$$Fe^{2+} + H_2O_2 \rightarrow Fe^{3+} + OH^- + \cdot OH \qquad 40-80\,M^{-1}s^{-1} \quad (14)$$
$$Fe^{3+} + H_2O_2 \rightarrow Fe^{2+} + H^+ + \cdot HO_2 \qquad 9.1 \cdot 10^{-7}M^{-1}s^{-1} \quad (15)$$
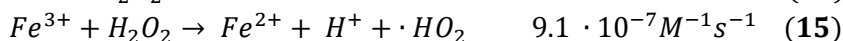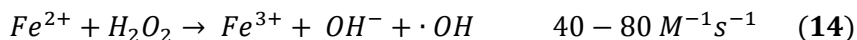
These two reactions are the sources of the two main radicals that are formed during the catalytic degradation of hydrogen peroxide. There are three main oxidating species that can be found in the solution: 1. Hydrogen peroxide (H_2O_2 $E^\circ_{vs\ NHE}$= +0.39 V), 2. Hydroperoxyl radical (OH_2 $E^\circ_{vs\ NHE}$= +1.05 V), and 3. Hydroxyl radical ($\cdot OH$ $E^\circ_{vs\ NHE}$= +2.31 V) [159]. The latter two are produced in the catalytic degradation of hydrogen peroxide involving two different iron species. The main oxidizing species are the hydroxyl radicals, since they have the highest oxidation potential, and are produced when the Fe(II) ions are involved in the catalytic breakdown of

hydrogen peroxide. Of course, some side reactions can reduce the efficiency and control the overall rate of the organics mineralization reaction, by "neutralizing" the oxidative species mentioned above:

$$Fe^{2+} + \cdot OH \rightarrow Fe^{3+} + OH^- \qquad 2.5 - 5 \cdot 10^8 M^{-1}s^{-1} \qquad (16)$$
$$Fe^{3+} + \cdot HO_2 \rightarrow Fe^{2+} + H^+ + O_2 \quad 0.33 - 2.1 \cdot 10^6 M^{-1}s^{-1} \quad (17)$$
$$Fe^{2+} + \cdot HO_2 \rightarrow Fe^{2+} + HO_2^- \qquad 0.72 - 1.5 \cdot 10^{-7} M^{-1}s^{-1} \quad (18)$$
$$\cdot OH + H_2O_2 \rightarrow H_2O + \cdot HO_2 \qquad (19)$$
$$2H_2O_2 \rightarrow 2H_2O + O_2 \qquad (20)$$
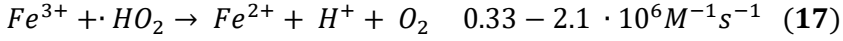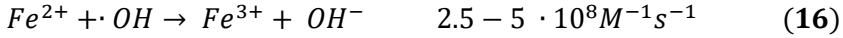
As it can be seen, the hydrogen peroxide can be considered as a hydroxyl radical scavenger, and at high enough concentrations it can react producing less active hydroperoxyl radical, which has weaker oxidating power. Also at high concentrations, the hydrogen peroxide in the acidic media can disproportionate into water and oxygen. It is very important to correctly choose appropriate concentrations of hydrogen peroxide for the Fenton reaction trying to obtain the highest mineralization rate. At too low hydrogen peroxide concentrations the full discoloration and/or mineralization cannot be fully achieved.

In our case, we also use highly porous Cu foams for substrate, and as can be seen from SEM images, the copper foam substrate is not fully covered by the iron layer, or parts of it are being uncovered with ongoing iron corrosion. This is especially the case using lower potentials and shorter deposition times. The exposed copper can also dissolve and catalyze a Fenton-like reaction [134, 160]

$$Cu^0 \rightarrow Cu^+ + e^- \qquad E^0_{Cu/Cu^+} = 0.342 \, V \qquad (21)$$

$$Cu^+ \rightarrow Cu^{2+} + e^- \qquad E^0_{Cu^+/Cu^{2+}} = 0.153 \, V \qquad (22)$$
$$Cu^0 \rightarrow Cu^{2+} + 2e^- \qquad E^0_{Cu/Cu^{2+}} = 0.521 \, V \qquad (23)$$
$$Cu^+ + H_2O_2 \rightarrow Cu^{2+} + \cdot OH + OH^- \qquad (24)$$
$$Cu^{2+} + H_2O_2 \rightarrow Cu^+ + \cdot HO_2 + OH^- \qquad (25)$$
$$Fe^{3+} + Cu^+ \rightarrow Fe^{2+} + Cu^{2+} \qquad \Delta E^0 = 0.6 \, V \qquad (26)$$
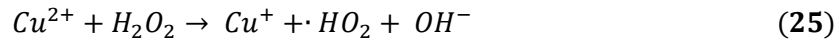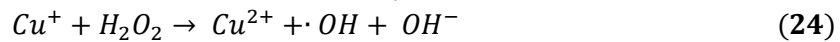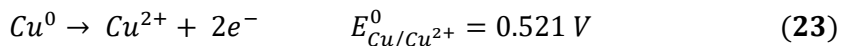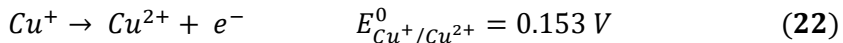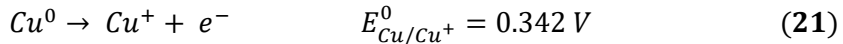
Copper can also help to decrease the concentration of Fe(III) ions by reducing them to Fe(II) ions (Eq. 26). This increases the overall efficiency and rate of the heterogeneous Fenton-like catalytic concentration. The main process - dye oxidation, can be expressed via such a simplified reaction:

$$\cdot OH + Dye \rightarrow Oxidised \, Dye + H_2O$$
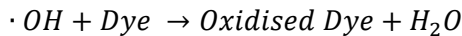
3.4.3. Investigation of heterogeneous Fenton reaction

The chosen MO solution composition and its pH for the investigation of our catalyst were not incidental. Characteristics of effluents from various processes of textiles' wet processing have been evaluated; chosen compositions and temperatures are in the range of the real conditions [161]. Usually, the Fenton process is used for the degradation of comparatively low concentrations of organic matter (up to 20 mg/L), however in this case we decided to test the capabilities of our catalyst using MO concentrations closer to the real conditions with much higher concentrations [111,161].

The discoloration speed was tracked using spectrophotometric data obtained by scanning from 620 to 320 nm region at 2 nm step. Such narrow window was chosen because the adsorption peak for MO is around 470-490 nm and is slightly dependant on the concentration of MO in the solution, and also on the pH of the solution [101]. This wavelength window was also chosen to try to prevent the solution's exposure to UV irradiation, where it could affect the catalytic degradation of hydrogen peroxide. A typical spectrophotometric measurement can be seen in **Fig. 32.**
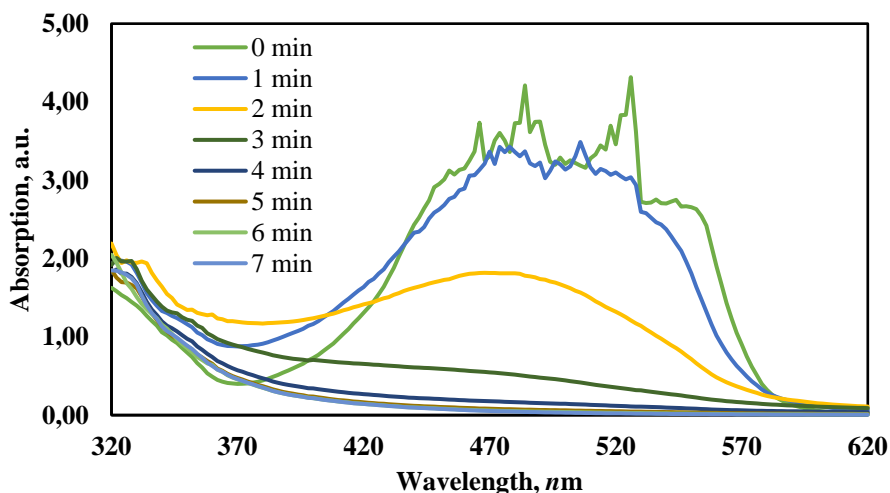
Fig. 32. Time dependence UV/Vis light absorption of 100mL of 70 mg/L MO solution during degradation at pH 3 and 30° C, with 50 µL H$_2$O$_2$. Catalyst obtained at -1.5 V vs Ag/AgCl; q = 300 C.

The chosen pH 3, was used to facilitate the iron/copper corrosion. There have been plenty of investigations, regarding Fenton catalysts activity at different pH, and it was found that optimal pH is around 2,8-3 [111,121,126]. At such a value corrosion rate is high, and the formation of insoluble iron hydroxides does not occur, hampering the activity of

mineralization. At pH < 1 the oxidation of formation of Fe(II) aqua complexes occurs, inhibiting the cleavage of H_2O_2 and formation of oxidative species.

The signal at around 480 nm can be attributed to -N=N- chromophoric bond in MO molecule. The reduction of light absorption at this wavelength is attributed to the first step in the MO mineralization pathway [126]. Hence, tracking the light absorption at this wavelength allows to easily estimate the MO degradation rate. As can be seen from **Fig. 32** the discoloration of MO solution started immediately upon immersion of the catalyst into the solution and under current conditions was complete in around 5 minutes. Since the solutions contained an unusually high concentration of organic content, the light absorption at desired wavelength window is above 1. So the spectrophotometric measurements were used as a qualitative tool to determine when the full discoloration would occur (A ≤ 0.06). Because of measurement specifics, all the discoloration times obtained have up to 30 seconds error.

3.4.4. Effect of hydrogen peroxide on Fentons reaction rate

The Fenton reaction mechanism is quite complicated, because of interdependencies between concentrations of organic matter, iron ions, and hydrogen peroxide, as well as a plethora of various reactions that might occur. To determine optimal H_2O_2 concentration at 3 chosen concentrations of MO we used a catalyst with an excessive amount of iron (obtained at -1.9 V vs Ag/AgCl q = 450 C). We chose two temperatures for tests – 30 and 40° C, examples of measurements can be seen in **Fig. 33**.

As we can see from the **inset** of **Fig. 33** a degradation reaction has the highest rate when 50 µL of H_2O_2 is used. Even adding a large surplus of H_2O_2 the rate of discoloration does not increase, meaning choosing the correct ratio is much more important. Using a too low concentration of peroxide results in either a partial discoloration of the solution or a slower discoloration and partial mineralization (10 to 30 µL in this case). The highest reaction rate was achieved using 50 µL of hydrogen peroxide.

As can be seen from the data, increasing the MO concentration to 70 and 100 mg/L, the optimal ratio between MO and hydrogen peroxide concentrations remains the same. So, for 70 mg/L MO the optimal concentration is 90 µL of 30 % v/v hydrogen peroxide, and for 100 mg/L – 120 µL. We can see a discoloration rate increase at 120 µL of hydrogen peroxide in the 70 mg/L solutions, however, almost the same reaction rate was achieved using 90 µL. Trying to save resources, the chosen amount of

hydrogen peroxide was 90 μL. As can be seen from the presented data, the experiments were performed at first testing the optimal concentration of H_2O_2 with increased MO concentration, however, the ratio was off and discoloration did not occur. So at tested MO concentrations, the ratio between MO and H_2O_2 remained the same.
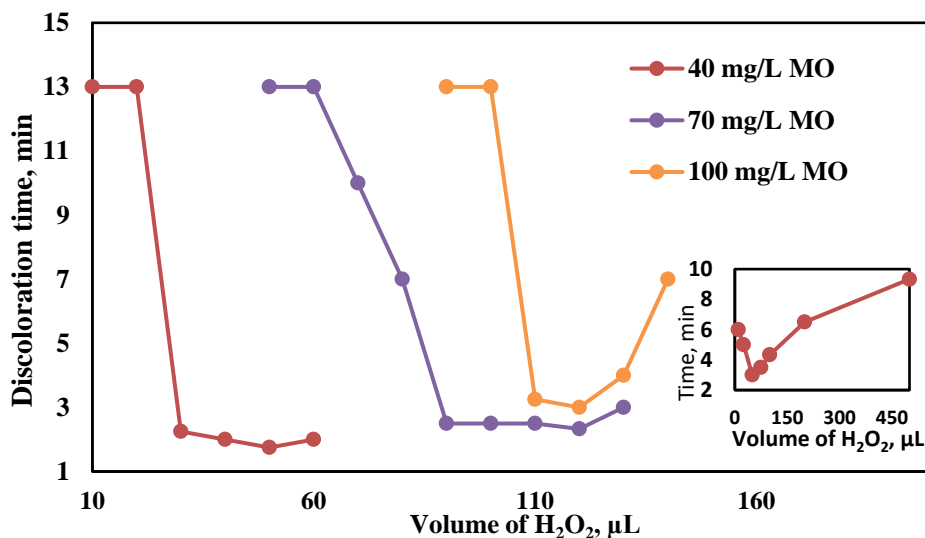
Fig. 33. Effect of H_2O_2 concentration on discoloration time at various MO concentrations at 40°C. The catalyst used for analysis was obtained at -1.9 V vs Ag/AgCl; q = 450 C. Inset shows the effect of hydrogen peroxide concentration on MO solutions discoloration time of 40 mg/L MO at 30°C.

When looking into the influence of temperature on the reaction rate at 40 mg/L MO (**Fig. 33** and its inset), it was determined that the overall rate of the reaction increases with the temperature. The optimal hydrogen concentration remains the same, namely - 50μL, but the time of discoloration from approximately 3 min at 30°C decreases to around 1 min 45 s at 40°C. This shows that the obtained ratio of hydrogen peroxide to MO works well, and at these conditions, the reaction is most likely dependant on the rate of iron corrosion.

3.4.5. The effect of Fe deposition condition on Fentons reaction rate

To evaluate the effects of the amount of deposited iron and the applied deposition potential (changes in morphology) on the heterogenous Fentons reaction rate, the catalysts have been electrochemically formed at three

distinct potentials with 5 different amounts of charge passed. The evaluation was performed at 30°C using tracking the average discoloration time of 70 mg/L MO solution (**Fig. 34**).
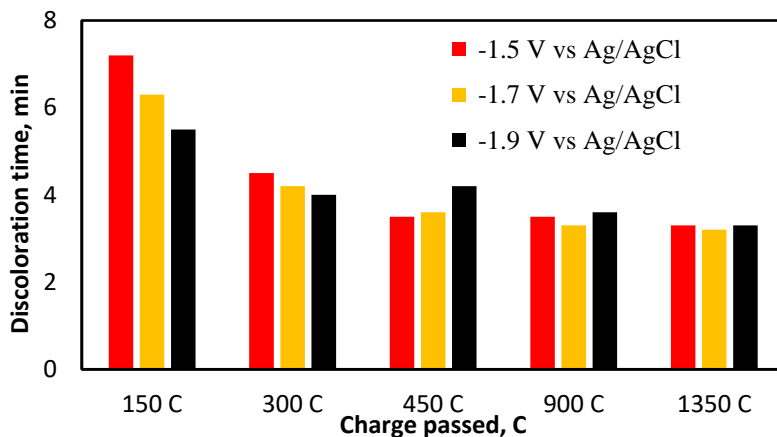
Fig. 34. *Effect of electrochemical deposition conditions (potential applied and charge passed) on discoloration time of 70 mg/L MO solution at 30°C.*

In the case of 150 C and 300 C, it can be seen that the discoloration time is dependant both on the potential and the amount of passed charge. At higher potentials, the iron layer has more bumps and almost foam-like structure, and in turn more potential active sites. This can be seen when comparing discoloration times at 150 C. However, when increasing the deposition time (charge passed) the difference, between potentials applied for deposition, disappears. There has to be a certain amount of iron deposited on the copper foam, for Fenton's reaction to proceed at a high enough rate. Since iron corrosion occurs very quickly, the layer has to be sufficient for enough Fe^{2+} ions to be produced (the first 8 reactions (**Eq. 6-13**)), Fe^{2+} ions then later participate in catalytical degradation of the hydrogen peroxide into hydroxyl radicals (**Eq. 14**). Further increasing the deposition time and amount of iron on the copper foam surface had no effect on the discoloration rate. However, increasing the amount of iron on the copper foam could reduce the mineralization efficiency, because of possible side reactions (**Eq. 16-20**). The thick iron layer also prevents Cu foam to participate in a Fenton-like reaction (**Eq. 24** and **25**) by preventing the conversion of Fe^{3+} ions into highly active Fe^{2+} ions. (**Eq. 26**).

3.4.6. The effect of MO concentration

The concentration of organic matter is also a very important parameter trying to determine the correct ratio of other constituents. Three concentrations (40, 70, and 100 mg/L) of methyl orange have been investigated, alongside the amount of deposited iron on Cu foam, and how it affects the discoloration time (**Fig. 35**). These concentrations have been chosen trying to simulate the real data [161].
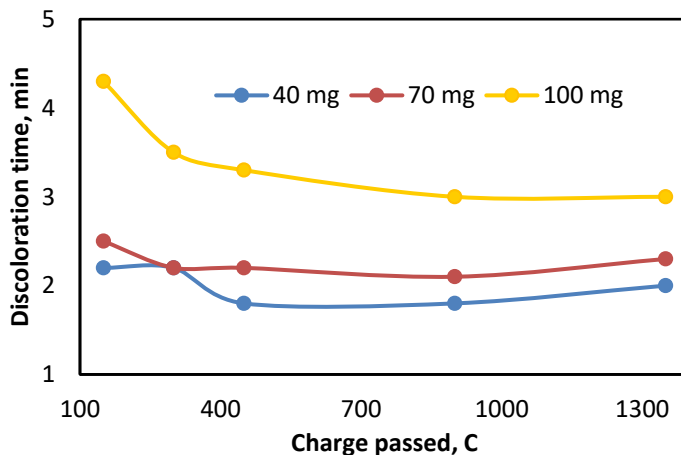
Fig. 35. Discoloration time dependence on MO concentration and catalyst deposition length (charge passed), at 40°C, 90 μL H_2O_2. The catalyst was electrochemically deposited using -1.9 V vs/AgAgCl potential.

Usually, Fentons reaction is used when the total carbon amount does not exceed 20 mg/L, but it was decided to test the capabilities of the current catalyst system using much higher concentrations. The catalyst obtained at -1.9 V vs Ag/AgCl was used because it displayed the best results at lower deposition times. As can be seen from **Fig. 35** similar dependence of discoloration time on deposition time can be seen. However, since higher concentrations of MO have been used, trying to ensure good solubility experiments were carried out at 40 °C temperature. An increase of solutions temperature also caused the speed-up of discoloration by around 3 minutes at low iron concentrations, and approx.. by 1 minute at 450 C or higher amounts of coulombs. This proves that the corrosion rate of iron on the copper foam is the limiting step.

Also, a nonlinear relationship between MO concentration and discoloration time can be seen. This could mean that at the current set up the optimal ratio between Fe^{2+}, H_2O_2, and MO concentration has not been

reached yet, and further optimization could decrease the discoloration times and increase the mineralization efficiency.

3.4.7. Temperature effects on Fenton's reaction rate

Usually, the effluents from textile wet processing facilities are from 30 to 60 °C [161]. Trying to simulate real effluents and investigate what effects temperature has on the degradations rate of methyl orange, we chose three distinct temperature values for investigation: 30,40, and 50 °C. Discoloration time was tracked at chosen temperatures, using 70 mg/L MO solution (**Fig. 36**). Judging from the previous results, catalysts obtained at -1.9 V vs Ag/AgCl potential, showed the best results even using short deposition times. Consequently, samples obtained at this potential were used for temperature effect research.

According to Lin & Lo that investigated Fenton's process in wastewater containing polyvinyl alcohol, Blue G and Black b dyes found that optimal temperature is around 30°C [162]. However, when looking at MO degradation it can be seen that the first step – cleavage of –N=N- bond, occurs faster with the increase of the temperature.
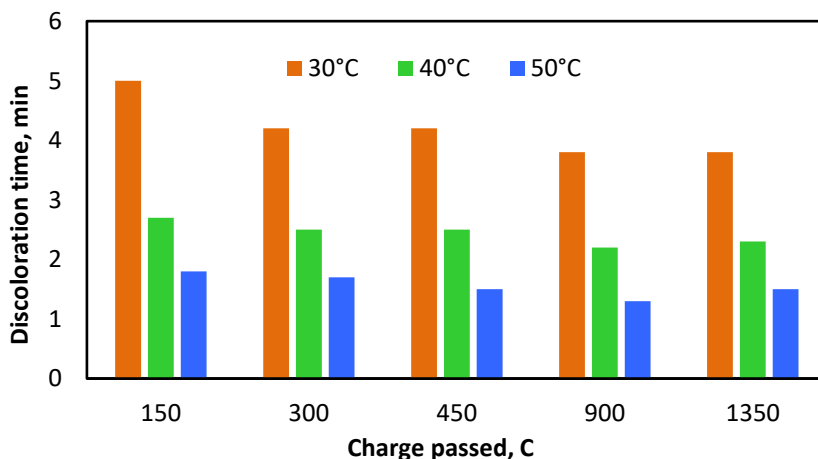
Fig. 36. Discoloration time dependence of MO solution on temperature and catalyst deposition conditions, MO concentration 70 mg/L, H_2O_2 conc. – 90 µL. The catalyst was electrochemically deposited using -1.9 V vs/AgAgCl potential.

The discoloration time difference between 30° and 50°C is almost is around 3 mins and is virtually independent of the amount of iron on the copper foam (**Fig. 36**). Using 30°C we can see that maximum efficiency is reached when 450 C has been passed during deposition. With an increase of the temperature to 40 and 50°C, even a lower amount of iron on copper foam

is enough to reach peak discoloration rate, and there is not much change with an increase of charge passed. Similar to the increase of hydrogen peroxide concentration (**Fig. 33**). This further proves that under current conditions the overall reaction rate is being controlled by the iron corrosion rate, as well as the amount of iron deposited.
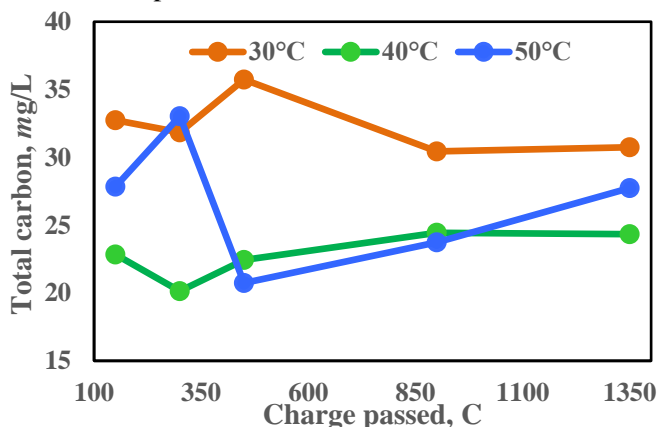
Fig. 37. *TC results dependence after 10min of degradation with immersed catalyst (obtained at -1.9 V vs Ag/AgCl) on solution temperature and amount of iron on it.*

Trying to further evaluate the efficiency of the catalyst mineralization efficiency has been investigated. The total amount of carbon left in the solution has been determined using catalyzed oxidation of all organic matter at high temperatures. As can be seen from **Fig. 37** the total MO degradation rate into carbon dioxide and water does not follow the same tendencies as discoloration rate dependence on the temperature. The mineralization efficiency peaks at 40°C (~30 % all organic matter mineralized in 10min) with all tested amounts of iron when compared to other temperatures. This could be explained that even though with increasing temperature the first degradation step – discoloration occurs the fastest, the reactions are shown in **Eq. 19-20** start to dominate. Additionally, the very active ·OH radicals are used up elsewhere.

CONCLUSIONS

1. Co and Co-Pt foams have been successfully electrodeposited using a dynamic hydrogen bubbles template and by rigorous control of the deposition conditions: bath composition, current density, the angle between the WE and counter electrode. Electrochemically active surface area is an important parameter of 3D materials, which was ~100 times higher than for 2D films. The obtained Co and Co-Pt foams showed promising catalytic activity towards HER, but the long-term stability of those catalysts should be considered. Thus, the overpotential required to reach 10 mA current was 220mV for Co and only 120 mV for Co-Pt. However, the Tafel slope was inferior for Co-Pt foam. The Co foams can also be used as catalysts for OER in alkaline media, after appropriate modifications.

2. Cobalt hexacyanoferrate formed on Co foams formed by means of cyclic voltammetry was evaluated as a sensor for detection of free chlorine in the water. The best results were obtained for modifying Co foam by scanning from 0 to -0.8 V for 40 cycles and 100 mV/s scan rate. The obtained sensor was tested at -0.45 V. It had good detection limits: the notable increase of cathodic current even at the addition of a very small amount of chlorine into the water. The calculated limit of blank solution (LOB = 1.65σ) was 3.06 ppb. The obtained limit of detection (LOD = 3σ) was 5.57 ppb and the limit of quantification (LOQ = 10σ) was 18.86 ppb. These results show great potential application for this sensor since the concentration of residual chlorine in tap water is usually between 0.2 and 1 ppm.

3. A comprehensive investigation of the electrodeposition of Cu onto 2D (plate) and 3D (foam) Cu substrates has been carried out. In order to produce an advanced 3D cathode for electrowinning. The main processes occurring on the electrode are the charge-up of double electric layer, charge transfer, and diffusion, which is the rate-determining step for Cu deposition. The electrochemically active area estimated from double electric layer capacitance data was 7–14 times higher than on the 2D electrode. Also, the charge transfer resistance on the 3D electrode was lower, which increases the charge transfer rate by ~2 times. The Cu^{2+} ions mass transfer and the Cu deposition rate is up to 3 times faster on the foam surface in comparison with a flat surface having the same geometric area in the same range of potentials.

4. Effective heterogeneous Fenton catalyst has been obtained by electrodeposition of Fe onto Cu foam. The influence of temperature, H_2O_2 concentration, deposition conditions, and dye concentration on methyl orange degradation has been investigated. The main impact on the

degradation rate has the surface area and the catalyst loading (formed deposit under given potential and charge passed). The highest discoloration rate was achieved for Fe/Cu catalysts deposited at -1.9 V (100 mg/L MO solution, V = 100 mL in 90 s). By increasing the temperature even higher discoloration rate was attained, however, the mineralization efficiency (ME) decreases. The highest ME was reached at 40°C: ~30% of all organic material degrades in 10 mins.

REFERENCES

[1] X. Li, R. Zhang, Y. Luo, Q. Liu, S. Lu, G. Chen, S. Gao, S. Chen, X. Sun, A cobalt-phosphorus nanoparticle decorated N-doped carbon nanosheet array for efficient and durable hydrogen evolution at alkaline pH, Sustain. Energy Fuels. 4 (2020) 3884–3887. https://doi.org/10.1039/d0se00240b.

[2] V.V.T. Doan-Nguyen, S. Zhang, E.B. Trigg, R. Agarwal, J. Li, D. Su, K.I. Winey, C.B. Murray, Synthesis and X-ray Characterization of Cobalt Phosphide (Co2P) Nanorods for the Oxygen Reduction Reaction, ACS Nano. 9 (2015) 8108–8115. https://doi.org/10.1021/acsnano.5b02191.

[3] C. Wang, J. Jiang, X. Zhou, W. Wang, J. Zuo, Q. Yang, Alternative synthesis of cobalt monophosphide@C core-shell nanocables for electrochemical hydrogen production, Elsevier Ltd, 2015. https://doi.org/10.1016/j.jpowsour.2015.04.002.

[4] T.F. Hung, H.C. Kuo, C.W. Tsai, H.M. Chen, R.S. Liu, B.J. Weng, J.F. Lee, An alternative cobalt oxide-supported platinum catalyst for efficient hydrolysis of sodium borohydride, J. Mater. Chem. 21 (2011) 11754–11759. https://doi.org/10.1039/c1jm11720c.

[5] N. Diab, D.M. Morales, C. Andronescu, M. Masoud, W. Schuhmann, A sensitive and selective graphene/cobalt tetrasulfonated phthalocyanine sensor for detection of dopamine, Sensors Actuators, B Chem. 285 (2019) 17–23. https://doi.org/10.1016/j.snb.2019.01.022.

[6] G. Baldi, D. Bonacchi, C. Innocenti, G. Lorenzi, C. Sangregorio, Cobalt ferrite nanoparticles: The control of the particle size and surface state and their effects on magnetic properties, J. Magn. Magn. Mater. 311 (2007) 10–16. https://doi.org/10.1016/j.jmmm.2006.11.157.

[7] G. Leofanti, M. Padovan, G. Tozzola, B. Venturelli, Surface area and pore texture of catalysts, Catal. Today. 41 (1998) 207–219. https://doi.org/10.1016/S0920-5861(98)00050-9.

[8] J. Banhart, Metal foams: Production and stability, Adv. Eng. Mater. 8 (2006) 781–794. https://doi.org/10.1002/adem.200600071.

[9] A. Bhattacharya, V. V. Calmidi, R.L. Mahajan, Thermophysical properties of high porosity metal foams, Int. J. Heat Mass Transf. 45 (2002) 1017–1031. https://doi.org/10.1016/S0017-9310(01)00220-4.

[10] J. Banhart, Manufacture, characterisation and application of cellular metals and metal foams, Prog. Mater. Sci. 46 (2001) 559–632. https://doi.org/10.1016/S0079-6425(00)00002-5.

[11] A. Angelescu, I. Kleps, M. Mihaela, M. Simion, T. Neghina, S. Petrescu, N. Moldovan, C. Paduraru, A. Raducanu, Porous silicon matrix for applications in biology, Rev. Adv. Mater. Sci. 5 (2003) 440–449.

[12] D. Van Noort, C.F. Mandenius, Porous gold surfaces for biosensor applications, Biosens. Bioelectron. 15 (2000) 203–209. https://doi.org/10.1016/S0956-5663(00)00061-0.

[13] L. Heinke, C. Wöll, Surface-Mounted Metal–Organic Frameworks: Crystalline and Porous Molecular Assemblies for Fundamental Insights and Advanced Applications, Adv. Mater. 31 (2019). https://doi.org/10.1002/adma.201806324.

[14] M.F. Ashby, A. Evans, N. a Fleck, L.J. Gibson, J.W. Hutchinson, H.N.. Wadley, Metal foams: a design guide, Mater. Des. 23 (2002) 119. https://doi.org/10.1016/S0261-3069(01)00049-8.

[15] S. Vesztergom, A. Dutta, M. Rahaman, K. Kiran, I. Zelocualtecatl Montiel, P. Broekmann, Hydrogen Bubble Templated Metal Foams as Efficient Catalysts of CO_2 Electroreduction, ChemCatChem. 13 (2021) 1039–1058. https://doi.org/10.1002/cctc.202001145.

[16] J.S. Katz, C. Zhang, M.T. Barako, H.J.K. Kim, M. Asheghi, T.W. Kenny, K.E. Goodson, Bicontinuous Mesoporous Metal Foams with Enhanced Conductivity and Tunable Pore Size and Porosity via Electrodeposition for Electrochemical and Thermal Systems, ACS Appl. Nano Mater. 3 (2020) 12408–12415. https://doi.org/10.1021/acsanm.0c02970.

[17] W. Jiang, S.S. Sundarram, W. Li, Fabrication of microcellular metal foams with sphere template electrodeposition, Manuf. Lett. 2 (2014) 118–121. https://doi.org/10.1016/j.mfglet.2014.08.001.

[18] A. Diani, K.K. Bodla, L. Rossetto, S. V. Garimella, Numerical investigation of pressure drop and heat transfer through reconstructed metal foams and comparison against experiments, Int. J. Heat Mass Transf. 88 (2015) 508–515. https://doi.org/10.1016/j.ijheatmasstransfer.2015.04.038.

[19] H.C. Shin, M. Liu, Copper foam structures with highly porous nanostructured walls, Chem. Mater. 16 (2004) 5460–5464. https://doi.org/10.1021/cm048887b.

[20] A. Inayat, H. Freund, T. Zeiser, W. Schwieger, Determining the specific surface area of ceramic foams: The tetrakaidecahedra model revisited, Chem. Eng. Sci. 66 (2011) 1179–1188. https://doi.org/10.1016/j.ces.2010.12.031.

[21] S. Cunsolo, M. Oliviero, W.M. Harris, A. Andreozzi, N. Bianco, W.K.S. Chiu, V. Naso, Monte Carlo determination of radiative properties of metal foams: Comparison between idealized and real cell structures, Int. J. Therm. Sci. 87 (2015) 94–102. https://doi.org/10.1016/j.ijthermalsci.2014.08.006.

[22] M.L. Tremblay, M.H. Martin, C. Lebouin, A. Lasia, D. Guay, 22 Determination of the real surface area of powdered materials in cavity

microelectrodes by electrochemical impedance spectroscopy, Electrochim. Acta. 55 (2010) 6283–6291. https://doi.org/10.1016/j.electacta.2009.11.006.

[23] M. Shao, J.H. Odell, S. Il Choi, Y. Xia, Electrochemical surface area measurements of platinum- and palladium-based nanoparticles, Electrochem. Commun. 31 (2013) 46–48. https://doi.org/10.1016/j.elecom.2013.03.011.

[24] E. Rouya, S. Cattarin, M.L. Reed, R.G. Kelly, G. Zangari, Electrochemical Characterization of the Surface Area of Nanoporous Gold Films, J. Electrochem. Soc. 159 (2012) K97–K102. https://doi.org/10.1149/2.097204jes.

[25] J.B. Raoof, R. Ojani, A. Kiani, S. Rashid-Nadimi, Fabrication of highly porous Pt coated nanostructured Cu-foam modified copper electrode and its enhanced catalytic ability for hydrogen evolution reaction, Int. J. Hydrogen Energy. 35 (2010) 452–458. https://doi.org/10.1016/j.ijhydene.2009.10.069.

[26] Z. Dai, A. Yang, X. Bao, R. Yang, Facile Non-Enzymatic Electrochemical Sensing, Sensors. 19 (2019) 1–13.

[27] J. Shi, Z. Ai, L. Zhang, Fe@Fe2O3 core-shell nanowires enhanced Fenton oxidation by accelerating the Fe(III)/Fe(II) cycles, Water Res. 59 (2014) 145–153. https://doi.org/10.1016/j.watres.2014.04.015.

[28] T.M. Do, J.Y. Byun, S.H. Kim, An electro-Fenton system using magnetite coated metallic foams as cathode for dye degradation, Catal. Today. 295 (2017) 48–55. https://doi.org/10.1016/j.cattod.2017.05.016.

[29] P. Abdi, A. Farzi, A. Karimi, Application of a hybrid enzymatic and photo-fenton process for investigation of azo dye decolorization on TiO2/metal-foam catalyst, J. Taiwan Inst. Chem. Eng. 71 (2017) 137–144. https://doi.org/10.1016/j.jtice.2016.11.022.

[30] W. Wan, Y. Zhang, R. Ji, B. Wang, F. He, Metal Foam-Based Fenton-Like Process by Aeration, ACS Omega. 2 (2017) 6104–6111. https://doi.org/10.1021/acsomega.7b00977.

[31] Yu, H.; Chen, H.; Pan, M.; Tang, Y.; Zeng, K.; Peng, F.; Wang, H. Effect of the metal foam materials on the performance of methanol steam micro-reformer for fuel cells. *Appl. Catal. A Gen.* **2007**, *327*, 106–113.

[32] Shahbazi, P.; Kiani, A. Fabricated Cu2O porous foam using electrodeposition and thermal oxidation as a photocatalyst under visible light toward hydrogen evolution from water. *Int. J. Hydrog. Energy* **2016**, *41*, 2–11.

[33] Liu, H.; Zeng, S.; He, P.; Dong, F.; He, M.; Zhang, Y.; Wang, S.; Li, C.; Liu, M.; Jia, L. Samarium oxide modified Ni-Co nanosheets based three-dimensional honeycomb film on nickel foam: A highly efficient electrocatalyst for hydrogen evolution reaction. *Electrochim. Acta* **2019**, *299*, 405–414.

[34] Siwek, K.I.; Eugénio, S.; Santos, D.M.F.; Silva, M.T.; Montemor, M.F. 3D nickel foams with controlled morphologies for hydrogen evolution

reaction in highly alkaline media. *Int. J. Hydrog. Energy* **2019**, *44*, 1701–1709.

[35] Dong, Y.; Sun, F.; Li, X.; Chu, M.; Li, N.; Li, X.; Wang, L.; Qu, D.; Dong, Y.; Xie, Z.; et al. A porous FeCuNi-based electrocatalyst supported by nickel foam for oxygen evolution reaction in alkaline conditions. *J. Electrochem. Soc.* **2018**, *165*, F1127–F1132.

[36] Jin, J.; Xia, J.; Qian, X.; Wu, T.; Ling, H.; Hu, A.; Li, M.; Hang, T. Exceptional electrocatalytic oxygen evolution efficiency and stability from electrodeposited NiFe alloy on Ni foam. *Electrochim. Acta* **2019**, *299*, 567–574.

[37] Pei, Y.; Ge, Y.; Chu, H.; Smith, W.; Dong, P.; Ajayan, P.M.; Ye, M.; Shen, J. Controlled synthesis of 3D porous structured cobalt-iron based nanosheets by electrodeposition as asymmetric electrodes for ultra-efficient water splitting. *Appl. Catal. B Environ.* **2019**, *244*, 583–593.

[38] Ma, Y.; Wang, H.; Feng, H.; Ji, S.; Mao, X.; Wang, R. Three-dimensional iron, nitrogen-doped carbon foams as efficient electrocatalysts for oxygen reduction reaction in alkaline solution. *Electrochim. Acta* **2014**, *142*, 317–323.

[39] Sanzó, G.; Taurino, I.; Antiochia, R.; Gorton, L.; Favero, G.; Mazzei, F.; De Micheli, G.; Carrara, S. Bubble electrodeposition of gold porous nanocorals for the enzymatic and non-enzymatic detection of glucose. *Bioelectrochemistry* **2016**, *112*, 125–131.

[40] Nam, D.-H.; Kim, R.-H.; Lee, C.-L.; Kwon, H.-S. Highly reversible Sn-Co alloy anode using porous Cu foam substrate for Li-Ion batteries. *J. Electrochem. Soc.* **2012**, *159*, A1822–A1826.

[41] Trahey, L.; Vaughey, J.T.; Kung, H.H.; Thackeray, M.M. High-capacity, microporous Cu_6Sn_5–Sn anodes for Li-ion batteries. *J. Electrochem. Soc.* **2009**, *156*, A385.

[42] Xu, J.; Ji, X.; Zhang, W.; Liu, G. Pool boiling heat transfer of ultra-light copper foam with open cells. *Int. J. Multiph. Flow* **2008**, *34*, 1008–1022.

[43] Hong, S.T.; Herling, D.R. Open-cell aluminum foams filled with phase change materials as compact heat sinks. *Scr. Mater.* **2006**, *55*, 887–890.

[44] Shin, H.C.; Dong, J.; Liu, M. Nanoporous structures prepared by an electrochemical deposition process. *Adv. Mater.* **2003**, *15*, 1610–1614.

[45] Raoof, J.B.; Ojani, R.; Kiani, A.; Rashid-Nadimi, S. Fabrication of highly porous Pt coated nanostructured Cu-foam modified copper electrode and its enhanced catalytic ability for hydrogen evolution reaction. *Int. J. Hydrog. Energy* **2010**, *35*, 452–458.

[46] Lange, G.A.; Eugénio, S.; Duarte, R.G.; Silva, T.M.; Carmezim, M.J.; Montemor, M.F. Characterisation and electrochemical behaviour of electrodeposited Cu-Fe foams applied as pseudocapacitor electrodes. *J. Electroanal. Chem.* **2015**, *737*, 85–92.

[47] Eugénio, S.; Silva, T.M.; Carmezim, M.J.; Duarte, R.G.; Montemor, M.F. Electrodeposition and characterization of nickel-copper metallic foams for application as electrodes for supercapacitors. *J. Appl. Electrochem.* **2014**, *44*, 455–465.

[48] Niu, J.; Liu, X.; Xia, K.; Xu, L.; Xu, Y.; Fang, X.; Lu, W. Effect of electrodeposition parameters on the morphology of three-dimensional porous copper foams. *Int. J. Electrochem. Sci.* **2015**, *10*, 7331–7340.

[49] Marozzi, C.A.; Chialvo, A.C. Development of electrode morphologies of interest in electrocatalysis. Part 1: Electrodeposited porous nickel electrodes. *Electrochim. Acta* **2000**, *45*, 2111–2120.

[50] Kim, J.H.; Kim, R.H.; Kwon, H.S. Preparation of copper foam with 3-dimensionally interconnected spherical pore network by electrodeposition. *Electrochem. commun.* **2008**, *10*, 1148–1151.

[51] M.A. Pasquale, D.P. Barkey, A.J. Arvia, Influence of Additives on the Growth Velocity and Morphology of Branching Copper Electrodeposits, J. Electrochem. Soc. 152 (2005) C149. doi:10.1149/1.1860514.

[52] J.J. Kim, S.K. Kim, Y.S. Kim, Catalytic behavior of 3-mercapto-1-propane sulfonic acid on Cu electrodeposition and its effect on Cu film properties for CMOS device metallization, J. Electroanal. Chem. 542 (2003) 61–66. doi:10.1016/S0022-0728(02)01450-X.

[53] Ribeiro, C.P.; Mewes, D. The effect of electrolytes on the critical velocity for bubble coalescence. Chem. Eng. J. 1993, 97, 10192–10197.

[54] S. Tension, B.C. Phenomena, A. Solutions, Surface Tension and Bubble Coalescence Phenomena, (1996) 1422–1426.

[55] Popov, K.I.; Nikolić, N.D.; Živković, P.M.; Branković, G. The effect of the electrode surface roughness at low level of coarseness on the polarization characteristics of electrochemical processes. *Electrochim. Acta* **2010**, *55*, 1919–1925. 10.1016/j.electacta.2009.10.085

[56] Miranda-Hernández, M.; González, I.; Batina, N. Silver electrocrystallization onto carbon electrodes with different surface morphology: Active sites vs surface features. *J. Phys. Chem. B* **2001**, *105*, 4214–4223. 10.1021/jp002057d

[57] Menshykau, D.; Streeter, I.; Compton, R.G. Influence of electrode roughness on cyclic voltammetry. *J. Phys. Chem. C* **2008**, *112*, 14428–14438. 10.1021/jp8047423

[58] Kostevšek, N.; Rožman, K.Ž.; Pečko, D.; Pihlar, B.; Kobe, S. 33NN A comparative study of the electrochemical deposition kinetics of iron-palladium alloys on a flat electrode and in a porous alumina template. *Electrochim. Acta* **2014**, *125*, 320–329. 10.1016/j.electacta.2014.01.115.

[59] Karimi Shervedani, R.; Lasia, A. Evaluation of the surface roughness of microporous Ni-Zn-P electrodes by in situ methods. *J. Appl. Electrochem.* **1999**, *29*, 979–986. 10.1023/A:1003577631897

[60] Gira, M.J.; Tkacz, K.P.; Hampton, J.R. Physical and Electrochemical Area Determination of Electrodeposited Ni, Co, and NiCo Thin Films. *Nano Converg.* **2015**, 1–8. 10.1186/s40580-016-0063-0

[61] Zankowski, S.P.; Vereecken, P.M. Electrochemical Determination of Porosity and Surface Area of Thin Films of Interconnected Nickel Nanowires. *J. Electrochem. Soc.* **2019**, *166*, D227–D235. 10.1149/2.0311906jes

[62] Tadros Th. F.; Lyklema J. Adsorption of potential - determining ions at the silica - aqueous electrolyte interface and the role of some cations.*Electroanalytical Chemistry and Interfacial Electrochemistry* **1968**, *17*, 267–275.

[63] Schneider, I.A.; Kramer, D.; Wokaun, A.; Scherer, G.G. Effect of inert gas flow on hydrogen underpotential deposition measurements in polymer electrolyte fuel cells. *Electrochem. commun.* **2007**, *9*, 1607–1612. 10.1016/j.elecom.2007.03.002

[64] Green, C.L.; Kucernak, A. Determination of the platinum and ruthenium surface areas in platinum-ruthenium alloy electrocatalysts by underpotential deposition of Copper. I. Unsupported catalysts. *J. Phys. Chem. B* **2002**, *106*, 1036–1047. 10.1021/jp0131931

[65] Yamaguchi, R.; Kurosu, S.; Suzuki, M. Hydroxyl radical generation by zero-valent iron/Cu (ZVI/Cu) bimetallic catalyst in wastewater treatment: Heterogeneous Fenton/Fenton-like reactions by Fenton reagents formed in-situ under oxic conditions. *Chem. Eng. J.* **2018**, *334*, 1537–1549. 10.1016/j.cej.2017.10.154

[66] Macht, F.; Eusterhues, K.; Pronk, G.J.; Totsche, K.U. Specific surface area of clay minerals: Comparison between atomic force microscopy measurements and bulk-gas (N_2) and -liquid (EGME) adsorption methods. *Appl. Clay Sci.* **2011**, *53*, 20–26. 10.1016/j.clay.2011.04.006

[67] Sharifi-Viand, A.; Mahjani, M.G.; Jafarian, M. Determination of fractal rough surface of polypyrrole film: AFM and electrochemical analysis. *Synth. Met.* **2014**, *191*, 104–112. 10.1016/j.synthmet.2014.02.021

[68] Wongmanerod, C.; Zangooie, S.; Arwin, H. Determination of pore size distribution and surface area of thin porous silicon layers by spectroscopic ellipsometry. *Appl. Surf. Sci.* **2001**, *172*, 117–125. 10.1016/S0169-4332(00)00847-3

[69] Shahbazi, P.; Kiani, A. Fabricated Cu2O porous foam using electrodeposition and thermal oxidation as a photocatalyst under visible light toward hydrogen evolution from water. *Int. J. Hydrogen Energy* **2016**, 2–11. 10.1016/j.ijhydene.2016.07.080

[70] Lange, G.A.; Eugénio, S.; Duarte, R.G.; Silva, T.M.; Carmezim, M.J.; Montemor, M.F. Characterisation and electrochemical behaviour of

electrodeposited Cu-Fe foams applied as pseudocapacitor electrodes. *J. Electroanal. Chem.* **2015**, *737*, 85–92. 10.1016/j.jelechem.2014.10.025

[71] Mattarozzi, L.; Cattarin, S.; Comisso, N.; Gerbasi, R.; Guerriero, P.; Musiani, M.; Vazquez-Gomez, L.; Verlato, E. Electrodeposition of Cu-Ni Alloy Electrodes with Bimodal Porosity and Their Use for Nitrate Reduction. *ECS Electrochem. Lett.* **2013**, *2*, D58–D60. 10.1149/2.004311eel

[72] Damian, A.; Omanovic, S. Dependance of Ni and Ni{single bond}Mo hydrogen evolution electrocatalysts electrodeposited in a polyaniline matrix. *J. Power Sources* **2006**, *158*, 464–476. 10.1016/j.jpowsour.2005.09.007

[73] Kandalkar, S.G.; Lee, H.M.; Chae, H.; Kim, C.K. Structural, morphological, and electrical characteristics of the electrodeposited cobalt oxide electrode for supercapacitor applications. *Mater. Res. Bull.* **2011**, *46*, 48–51. 10.1016/j.materresbull.2010.09.041

[74] Song, H.; Song, H.; Jung, Y.; Jung, Y.; Lee, K.; Lee, K.; Dao, L.H.; Dao, L.H. Electrochemical impedance spectroscopy of porous electrodes: the effect of pore size distribution. *Electrochim. Acta* **1999**, *44*, 3513–3519. 10.1016/S0013-4686(99)00121-8

[75] Ogihara, N.; Itou, Y.; Sasaki, T.; Takeuchi, Y. Impedance spectroscopy characterization of porous electrodes under different electrode thickness using a symmetric cell for high-performance lithium-ion batteries. *J. Phys. Chem. C* **2015**, *119*, 4612–4619. 10.1021/jp512564f

[76] Yan, B.; Li, M.; Li, X.; Bai, Z.; Dong, L.; Li, D. Electrochemical impedance spectroscopy illuminating performance evolution of porous core-shell structured nickel/nickel oxide anode materials. *Electrochim. Acta* **2015**, *164*, 55–61. 10.1016/j.electacta.2015.02.178

[77] Liu, X.; Tanaka, M.; Matsui, Y. Generation amount prediction and material flow analysis of electronic waste: A case study in Beijing, China. *Waste Manag. Res.* **2006**, *24*, 434–445. 10.1177/0734242X06067449

[78] Jain, A.; Sareen, R. E-waste assessment methodology and validation in India. *J. Mater. Cycles Waste Manag.* **2006**, *8*, 40–45. 10.1007/s10163-005-0145-2

[79] Eurostat, Statistics Explained. https://ec.europa.eu/eurostat/statistics-explained/index.php/Waste_statistics_-_electrical_and_electronic_equipment, (accessed on 22-06-2021)

[80] Vegliò, F.; Quaresima, R.; Fornari, P.; Ubaldini, S. Recovery of valuable metals from electronic and galvanic industrial wastes by leaching and electrowinning. *Waste Manag.* **2003**, *23*, 245–252. 10.1016/S0956-053X(02)00157-5

[81] Grimshaw, P.; Calo, J.M.; Hradil, G. Cyclic electrowinning/precipitation (CEP) system for the removal of heavy metal mixtures from aqueous solutions. *Chem. Eng. J.* **2011**, *175*, 103–109. 10.1016/j.cej.2011.09.062

[82] Bertuol, D.A.; Amado, F.D.R.; Veit, H.; Ferreira, J.Z.; Bernardes, A.M. Recovery of Nickel and Cobalt from Spent NiMH Batteries by Electrowinning. *Chem. Eng. Technol.* **2012**, *35*, 2084–2092. 10.1002/ceat.201200283

[83] L. Chong, J. Wen, J. Kubal, F.G. Sen, J. Zou, J. Greeley, M. Chan, H. Barkholtz, W. Ding, D.J. Liu, Ultralow-loading platinum-cobalt fuel cell catalysts derived from imidazolate frameworks, Science (80-.). 362 (2018) 1276–1281. doi:10.1126/science.aau0630.

[84] A. Ashok, A. Kumar, R.R. Bhosale, F. Almomani, M.A.H. Saleh Saad, S. Suslov, F. Tarlochan, Influence of fuel ratio on the performance of combustion synthesized bifunctional cobalt oxide catalysts for fuel cell application, Int. J. Hydrogen Energy. (2019) 436–445. doi:10.1016/j.ijhydene.2018.02.111.

[85] P. Quaino, F. Juarez, E. Santos, W. Schmickler, Volcano plots in hydrogen electrocatalysis-uses and abuses, Beilstein J. Nanotechnol. 5 (2014) 846–854. doi:10.3762/bjnano.5.96..

[86] C.G. Morales-Guio, L. Liardet, X. Hu, Oxidatively Electrodeposited Thin-Film Transition Metal (Oxy)hydroxides as Oxygen Evolution Catalysts, J. Am. Chem. Soc. 138 (2016) 8946–8957. doi:10.1021/jacs.6b05196.

[87] J. Sriwannaboot, A. Kannan, N. Tantavichet, Pulse-reverse electrodeposition of Pt–Co bimetallic catalysts for oxygen reduction reaction in acidic medium, Int. J. Hydrogen Energy. 45 (2020) 7025–7035. doi:10.1016/j.ijhydene.2019.12.191.

[88] W. Li, Z.Y. Hu, Z. Zhang, P. Wei, J. Zhang, Z. Pu, J. Zhu, D. He, S. Mu, G. Van Tendeloo, Nano-single crystal coalesced PtCu nanospheres as robust bifunctional catalyst for hydrogen evolution and oxygen reduction reactions, J. Catal. 375 (2019) 164–170. doi:10.1016/j.jcat.2019.05.031.

[89] H. Bin Meng, X.F. Zhang, Y.L. Pu, X.L. Chen, J.J. Feng, D.M. Han, A.J. Wang, One-pot solvothermal synthesis of reduced graphene oxide-supported uniform PtCo nanocrystals for efficient and robust electrocatalysis, J. Colloid Interface Sci. 543 (2019) 17–24. doi:10.1016/j.jcis.2019.01.110.

[90] J.R.C. Salgado, E. Antolini, E.R. Gonzalez, Structure and activity of carbon-supported Pt - Co electrocatalysts for oxygen reduction, J. Phys. Chem. B. 108 (2004) 17767–17774. doi:10.1021/jp0486649.

[91] P. Yu, M. Pemberton, P. Plasse, PtCo/C cathode catalyst for improved durability in PEMFCs, J. Power Sources. 144 (2005) 11–20. doi:10.1016/j.jpowsour.2004.11.067.

[92] Salazar, P.; Martín, M.; García-García, F.J.; González-Mora, J.L.; González-Elipe, A.R. A novel and improved surfactant-modified Prussian

Blue electrode for amperometric detection of free chlorine in water. Sens. Actuators B Chem. 2015, 213, 116–123.

[93] Salazar, P.; Martín, M.; González-Mora, J.L.; González-Elipe, A.R. Application of prussian blue electrodes for amperometric detection of free chlorine in water samples using flow injection analysis. Talanta 2016, 146, 410–416

[94] de Tacconi, N.R.; Rajeshwar, K.; Lezna, R.O. Metal hexacyanoferrates: electrosynthesis, in situ characterization, and applications. *Chem. Mater.* **2003**, *15*, 3046–3062.

[95] Kumar, A.; Kanagare, A.; Banerjee, S.; Kumar, P.; Kumar, M.; Sudarsan, V. Synthesis of cobalt hexacyanoferrate nanoparticles and its hydrogen storage properties. *Int. J. Hydrog. Energy* **2018**, *43*, 7998–8006.

[96] Cai, C.-X.; Xue, K.-H.; Xu, S.-M. Electrocatalytic activity of a cobalt hexacyanoferrate modified glassy carbon electrode toward ascorbic acid oxidation. *J. Electroanal. Chem.* **2000**, *486*, 111–118.

[97] Hegner, F.S.; Herraiz-Cardona, I.; Cardenas-Morcoso, D.; López, N.; Galán-Mascarós, J.R.; Gimenez, S. Cobalt hexacyanoferrate on $BiVO_4$ photoanodes for robust water splitting. *ACS Appl. Mater. Interfaces* **2017**, *9*, 37671–37681.

[98] Ho, K.C.; Chen, C.Y.; Hsu, H.C.; Chen, L.C.; Shiesh, S.C.; Lin, X.Z. Amperometric detection of morphine at a Prussian blue-modified indium tin oxide electrode. *Biosens. Bioelectron.* **2004**, *20*, 3–8.

[99] Ricci, F.; Palleschi, G. Sensor and biosensor preparation, optimisation and applications of Prussian Blue modified electrodes. *Biosens. Bioelectron.* **2005**, *21*, 389–407.

[100] https://www.who.int/news-room/fact-sheets/detail/drinking-water

[101] Y. Sha, I. Mathew, Q. Cui, M. Clay, F. Gao, X.J. Zhang, Z. Gu, Rapid degradation of azo dye methyl orange using hollow cobalt nanoparticles, Chemosphere. 144 (2016) 1530–1535. https://doi.org/10.1016/j.chemosphere.2015.10.040.

[102] P. Li, Y. Song, S. Wang, Z. Tao, S. Yu, Y. Liu, Enhanced decolorization of methyl orange using zero-valent copper nanoparticles under assistance of hydrodynamic cavitation, Ultrason. Sonochem. 22 (2015) 132–138. https://doi.org/10.1016/j.ultsonch.2014.05.025.

[103] A.G. R Ananthashankar, Production, Characterization and Treatment of Textile Effluents: A Critical Review, J. Chem. Eng. Process Technol. 05 (2013) 1–18. https://doi.org/10.4172/2157-7048.1000182.

[104] K.C. Chen, J.Y. Wu, C.C. Huang, Y.M. Liang, S.C.J. Hwang, Decolorization of azo dye using PVA-immobilized microorganisms, J. Biotechnol. 101 (2003) 241–252. https://doi.org/10.1016/S0168-1656(02)00362-0.

[105] P.C. Vandevivere, R. Bianchi, W. Verstraete, Treatment and reuse of wastewater from the textile wet-processing industry: Review of emerging technologies, J. Chem. Technol. Biotechnol. 72 (1998) 289–302. https://doi.org/10.1002/(sici)1097-4660(199808)72:4<289::aid-jctb905>3.0.co;2-%23.

[106] V. Murali, S.A. Ong, L.N. Ho, Y.S. Wong, Decolorization of methyl orange using upflow anaerobic sludge blanket (UASB) reactor-An investigation of co-substrate and dye degradation kinetics, Desalin. Water Treat. 51 (2013) 7621–7630.
https://doi.org/10.1080/19443994.2013.782255.

[107] S. Tak, A. Kumar, Chlorination disinfection by-products and comparative cost analysis of chlorination and UV disinfection in sewage treatment plants: Indian scenario, Environ. Sci. Pollut. Res. 24 (2017) 26269–26278. https://doi.org/10.1007/s11356-017-0568-z.

[108] K. Dutta, S. Mukhopadhyay, S. Bhattacharjee, B. Chaudhuri, Chemical oxidation of methylene blue using a Fenton-like reaction, J. Hazard. Mater. 84 (2001) 57–71. https://doi.org/10.1016/S0304-3894(01)00202-3.

[109] W.H.. Glaze, Drinking-water treatment with ozone, Environmental Sci. Technol. 21 (1987) 224–230.
https://doi.org/10.1080/01919510208901636.

[110] H.J.H. Fenton, Oxidation of Tartatic Acid in Presence of Iron, J. Chem. Soc. Trans. 65 (1894) 899–910.

[111] M.I. Litter, An overview on Photo degradation of Methyl Orange an azo dye by zerovalent iron materials, (2017). doi:10.1515/jaots-2016-0164.

[112] S.H. Bossmann, E. Oliveros, S. Göb, S. Siegwart, E.P. Dahlen, L. Payawan, M. Straub, M. Wörner, A.M. Braun, New evidence against hydroxyl radicals as reactive intermediates in the thermal and photochemically enhanced fenton reactions, J. Phys. Chem. A. 102 (1998) 5542–5550. https://doi.org/10.1021/jp980129j.

[113] F. Haber, J. Weiss, P.R.S.L. A, The catalytic decomposition of hydrogen peroxide by iron salts, Proc. R. Soc. London. Ser. A - Math. Phys. Sci. 147 (1934) 332–351. https://doi.org/10.1098/rspa.1934.0221.

[114] V.L. Bohnson, The catalytic decomposition of hydrogen peroxide by ferric salts, J. Phys. Chem. 25 (1921) 19–54. https://doi.org/10.1021/j150208a003.

[115] K. Barbusiński, Controversy Over Fenton Mechanism, Ecol. Chem. Eng. S. 16 (2009) 347–358.

[116] S. Karthikeyan, A. Titus, A. Gnanamani, A.B. Mandal, G. Sekaran, Treatment of textile wastewater by homogeneous and heterogeneous Fenton oxidation processes, Desalination. 281 (2011) 438–445. doi:10.1016/j.desal.2011.08.019.

[117] A.I. Zárate-Guzmán, L. V. González-Gutiérrez, L.A. Godínez, A. Medel-Reyes, F. Carrasco-Marín, L.A. Romero-Cano, Towards understanding of heterogeneous Fenton reaction using carbon-Fe catalysts coupled to in-situ H2O2 electro-generation as clean technology for wastewater treatment, Chemosphere. 224 (2019) 698–706. https://doi.org/10.1016/j.chemosphere.2019.02.101.

[118] A.K. Biń, S. Sobera-Madej, Comparison of the Advanced Oxidation Processes (UV, UV/H 2O 2 and O 3) for the Removal of Antibiotic Substances during Wastewater Treatment, Ozone Sci. Eng. 34 (2012) 136–139. doi:10.1080/01919512.2012.650130.

[119] B. Kakavandi, A.A. Babaei, Heterogeneous Fenton-like oxidation of petrochemical wastewater using a magnetically separable catalyst (MNPs@C): Process optimization, reaction kinetics and degradation mechanisms, RSC Adv. 6 (2016) 84999–85011. https://doi.org/10.1039/c6ra17624k.

[120] N. Wang, T. Zheng, G. Zhang, P. Wang, A review on Fenton-like processes for organic wastewater treatment, Journal of Environmental Chemical Engineering , Biochem. Pharmacol. 4 (2016) 762–787. https://doi.org/10.1016/j.jece.2015.12.016.

[121] J. He, X. Yang, B. Men, D. Wang, Interfacial mechanisms of heterogeneous Fenton reactions catalyzed by iron-based materials: A review, JES. (2015) 1–14. https://doi.org/10.1016/j.jes.2015.12.003.

[122] L.G. Devi, S.G. Kumar, K.M. Reddy, C. Munikrishnappa, Photo degradation of Methyl Orange an azo dye by Advanced Fenton Process using zero valent metallic iron : Influence of various reaction parameters and its degradation mechanism, 164 (2009) 459–467. https://doi.org/10.1016/j.jhazmat.2008.08.017.

[123] Z. Jia, J. Kang, W.C. Zhang, W.M. Wang, C. Yang, H. Sun, D. Habibi, L.C. Zhang, Applied Catalysis B : Environmental Surface aging behaviour of Fe-based amorphous alloys as catalysts during heterogeneous photo Fenton-like process for water treatment, "Applied Catal. B, Environ. 204 (2017) 537–547. https://doi.org/10.1016/j.apcatb.2016.12.001.

[124] J. Singh, Y. Chang, J.R. Koduru, J. Yang, D.P. Singh, Rapid Fenton-like degradation of methyl orange by ultrasonically dispersed nano-metallic particles, 22 (2017) 245–254.

[125] H. Zhang, Y. Feng, Y. Cheng, M.D. Baró, A. Altube, E. García-Lecina, F. Alcaide, E. Pellicer, T. Zhang, J. Sort, Nanoporous Fe-Based Alloy Prepared by Selective Dissolution: An Effective Fenton Catalyst for Water Remediation, ACS Omega. 2 (2017) 653–662. https://doi.org/10.1021/acsomega.7b00043.

[126] U.A. Sanjidah, K. ASW, G. Fahmida, Decolorization of Methyl Orange Using Mill Scale by Photo-Fenton Reaction, Pocedia Eng. 105 (2015) 844–851. doi:10.1016/j.proeng.2015.05.100.

[127] L.G. Devi, S.G. Kumar, K.S.A. Raju, K.E. Rajashekhar, Photo-Fenton and photo-Fenton-like processes for the degradation of methyl orange in aqueous medium : Influence of oxidation states of iron, 64 (2010) 378–385. doi:10.2478/s11696-010-0011-0.

[128] G. Centi, S. Perathoner, T. Torre, M.G. Verduna, Catalytic wet oxidation with H2O2 of carboxylic acids on homogeneous and heterogeneous Fenton-type catalysts, Catal. Today. 55 (2000) 61–69. doi:10.1016/S0920-5861(99)00226-6.

[129] M.A. Fontecha-Cámara, M.A. Álvarez-Merino, F. Carrasco-Marín, M.V. López-Ramón, C. Moreno-Castilla, Heterogeneous and homogeneous Fenton processes using activated carbon for the removal of the herbicide amitrole from water, Appl. Catal. B Environ. 101 (2011) 425–430. doi:10.1016/j.apcatb.2010.10.012.

[130] J. Wang, C. Liu, L. Tong, J. Li, R. Luo, J. Qi, Y. Li, L. Wang, Iron-copper bimetallic nanoparticles supported on hollow mesoporous silica spheres: An effective heterogeneous Fenton catalyst for orange II degradation, RSC Adv. 5 (2015) 69593–69605. doi:10.1039/c5ra10826h.

[131] A.N. Pham, G. Xing, C.J. Miller, T.D. Waite, Fenton-like copper redox chemistry revisited: Hydrogen peroxide and superoxide mediation of copper-catalyzed oxidant production, J. Catal. 301 (2013) 54–64. doi:10.1016/j.jcat.2013.01.025.

[132] J. Peng, H. Shi, J. Li, L. Wang, Z. Wang, S. Gao, Bicarbonate enhanced removal of triclosan by copper(II) catalyzed Fenton-like reaction in aqueous solution, Chem. Eng. J. 306 (2016) 484–491. doi:10.1016/j.cej.2016.07.088.

[133] C. Bao, H. Zhang, L. Zhou, Y. Shao, J. Ma, Q. Wu, Preparation of copper doped magnetic porous carbon for removal of methylene blue by a heterogeneous Fenton-like reaction, RSC Adv. 5 (2015) 72423–72432. doi:10.1039/c5ra12621e.

[134] A.F. Rossi, R.C. Martins, R.M. Quinta-Ferreira, Composition effect of iron-copper composite catalysts in the fenton heterogeneous process efficiency and cooxidation synergy assessment, Ind. Eng. Chem. Res. 53 (2014) 15369–15373. doi:10.1021/ie501193x.

[135] Y. Wang, H. Zhao, G. Zhao, Iron-copper bimetallic nanoparticles embedded within ordered mesoporous carbon as effective and stable heterogeneous Fenton catalyst for the degradation of organic contaminants, Appl. Catal. B Environ. 164 (2015) 396–406. doi:10.1016/j.apcatb.2014.09.047.

[136] S.S. Belevskii, A. V. Gotelyak, S.P. Yushchenko, A.I. Dikusar, Electrodeposition of Nanocrystalline Fe—W Coatings from a Citrate Bath, Surf. Eng. Appl. Electrochem. 55 (2019) 119–129. doi:10.3103/S1068375519020054.

[137] S.S. Belevskii, V. V. Danilchuk, A. V. Gotelyak, M. Lelis, S.P. Yushchenko, A.I. Dikusar, Electrodeposition of Fe–W Alloys from Citrate Bath: Impact of Anode Material, Surf. Eng. Appl. Electrochem. 56 (2020). doi:10.3103/S1068375520010020.

[138] A. Nicolenco, N. Tsyntsaru, J. Fornell, E. Pellicer, J. Reklaitis, D. Baltrunas, H. Cesiulis, J. Sort, Mapping of magnetic and mechanical properties of Fe-W alloys electrodeposited from Fe(III)-based glycolate-citrate bath, Mater. Des. 139 (2018) 429–438. doi:10.1016/j.matdes.2017.11.011.

[139] X. Zhang, J. Dong, Z. Hao, W. Cai, F. Wang, Fe – Mn / MCM - 41 : Preparation , Characterization , and Catalytic Activity for Methyl Orange in the Process of Heterogeneous Fenton Reaction, Trans. Tianjin Univ. 24 (2018) 361–369. doi:10.1007/s12209-018-0122-1.

[140] N.E. Séverin, S.E. Aimé, D. Donourou, B.O. Diby, M.Y. Jocelin, Catalytic activity of using tungsten oxide with hydrogen peroxide for methyl orange degradation, African J. Pure Appl. Chem. 14 (2020) 69–80. https://doi.org/10.5897/ajpac2019.0827.

[141] Nam, D.; Kim, R.; Han, D.; Kim, J.; Kwon, H. Effects of (NH4)2SO4 and BTA on the nanostructure of copper foam prepared by electrodeposition. *Electrochim. Acta* **2011**, *56*, 9397–9405. 10.1016/j.electacta.2011.08.025

[142] Berkh, O.; Shacham-Diamand, Y.; Gileadi, E. Reduction of ammonium ion on Pt electrodes. J. Electrochem. Soc. 2008, 155, F223.

[143] Tsyntsaru, N.; Cesiulis, H.; Pellicer, E.; Celis, J.P.; Sort, J. Structural, magnetic, and mechanical properties of electrodeposited cobalt-tungsten alloys: Intrinsic and extrinsic interdependencies. Electrochim. Acta 2013, 104, 94–103.

[144] Liu, X.; Wu, N.; Zhou, P.; Bi, N.; Or, S.W.; Cui, C.; Sun, Y. Large scale synthesis of superparamagnetic face-centered cubic Co/C nanocapsules by a facile hydrothermal method and their microwave absorbing properties. Mater. Res. 2015, 18, 756–762.

[145] Liu, B.H.; Li, Z.P.; Suda, S. Nickel- and cobalt-based catalysts for hydrogen generation by hydrolysis of borohydride. J. Alloy. Compd. 2006, 415, 288–293.

[146] Staszak-Jirkovský, J.; Malliakas, C.D.; Lopes, P.P.; Danilovic, N.; Kota, S.S.; Chang, K.-C.; Genorio, B.; Strmcnik, D.; Stamenkovic, V.R.; Kanatzidis, M.G.; et al. Design of active and stable Co–Mo–Sx chalcogels as pH-universal catalysts for the hydrogen evolution reaction. Nat. Mater. 2015, 15, 197–203.

[147] Lupi, C.; Dell'Era, A.; Pasquali, M. Nickel-cobalt electrodeposited alloys for hydrogen evolution in alkaline media. Int. J. Hydrog. Energy 2009, 34, 2101–2106.

[148] Mulder, W.; Sluyters, J.; Pajkossy, T.; Nyikos, L. Tafel current at fractal electrodes: Connection with admittance spectra. J. Electroanal. Chem. Interfacial Electrochem. 1990, 285, 103–115.

[149] Łosiewicz, B.; Budniok, A.; Rówiński, E.; Łągiewka, E.; Lasia, A. Effect of heat-treatment on the mechanism and kinetics of the hydrogen evolution reaction on Ni-P + TiO2 + Ti electrodes. J. Appl. Electrochem. 2004, 34, 507–516.

[150] Damian, A.; Omanovic, S. Ni and nimo hydrogen evolution electrocatalysts electrodeposited in a polyaniline matrix. J. Power Sources 2006, 158, 464–476.

[151] Łosiewicz, B.; Budniok, A.; Rówiński, E.; Łagiewka, E.; Lasia, A. The structure, morphology and electrochemical impedance study of the hydrogen evolution reaction on the modified nickel electrodes. Int. J. Hydrog. Energy 2004, 29, 145–157.

[152] Cheng, C.Y.; Kelsall, G.H. Models of hypochlorite production in electrochemical reactors with plate and porous anodes. J. Appl. Electrochem. 2007, 37, 1203–1217

[153] Kaufmann, B.Y.K. Transfer function simulation for electrochemical impedance spectroscopy (EIS). Rev. Colomb. Fis. 2005, 37, 25–27.

[154] Mahato, N.; Singh, M.M. Investigation of passive film properties and pitting resistance of AISI 316 in aqueous ethanoic acid containing chloride ions using electrochemical impedance spectroscopy(EIS). Port. Electrochim. Acta 2011, 29, 233–251.

[155] Hsu, C.H.; Mansfeld, F. concerning the conversion of the constant phase element parameter Y0 into a capacitance. Corrosion 2001, 57, 747–748.

[156] Krzewska, S. Impedance investigation of the mechanism of copper electrodeposition from acidic perchlorate electrolyte. Electrochim. Acta 1997, 42, 3531–3540.

[157] Halsey, T.C. Frequency dependence of the double-layer impedance at a rough surface. Phys. Rev. A 1987, 35, 3512–3521

[158] Hirschorn, B.; Orazem, M.E.; Tribollet, B.; Vivier, V.; Frateur, I.; Musiani, M. Determination of effective capacitance and film thickness from constant-phase-element parameters. Electrochim. Acta 2010, 55, 6218–6227.

[159] W.H. Koppenol, D.M. Stanbury, P.L. Bounds, Electrode potentials of partially reduced oxygen species, from dioxygen to water, Free Radic. Biol. Med. 49 (2010) 317–322. https://doi.org/10.1016/j.freeradbiomed.2010.04.011.

[160] Q. Zhang, Z. Zhu, P. Liu, J. Zhang, F. Cao, Corrosion Electrochemical Kinetic Study of Copper in Acidic Solution using Scanning Electrochemical Microscopy, J. Electrochem. Soc. 166 (2019) C401–C409. https://doi.org/10.1149/2.0061913jes.

[161] D.A. Yaseen, M. Scholz, Textile dye wastewater characteristics and constituents of synthetic effluents: a critical review, Springer Berlin Heidelberg, 2019. https://doi.org/10.1007/s13762-018-2130-z.

[162] S.H. Lin, C.C. Lo, Fenton process for treatment of desizing wastewater, Water Res. 31 (1997) 2050–2056. doi:10.1016/S0043-1354(97)00024-9.

ACKNOWLEDGEMENTS

This work was a real journey, so I would like to thank the people that have contributed to the work presented in this thesis. First of all, I would like to express my deep gratitude to my supervisor prof. Henrikas Cesiulis and scientific consultant associate prof. dr. Natalia Tsyntsaru who have helped me all the way, with their guidance, patience, insights, various life-changing opportunities, and splendid editorial work.

I would also like to extend my sincerest thanks to the colleagues that have helped me along the way, have listened to my concerns, the very interesting discussions, and good vibes in the workplace. I would like to thank Ramūnas for his irony and sarcasm, Edita for her sincerity and honest concern. I would also like to thank Inga, Aura, and Tomas for their overall support, ever listening to my rants, and also keep up the spirits. Special thanks to all the members of the Department of Physical Chemistry that have helped me along this journey.

I am very grateful to all the members of foreign institutions that have helped me during my research. I had the luck to work alongside some of the brightest minds in electrochemistry in the USA, Belarus, and Moldova. I wish them all the best in their personal and professional lives.

And finally, I would like to thank my family for their support during these years, their patience, and understanding. This could not be possible without them.

List of attended international conferences

1. **M.Vainoris**, N. Tsyntsaru, H. Cesiulis, Electrodeposition of Co onto Anodized W, Photoelectrochemical properties of obtained layers, 9th Nanoconference Advances in Bioelectrochemistry and Nanomaterials, Vilnius, Lithuania, 20/10/2016 – 22/10/2016. Oral presentation.
2. **M.Vainoris**, N. Tsyntsaru, H. Cesiulis, Electrodeposited cobalt foams as catalysts for water electrolysis, Open Readings 2017 60th International Conference for Students of Physics and Natural Sciences, Vilnius, Lithuania, 2017 03 14 - 2017 03 -17. Poster presentation.
3. E. Vernickaitė, **M.Vainoris**, N. Tsyntsaru, H. Cesiulis, One-step electrodeposition of cobalt foams for water electrocatalysis, ECHEMS 2017, Milano Marittima, Italy, 2017 06 06 – 2018 06 09, Oral presentation
4. **M.Vainoris**, N. Tsyntsaru, H. Cesiulis, Electrochemical deposition of Cobalt Foams for Water Electrocatalysis, 19th International Conference-School Advanced Materials and Technologies 2017, Palanga, Lithuania, 2017 08 27 - 2017 08 31. Poster presentation.
5. **M.Vainoris**, N. Tsyntsaru, H. Cesiulis, One-step electrodeposition of cobalt foams for water electrocatalysis, 10th International Nanoconference Current Trends in Electrochemistry and Material Sciences, Vilnius, Lithuania, 2017 10 24 - 2017 10 25. Oral presentation.
6. **M.Vainoris**, N. Tsyntsaru, H. Cesiulis, Electrochemical deposition of cobalt foams and investigation of deposition conditions, Open Readings 2018 61st International Conference for Students of Physics and Natural Sciences, Vilnius, Lithuania, 2018 03 20 - 2018 03 23. Poster presentation.
7. **M.Vainoris**, N. Tsyntsaru, H. Cesiulis, Electrochemical production of Cobalt Foams for detection of Free Chlorine in Water, The 32nd International Conference on Surface Modification Technologies, San Sebastian, Spain, 2018 06 27- 2018 06 29. Oral presentation
8. **M.Vainoris**, N. Tsyntsaru, H. Cesiulis, Electrochemical Synthesis of Cobalt Foams as Sensors for Chlorine Detection in water, The 69th Annual Meeting of the International Society of Electrochemistry, Bolognia, Italy, 2018 09 02 - 2018 09 07. Poster presentation.
9. **M.Vainoris**, N. Tsyntsaru, H. Cesiulis, Electrodeposited Cobalt Foams as Catalysts and Sensors for Detection of Free Chlorine in water, 9th International Conference on Materials Science and Condensed Matter Physics (MSCMP 2018), Chisinau, Moldova, 2018 09 25 - 2018 09 28. Oral presentation.

10. **M. Vainoris**, N. Tsyntsaru, E. Podlaha-Murphy, J. Sort, H. Cesiulis, Fabrication of porous Co-Pt nanowires, Open Readings 2019 62nd International Conference for Students of Physics and Natural Sciences, Vilnius, Lithuania, 2019 03 19 - 2019 03 22 Poster presentation.

11. **M. Vainoris**, N. Tsyntsaru, E. Podlaha-Murphy, J. Sort, H. Cesiulis, Template assisted electrodeposited Co-Pt nanowires for magnetic applications, The 33rd International Conference on Surface Modification Technologies, Neaples, Italy, 2019 06 23 – 2019 06 30. Poster presentation

12. A. Nicolenco, **M. Vainoris**, F. Alcaide, N. Tsyntsaru, H. Cesiulis, Fabrication of bimetallic Fe/Cu catalyst for heterogeneous Fenton process catalysis, 21st International Conference-School Advanced Materials and Technologies 2019, Palanga, Lithuania, 2019 08 19 – 2019 08 23. Poster presentation

13. A. Nicolenco, **M. Vainoris,** F. Alcaide, N. Tsyntsaru, H. Cesiulis, Electrochemical synthesis of bimetallic Fe/Cu catalyst for heterogeneous Fenton process catalysis, 9th International Conference on Nanomaterials: Applications & Properties 2019, Odesa, Ukraine, 2019 09 14 – 2019 09 21. Oral presentation.

14. **M.Vainoris**, N. Tsyntsaru, H. Cesiulis, Electrochemically deposited Iron onto Copper Foam as Catalyst for heterogeneous Fenton's reaction, Open Readings 2020 63rd International Conference for Students of Physics and Natural Sciences, Vilnius, Lithuania, 2020 03 17 - 2020 03 20. Poster presentation

15. **M.Vainoris**, N. Tsyntsaru, H. Cesiulis, Electrodeposition of Co and Co-Pt metal foams for water electrocatalysis, ECRES 2020 European Conference on Renewable Energy Systems, Istanbul, Turkey , 2020 08 24 - 2020 08 25. Oral presentation

16. **M.Vainoris**, H. Cesiulis, A. Nicolenco, N. Tsyntsaru, Electrochemically deposited Fe/Cu foam as Fenton reagent for catalytic mineralization of Methyl Orange, 29th Topical Meeting of ISE, 2021 04 18 – 2021 04 21. Oral presentation

SANTRAUKA

ĮVADAS

Šioje daktaro disertacijoje aprašytos porėtų Co ir Co-Pt sluoksnių nusodinimo ypatybės, taip pat jų savybių tyrimas, bei aptariami porėtų sluoksnių modifikavimo ypatumai. Taip pat buvo tiriamos ir komercinės Cu putos, bei tiriamos pastarųjų savybės, bei modifikavimo ir pritaikymo galimybės.

Kobaltas susilaukė daug dėmesio dėl savo puikų katalizinių savybių elektrochemiškai skaidant vandenį, ir jis galėtų būti puikia alternatyva brangiems Pt ar Ir katalizatoriams [1-4]. Kobaltas taip pat turi ir kitų įdomių cheminių bei fizinių savybių, kurios leidžia jį bei jo lydinius taikyti labai įvairiose srityse (katalizė, jutikliai, magnetiniai sluoksniai, ir t.t.). [1-6].

Katalizatoriaus ar jutiklio savitojo paviršiaus ploto padidinimas yra siektina savybė, nes paviršiaus ploto vienete padidėja aktyvių centrų skaičiaus, kur gali vykti įvairios specifinės reakcijos [7,8]. Tokiu būdu katalizinės reakcijos greitį ar jutiklio jautrumą/aktyvumą galima padidinti daugelį kartų, taip pat suteikti medžiagai neįprastų savybių (maža masė, atsparumas ugniai, magnetinės savybės, garso/vibracijų sugertis ir t.t.) [8-10]. Padidėjęs didelio paviršiaus ploto substrato aktyvumas suteikia galimybę naudoti pigesnes, lengvesnes, bet mažiau aktyvias medžiagas ar lydinius, panaudoti įvairiose srityse[8-13].

Siekiant susintetinti įvarius poringus ar tekstūruotus paviršus (metalo putos, nanolaidai, aerogeliai, ir t.t.) pastaraisiais metais atlikta nemažai tyrimų, [8-10, 14]. Daugumai poringų paviršių sintezės metodų reikalinga itin specifinė ir brangi įranga. Deja dauguma poringų paviršių sintezės metodų yra stipriai priboti elementine sudėtimi, galimu pasiekti porėtos medžiagos tankiu, porų diametrų, taipogi ar poros yra atviros ar uždaros [10, 14]. Elektrocheminio nusodinimo metodu galima susintetinti putas iš visų elektrochemiškai nusodinamų elementų, ir tai padaryti daug pigiau ir paprasčiau, taip pat lengvai reguliuojant svarbias putų savybes [15-17]. Yra du pagrindiniai būdai elektrochemiškai nusodinti metalines putas – naudojant porėtą laidų šabloną (paprastai pagamintą iš laidaus polimero ar kito metalo), arba naudoti dinaminį vandenilio burbulų šabloną. Naudojant dinaminį šabloną metalo jonai yra redukuojami tik tarp vandenilio burbulų, taip formuojant reguliuojamo tankio ir sudėties metalo putas [10,14,15]. Naudojantis šiuo šablonu galima suuformuoti metalo putas praktiškai ant bet kokio laidaus paviršiaus.

Elektrochemiškai nusodintos vario putos yra vienos daugiausiai dėmesio susilaukusių metalinių putų [15, 18, 19]. Pastaruoju metu kobaltas ir įvairūs kiti metalai nesulaukė tokio didelio tyrėjų dėmesio. Pastaruoju metu didžiausias dėmesys buvo kreipiamas į metalo putų sintezę, bet deja ne į porėtumo priklausomybę nuo nusodinimo sąlygų. Dažniausiai putos buvo naudojamos kaip šablonas electrocheminio katalizatoriaus/jutiklio formavimui, tačiau elektrochemikai aktyvus paviršiaus plotas nebūdavo tiksliai nustatomas ar bent įvertinamas.

Porėtas paviršius kelia daug iššūkių siekiant įvertinti tikrąjį paviršiaus plotą, nebūtinai naudojant elektrocheminius metodus [20,21]. Tokie metodai kaip Brunauer'io – Emett'o – Teller'io (BET) dujų kondensacija leidžia įverinti tikrąjį viso mėginio paviršiaus plotą. Deja šiuo metodu gauti rezultatai gali būti netikslūs stengiantis įvertinti katalizatoriaus aktyvumą, kuris bus įmerktas į vandeninį tirpalą, dėl skirtingų vandens ir dujų skvarbos [22]. Taigi elektrocheminiai metodai leidžia teisingiau įvertintį tikrąjį paviršiaus plotą, elektrochemiškai aktyvų paviršiaus plotą, ir net aktyvių centrų kiekį [23, 24]. Elektrocheminiai metodai taip pat leidžia modifikuoti ir tiesiogiai pritaikyti gautus porėtus sluoksnius, panaudojant juos kaip katalizatorius ar jutiklius. Tokiu būdu porėtų sluoksnių elektrocheminiai sintezės metodai tampa itin efektyvūs laiko ir kainos atžvilgiu.

Metalinės putos, turinčios atviras poras (skystis gali judėti per visą putų tūrį), yra dažniausiai naudojamos kaip itin aktyvūs katalizatoriai, juktikliai ar tiesiog įvairios membranos [3,25,26]. Tokios metalo putos gali būti lengvai modifikuojamos ir pritaikomos, pavyzdžiui Fenton'o reakcijai geležį turinčiam katalizatoriui nuotėkų vandeniui valyti. Didelio paviršiaus ploto medžiagos jau buvo tirtos kaip katalizatoriai Fentono reakcijai [27-30]. Deja daugelio šių katalizatorių negalima naudoti ilgą laiką ar tiesiog kelis kartus iš eilės, bei turi kitokių nepageidaujamų savybių (aglomeracija, prastas aktyvumas ir t.t.).

Darbo tikslas elektrochemiškai susintetinti 3D medžiagas Co pagrindu bei Cu ir Fe ir ištirti nusodinimo sąlygų (srovės tankio, tirpalo sudėties ir t.t.) įtaką jų specifiniam paviršiaus plotui, siekiant panaudoti gautas medžiagas kaip katalizatorius, jutiklius ar katodą elektroektrakcijoje.

Darbui atlikti suformuoti uždaviniai:
1. Elektrochemiškai nusodinti Co ir Co-Pt metalines putas naudojantis dinaminiu vandenilio burbulų šablonu, ir pritaikyti jas kaip katalizatorius elektrocheminiam vandens skaldymui (HER ir OER)

2. Įvertinti Co putų, modifikuotų kobalto heksacianoferatu, galimą panaudojimą laisvojo chloro jutikliui vandeniniuose tirpaluose.

3. Įvertinti plokščių ir trimačių vario elektrodų galimą pritaikymą kaip katodą vario elektroekstrakcijai.

4. Elektrochemiškai nusodinti Fe ant Cu putų naudojant draugišką gamtai elektrolitą. Pritaikyti gautas modifikuotas putas katalizei Fenton'o reakcijoje skaidant metiloranžą.

Ginamieji teiginiai:

1. Elektrochemiškai nusodintos Co ir Co-Pt trimatės struktūros su dideliu specifiniu paviršiaus plotu, gali būti pritaikytos kaip efektyvūs katalizatoriai elektrocheminiam vandens skaidymui

2. Elektrochemiškai nusodintas Co putas galima modifikuoti ant pavišiaus suformuojant kobalto heksacianoferatą. Gautos modifikuotos putos gali būti panaudotos kaip jautrus jutiklis laisvojo chloro aptikimui bei jo koncentracijos nustatymui vandenyje.

3. Trimatės vario putos gali turėti žemesnę krūvio pernašos varžą ir geresnes masės pernašos savybes. Tokios putos gali būti panaudojamos kaip itin efektyvus katodas vario elektoekstrakcijai.

4. Elektrochemiškai nusodinta geležis ant Cu putų, naudojant draugišką gamtai elektrolitą, gali būti pritaikyta kaip katalizatorius Fentono reakcijoje skaidant metiloranžą.

REZULTATAI IR JŲ APTARIMAS

3.1. Elektrocheminis Co putų nusodinimas ir nusodinimo sąlygų tyrimas.

Elektrochemiškai nusodinant bet kokias metalo putas naudojantis dinaminiu vandenilio burbulų šablonu, itin svarbu teisingai pasirinkti nusodinimo sąlygas. Šiuo metodu nusodinant metalines putas naudojami dideli srovės tankiai (paprastai 0,6 A/cm² ir daugiau), kuomet išsiskiriant dideliam vandenilio kiekiui, tarp susidarusių burbulų redukuojami metalo jonai, taip suformuojant putų sturktūrą turinčias medžiagas (1 pav. 14 psl.). Norint ištirti kiekvieno komponento įtaką, buvo naudojami keli skirtingi tirpalai putų nusodinimui.

Siekiant paprastumo buvo bandyta nusodinti kobalto putas tiesiog naudojant žemą pH ir 0,2 M $CoCl_2$ arba 0,2 M $CoSO_4$ tirpalus. Deja nepavyko suformuoti putų net naudojant didelius srovės tankius. Siekiant padidinti porėtumą, ir palaikyti pH ne tik tirpale bet ir prie substrato

paviršiaus, buvo pridėta amonio chlorido arba amonio sulfato (1 lentelė, 24 psl.). Šie junginiai gali veikti ne tik kaip ligandai, bet ir sudaryti buferį vandeniniame tirpale. Taip pat šios medžiagos puikiai veikia ir tirpalo/dujų sąlyčio riboje, turi geras vandenilio burbulų koalescencijos prevencijos savybes [53]. Šiom sąlygomis nusodintų dangų morfologija gali būti stebima SEM nuotraukos (7 pav., 31 psl). Chloridiniuose tirpaluose putos susidarė esant didesniam nei 1,8 A/cm² katodiniam srovės tankiui, o porų diametras svyravo nuo 5 iki 100 μm. Sulfatiniuose tirpaluose sluoksniai buvo daug labiau nusėti poromis, kurių diametras buvo žymiai mažesnisir siekė 5-20 μm.

Siekiant dar labiau padidinti dangų porėtumą ir pagerinti trimatę struktūrą į tirpalus buvo pridėta 2 M izopropanolio, taip sumažinant paviršiaus įtempimą. Nusodintų dangų SEM nuotraukas galite matyti 8 pav, 32 psl. Nors porų diametras labai nepasikeitė, padaugėjo didesnių porų, ir akivaizdžiai sumažėjo dangos tankis, atsirado tarpusavje sujungtų porų. Naudojant tokius didelius katodinės srovės tankius (nuo 0,6 iki 2,5 A/cm²) srovės efektyvumai buvo palyginus nedideli (9 pav., 33 psl.). Iš Rentgeno difrakcijos spektroskopijos duomenų nustatyta, kad tokiuose dideliuose srovės tankiuose kobaltas sėdo formuodamas centruotojo paviršiaus kubinę struktūrą (fcc), vietoje įprastai formuojamos – heksagoninės.

Tikrąjį paviršiaus plotą nuspręsta įvertinti naudojantis elektrocheminio impedanso spektroskopijos duomenimis (12 pav, 37 psl.). Gauti spektrai modeliuoti naudojantis ekvivalentine elektrine schema pavaizduota tame pačiame paveiksle. Iš dvigubo elektrinio sluoksnio talpos duomenų nustatyta, kad nusodintų Co putų elektrochemiškai aktyvus paviršiaus plotas buvo nuo 100 iki 200 kartų didesnis nei plokščio paviršiaus. Putos turinčios didžiausias talpas gramui nusodintos medžiagos (~10 F/g), gautos naudojantis 0,2 M $CoSO_4$, 1 M $(NH_4)_2SO_4$ ir 2 M isopropanolio tirpale ir esant 2,5 A/cm² srovės tankiui (13 pav., 38 psl.)

3.1.3. Kampo tarp darbinio ir pagalbinio elektrodų įtaka Co putų poretumui

Siekiant plačiau patyrinėti nusodinimo sąlygų įtaką porėtumui, buvo tiriama kampo tarp elektrodų įtaka. Darbinis elektrodas buvo laikomas lygiagrečiai (0° kampu), 45° arba 90° kampu platinuotu titano tinklelio elektrodo atžvilgiu. Naudojantis šiuo metodu esant 90° kampui ant apatinės elektrodo pusės jau buvo sėkmingai suformuotas itin porėtas Co sluoksnis naudojant vos 0,2 A/cm² srovės tankį (14 pav., 39 psl.). Tokiu būduvandenilio burbulai yra ilgiau sulaikomi ant substrato paviršiaus apatinėje jo pusėje, leidžiant susidaryti mažesnio tankio porėtoms dangoms.

Pastebėta, kad didinat srovės tankį, skrtumai tarp viršunės ir apatinės substrato pusių dingsta, jų porėtumai supanašėja. Taip pat buvo tirta ir izopranolio įtaka. Sumažinus paviršiaus įtempimą, srovės efektyvumas sumažėjo vos iki ~ 4 % esant dideliems srovės tankiams (15 pav., 40 psl.). Toks sumažėjimas susijęs su skysčio pabviršiaus įtempimo sumažėjimu, todėl esant 90° kampui burbulai lengviau atitrūksta nuo substrato viršaus, atlaisvindami vietą susidaryti naujiems burbuliukams.

3.2.1. Katalitinis Co ir Co-Pt putų aktyvumas elektrocheminiame vandens skaidyme šarminėje terpėje

Kaip matyti iš poliarizacinių kreivių, kobaltas ir jo junginiai pagal savo adsorbcijos energijas gali būti itin aktyvūs katalizatoriai tiek vandenilio tiek ir deguonies skyrimosi reakcijose, elektrochemiškai skaidant vandenį [85, 86]. Tad buvo nuspręsta išbandyti gautas putas kaip katalizatorius šarminėje terpėje elektrochemiškai skaidant vandenį. Kobalto putoms esančioms 1 M KOH tirpale reikėjo suteikti 220 mV viršįtampį kad vandenilio skyrimosi reakcijoje pasiektume 10 mA srovę (16 pav., 41 psl.). Taip pat kiek neįprasta buvo matyti dvi tiesines priklausomybes, kur nuolinkio kampai buvo 22 to 44 mV/dec, o antrojo - 244 to 325 mV/dec. Pirmoji stadija turbūt apsprendžiama Tafelio ar Heyrovskio reakcijos, kitaip tariant krūvio pernaša įvyksta labai greitai, greičiausiai ribojama adsorbcijos proceso. O antroji tiesinė priklausomybė gali būti priskirta Volmero reakcijai. Antroji stadija galimai atsiranda dėl susidarusių difuzijos apribojjimų, kur dėl itin didelio burrbuliavimo, tirpalas negali iki galo užpildyti porų, tad veikia tik dalis katalizatoriaus paviršiaus.

Elektrocheminė deguonies skyrimosi katalizė vykdyta naudojant Co putas, papildomai jų nemodifikuojant. Buvo siekiama oksidus bei hidroksidus suformuoti tiesiogiai ant paviršiaus potencialo skleidimo metu. Tipinės kreivės 1 M KOH tirpale pavaizduotos 17 pav. (42 psl.) Čia kad būtų pasiekta 10 mA srovė katalizatoriui reikėjo suteikti ~330mV viršįtampį. Nuolinkio kampas buvo apie 130 mV/dec. Deja tiek viršįtampis tiek nuolinkio kampas leido nustatyti, kad gautas katalizatoriaus papildomai jo nemodifikuojant yra mažai aktyvus OER katalzėje.

Siekiant pagerinti Co putų aktyvumą buvo nusodintos $Co_{97}Pt_3$ sudėties putos (18 pav., 43 psl.). Pastarosios išbandytos tik HER reakcijai katalizuoti, kadangi siekėme vienu žingsniu pagaminti puikius katalizatorius (platinos oksidus ir hidroksidus reiktų papildomai formuoti). Kaip matyti, 1 M KOH tirpale (19 pav., 44 psl.) HER reakcijai pasiekti 10 mA srovę reikėjo suteikti 120 mV viršįtampį. Taigi aktyvumas gerokai išaugo, reikėjo suteikti 100 mV

mažesnį viršįtampį nei naudojant Co putas gautas tomis pačiomis sąlygomis. Deja nuolinkio kampas pablogėjo ir tapo tarp 270 ir 310 mV/dec, ir dingo itin aktyvus pirmasis etapas, tad procesas liko valdomas krūvio pernašos. Katalizines savybes būtų galima pagerinti nusodinant plonesnes, vos kelių mikrometrų storio ar net plonesnes putas, kad vandenilio ar deguonies burbulai pilnai neužblokuotų porų. Pastebėta kad elektrochemiškai nusodintų Co ir Co-Pt putų ilgalaikis katalizinis stabilumas yra gana prastas, tai turbūt susiję su prastu mechaniniu tvirtumu, nes skiriantis vandeniliui greičiausiai yra ardoma trimatė didelio paviršiaus ploto struktūra.

3.2.2. Kobalto putų modifikavimas ir laisvojo chloro vandenyje koncentracijos nustatymas

Gautos didelio paviršiaus ploto kobalto putos buvo modifikuotos naudojantis cikline voltamperometrija potencialą skleidžiant nuo 0 iki -0,8 V pagal Ag/AgCl. Nustatyta kad skleidžiant 100 mV/s greičiu po 40 ciklų ant paviršiaus susidaręs kobalto heksacianoferatas tolygiai padengia visą paviršių (20 pav., 45 psl.). Gautos modifikuotos putos naudotos kaip jutiklis nustatyti laisvojo chloro koncentraciją vandenyje (21 pav., 46 psl.). Nustatyta, kad tuščio mėginio riba (LOB = 1.65σ) buvo 3.06 ppb, aptikimo riba (LOD = 3σ) - 5.57 ppb, o nustatymo riba (LOQ = 10σ) - 18.86 ppb. Priklausomybė nėra itin tiesinė (R² = 0.943), nes laisvojo chloro nustatymas yra gana sudėtingas, dėl junginių lakumo, tačiau pakankamas gautą jutiklį naudoti nustatant laisvąjį chlorą geriamajame vandenyje, kuriame laisvojo chloro koncentracijos yra nuo 0.2 iki 1 ppm, t.y. įprastųkoncentracijų vandenyje ribose.

Vario putų katodas

3.3.1. Vario putų charakterizavimas

Tirtos komercinės Cu putos, kurių porų dydis svyruoja nuo 0,1 iki 1 mm pavaizduotos SEM nuotraukose (22 pav., 47 psl.). Siekiant išsiaiškinti kuo šių putų savybės skiriasi nuo plokščių varinių paviršių buvo atlikeami volatmperometriniai matavimai esant įvairioms Cu koncentracijoms (2 lentelė 26psl. ir 23 pav., 48-49 psl.). Nustatyta, kad nepriklausomai nuo naudojamo substrato, vario elektrocheminis sėdimas prasidėjo ties maždaug -0,075 V pagal Ag/AgCl, o vandenilio skyrimasis prasidėjo ties maždaug -1,1 V tirpaluose, kuriuose vario koncentracijos buvo 10 ir 50 mM, o 0,2 mM

koncentracijos tirpale vandenilio skyrimasis prasidėjo ties -0,75 V vs Ag/AgCl. Nustatyta, kad naudojant Cu putų katodus, teka maždaug 3 kartus didesnės srovės, nei ant tokio paties geometrinio ploto plokščių elektrodų.

Tolesni tyrimai vykdyti naudojant 0.1 M $CuSO_4$ ir 0.4 M Na_2SO_4 tirpalą esant 4 skirtingiems potencialams −0,1, −0,2, −0,4, ir −0,6 V pagal Ag/AgCl praleidžiant fiksuotą krūvio kiekį (q = 30 C). Rezultatai pateikti 4 lentelėje 49 psl. Elektrocheminio nusodinimo efektyvumas siekė beveik 100 % naudojant tiek plokščią tiek ir porėtą substratus. Buvo pastebėta, kad naudojant Cu putų elektrodą vario nusėdimas vyko ~3 kartus greičiau nepriklausomai nuo potencialo. Kaip matyti SEM nuotraukose (24 pav., 50 psl.) naudojant pasirinktus potencialus, varis sėdo formuodamas globulių tipo kristalitų aglomeratus.

3.2.2. Vario putų paviršiaus ploto bei difuzijos greičio nustatymas

Siekinat įvertinti Cu putų papviršiaus plotą bei išsiaiškinti Cu elektrocheminio nusėdimo metu vykstančius procesus ir jų parametrus buvo atlikti EIS matavimai esant 4 skirtingiems potencialams (-0.125, -0.15, -0.175, ir -0.2 V pagal Ag/AgCl) naudojant plokščius ir poringus paviršius (25 pav., 52 ir 53 psl.). Nepriklausomai nuo paviršiaus galima išskirti dvi talpines priklausomybes nuo dažnio - tai aukšto dažnio pusapskritimis (nuo 10000 iki 100 Hz) ir 45 ° tiesė (nuo 75-100 Hz). Aukšto dažnio pusapskritimis priskiriamas dvigubo elektrinio sluoksnio užsikrovimui bei krūvio pernašai, o žemo dažnio atsakas – Cu jonų difuzijai. Ekvivalentinė schema naudota modeliavimui pateikta 25 pav., 52 psl. o gautos kiekvieno elemento vertės pateiktos 5 lentelėje, 54 psl. Lyginant dvigubo elektrinio sluoksnio vertes ant lygių ir porėtų paviršių turinčių tą patį geometrinį paviršiaus plotą (26 pav., 55 psl), galima teigti, kad poringi paviršiai turi 7-14 kartų didesnį tikrąjį paviršiaus plotą. Taip pat Cu putos turėjo 1,5-1,7 karto žemesnę krūvio pernašos varžą visame tirtų potencialų srityje, tapogi esant įvairioms vario jonų koncentracijoms, tad redukcija ant porėtų paviršių galėjo vykti daug sparčiau. Lyginant difuziją modeliuojančių elementų vertes (27 pav., 56 psl.) ant plokščių ir poringų paviršių, matyti kad CPE(W) elemento vertės yra maždaug 2,5 karto didesnės, ir puikiai dera su nusodinimo greičio skirtumu, kuris iki galo gali būti paaiškintas lengvesne krūvio pernaša ir greitesne difuzija naudojant Cu putų elektrodus.

Siekiant plačiau ištirti Cu jonų difuziją, vykstant elektrocheminiam Cu nusodinimui, difuzijos elementų vertės buvo modeliuojamos plokštiems ir porėtiems paviršiams, ir gauti duomenys lyginami su realiais (28 pav., 58 psl.). Kaip matyti bendra difuzijos varža yra 2-4 kartus didesnė naudojant

plokščius elektrodus nei varža naudojant porėtus Cu elektrodus. Taip pat iš chornopotenciometrijos duomenų (29 pav., 59 psl.) buvo nustatytos limituojančios srovės vertės ir apskaičiuoti Cu(II) jonų difuzijos koeficientai, kurie buvo ~2,5 karto didesni naudojant Cu putų elektrodus.

Elektrocheminis Fe nusodinimas ant Cu putų, bei gautų putų katalitinio aktyvumo Fenton'o reakcijoje tyrimas

3.4.1. Geležies nusodinimas ant vario putų

Geležis buvo nusodinama iš gamtai draugiško citrinų ir glikolio rūgšties Fe(III) elektrolito. Siekiant nustatyti potencialo ir nusodinimo laiko poveikį paviršiaus morfologijai buvo pasirinktos 3 potencialo vertės (-1,5 V;-1,7 V; -1,9 V pagal Ag/AgCl) praleidžiant 5 fiksuotus elektros krūvius. Morfologijos pokyčiai priklausomai nuo naudoto potencialo pavaizduoti 30 pav., 61 psl. Esant -1,5 ir -1,7 V potencialams Fe sluoksnis tiesiog atkartodavo paviršių, tačiau naudojant -1,9 V gauti sluoksniai buvo gana nelygūs, beveik formavo putas ant vario putų paviršiaus. Taip pat tirta ir srovinės išeigos priklausomybė nuo nusodinimo sąlygų (31 pav., 62 psl.). Kaip matyti naudojant neigiamesnį potencialą išeiga auga dėl itin didelio paviršiaus ploto, irne visam vario putų paviršiaus plotui tenka pakankamas krūvis vykti nusodinimui. Didinant potencialą pakanka energijos Fe nusodinimui vykti ant viso paviršiaus panašiu greičiu. Tokiu būdu gaunamų dangų storis beveik vienodas visame Cu putų paviršiuje. Taip pat ilgėjant nusodinimo laikui, srovinė išeiga mažėja, dėl vandenilio skyrimosi nusodinimo metu, ir prastesnės Fe adhezijos dėl palyginus intensyvaus maišymo, nes dalis nusėdusio Fe nubyra.

3.4.2. Fenton'o reakcijos mechaizmas vykstant heterogeninei katalizei

Įprastai Fenton'o reakciją galima aprašyti kaip katalizinį vadenilio peroksido skilimo procesą susidarant OH• radikalams, kur skilimą katalizuoja Fe(II) jonai. Egzistuoja du skilimo mechanizmo paaiškinimai: Hauber'io –Weiss'o (kuriame dalyvauja radikalai) bei Kremer'io-Stein'o mechanizmas (joninis mechanizmas, kur dalyvauja FeO^{2+} / Fe(IV) jonai) [113, 114]. Paaiškinti vykstančioms reakcijoms buvo pasirinktas Hauber'io – Weiss'o mechanizmas. Čia reakcijos greitis priklauso nuo Fe(II) jonų išsiskyrimo pagal 16 reakciją.

Taip pat reakcijoje gali dalyvauti ir Cu (24 ir 25 reakcijos), bei redukuoti Fe(III) jonus į Fentono reakcijoje daug aktyvesnius Fe(II) jonus.

3.4. Heterogeninės Fenton'o reakcijos tyrimai

Metiloranžas buvo naudojamas kaip modelinis nitro dažas. Jo skilimas buvo sekamas naudojant spektrofotometrinius matavimus nuo 620 iki 320 nm bangos ilgių ribose (32 pav., 66 psl.). Tirtas ir vandenilio peroksido kiekio poveikis MO skaidymo greičiui (33 pav., 68 psl.). Tyrimai atlikti naudojant 3 skitingas metiloranžo koncentracijas 40, 70 ir 100 mg/L, ir nustatyta, kad atitinkamoms metiloranžo koncentracijoms optimalus kiekis vandenilio peroksido atitinkamai yra 50, 90 ir 120 µl. Taip pat tirta ir Fe nusodinimo sąlygų įtaka tirpalo nuskaidrėjimo greičiui (34 pav., 69 psl.).Nustatyta kad efektyviausi buvo katalizatoriai nusodinti ties -1,9 V pagal Ag/AgCl. Pastebėta, kad reakcijai vykti optimaliu greičiu yra reikalingas minimalus kiekis nusodintos geležies, kuris gaunamas praleidus maždaug 450 C elektros kiekį per elektrocheminę celę nepriklausomai nuo potencialo.

Tiriant nusodinimo laiko ir MO koncentracijos įtaką tirpalo išblukimo greičiui (35 pav., 70 psl.) nustatyta, kad taip pat reikalingas ir minimalus katalizatoriaus kiekis ant Cu putų. Šis kiekis nusodinamas praleidus 450 C elektros kiekį esant 40 ir 70 mg/L MO koncentracijoms, tačiau esant 100 mg/L MO reikia daugiau geležies norint pasiekti didesnį greitį, būtent 900 C.

Plačiau nagrinėjant temperatūros įtaką MO skilimo reakcijos greičiui (36 pav., 71 psl.) nustatyta, kad išblukimo greitis auga keliant temperatūrą. Didžiausias skirtumas tarp 30 ir 50°C temperatūrų, kur išblukimo laiko skirtumas bendru atveju nepriklausomai nuo nusodinimo sąlygų siekė apie 3 minutes. Taip pat pastebėta, kad keliant temperatūrą mažėja nusodinimo laiko įtaka, dėl pagreitėjusios Fe korozijos. Buvo tiriama ir temperatūros įtaka metiloranžo mineralizacijos greičiui (37 pav., 72 psl.). Nustatyta, kad didžiausias efektyvumas pasiektas easnt 40°C temperatūrai, kuomet per 10 min suskaidoma ~30% visos organikos esančios tirpale. Tad nors keliant temperatūrą iki 50°C pirmasis metiloranžo skilimo žingsnis – nuskaidrėjimas ir pagreitėja, tačiau mineralizacija sulėtėja dėl vykstančių pašalinių reakcijų (19 ir 20 lygtys).

IŠVADOS

1. Co ir Co-Pt putos buvo sėkmingai elektrochemiškai nusodintos naudojantis dinaminiu vandenilio burbulų šablonu, bei kontroliuojant nusodinimo sąlygas: elektrolito sudėtį, srovės tankį, kampą tarp darbinio ir pagalbinio elektrodų. Remiantis EIS duomenimis nustatytas elektrochemiškai aktyvus paviršiaus plotas, buvo ~100 kartų didenis nei plokščių paviršių. Gautos Co ir Co-Pt putos pasižymi geru kataliziniu aktyvumu vandenilio išsiskyrimo reakcijoje, tačiau turi prastą stabilumą reakcijai vykstant ilgesnį laiką. Viršįtampis, kuris reikalingas, pasiekti 10 mA srovę vandenilio išsiskyrimo reackcijoje buvo 220 mV Co putoms ir tik 120 mV Co-Pt putoms. Co-Pt putų Tafelio nuolinkio kampas deja buvo prastesnis nei Co. Kobalto putos taip pat gali būti panaudotos OER reakcijai šarminėje terpėje po atitinkamų modifikacijų suformuojant oksidus ir /ar hidroksidus jų paviršiuje.

2. Kobalto putos modifikuotos $K_3[Fe(CN)_6]$ tirpale naudojant ciklinę voltamperometriją suformavus kobalto heksacianoferatą. Gautas modifikuotas paviršius, išbandytas kaip jutiklis, skirtas nustatyti laisvojo chloro koncentraciją vandenyje. Jautriausias jutiklis suformuotas modifikuojant Co putas naudojant ciklinę voltamperometriją, skleidžiant potencialą nuo 0 iki -0,8 V pagal Ag/AgCl 40 ciklų 100 mV/s greičiu. Gautas jutiklis toliau naudotas chronoamperometriniuose matavimuose naudojant -0,45 V potencialą (Ag/AgCl elektrodo atžvilgiu). Jutiklis turėjo palyginus geras nustatymo ir aptikimo ribas, puikų jautrumą vandenyje esant itin nedideliems laisvojo chloro kiekiams. Apskaičiuota tuščio tirpalo riba (LOB = 1.65σ) buvo 3.06 ppb. Gauta aptikimo riba (LOD = 3σ) buvo 5.57 ppb, o nustatymo riba (LOQ = 10σ) buvo 18.86 ppb. Gautas modifikuotas paviršius gali būti naudojamas kaip jutiklis laisvojo chloro koncentracijos nustatymui vandenyje, tame tarpe ir geriamajame vandenyje, kur jo koncentracija paprastai svyruoja nuo 0,2 ir 1 ppm.

3. Nuodugniai ištirtas elektrocheminis vario nusodinimas ant dvimačių (plokštelių) ir trimačių (putų) elektrodų siekiant rasti tinkamiausią paviršių panaudoti kaip katodą vario elektroekstrakcijai. Vykstant vario elektronusodinimui vyksta šie pagrindiniai procesai – dvigubo elektrinio sluoksnio užsikrovimas, krūvio pernaša ir difuzija. Pastaroji yra proceso greitį limituojanti stadija. Iš dvigubo elektrinio sluoksnio talpos verčių buvo nustatyta kad putų elektrodo talpos yra nuo 7 iki 14 kartų didesnės nei dvimačių elektrodų. Taip pat nustatyta kad trimačiai elektrodai turėjo mažesnę krūvio pernašos varžą, tad krūvio pernašos greitis padidėjo ~2 kartus. Vario (II) jonų difuzijos greitis ant Cu putų elektrodų, yra apie 3

kartus didesnis. Panašus skirtumas gautas ir tarp nusodinimo greičių naudojant skirtingos geometrijos elektrodus.

4. Elektrochemiškai nusodinus geležį ant vario putų gautas efektyvus heterogeninis katalizatorius Fenton'o reakcijai. Buvo tiriama temperatūros, H_2O_2 koncentracijos, katalizatoriaus nusodinimo sąlygų bei dažo koncentracijos įtaka metiloranžo skaidymui. Pagrindinę įtaką skaidymo greičiui darė katalizatoriaus paviršiaus plotas, bei nusodinta geležies masė. Didžiausias tirpalo nuskaidrėjimo greitis užfiksuotas naudojant Fe/Cu putų katalizatorius elektrochemiškai suformuotus esant -1,9 V įtampai (pagal Ag/AgCl elektrodą). Esant 100 mg/L MO koncentracijai tirpalas nuskaidrėjo per 90 s. Keliant tirpalo temperatūrą stebimas didesnis tirpalo išblukimo greitis, tačiau mineralizacijos efektyvumas sumažėjo. Didžiausias mineralizacijos greitis buvo pasiektas esant 40°C temperatūrai, kuomet per 10 minučių apie 30% visos organinės fazės esančios tirpale buvo suskaidyta iki CO_2 ir vandens.

Copies of published articles

ARTICLE 1

Modified Electrodeposited Cobalt Foam Coatings as Sensors for Detection of Free Chlorine in Water

M. Vainoris, N. Tsytsaru and H. Cesiulis

Coatings, **2019**, *9*(5), 306

MDPI

Article

Modified Electrodeposited Cobalt Foam Coatings as Sensors for Detection of Free Chlorine in Water

Modestas Vainoris [1], Natalia Tsyntsaru [1,2] and Henrikas Cesiulis [1,*]

[1]   Department of Physical Chemistry, Vilnius University, Naugarduko str. 24, LT-03225 Vilnius, Lithuania; m.vainoris@gmail.com (M.V.); ashra_nt@yahoo.com (N.T.)
[2]   Institute of Applied Physics, Academiei str. 5, MD-2028 Chisinau, Republic of Moldova
[*]   Correspondence: henrikas.cesiulis@chf.vu.lt

check for updates

Abstract: Metal foams offer a substantial specific surface area and sturdy frame, which makes them great candidates for various applications such as catalysts, sensors, heat sinks, etc. Cobalt and its various compounds are being considered as a cheaper alternative for precious and rare metal catalysts. The cobalt foams have been electrodeposited under galvanostatic and current pulse modes; the porous surface was created using a dynamic hydrogen bubble template. In order to obtain the highest porosity, four different solutions were tested, as well as a wide current density window (0.6–2.5 A/cm^2), in addition many different combinations of pulse durations were applied. The effects of surfactant (isopropanol) on porosity were also investigated. The morphology of obtained foams was examined by SEM coupled with EDS, and XRD spectroscopy. True surface area was estimated based on the values of a double electric layer capacitance that was extracted from EIS data. Cobalt foams were modified using $K_3[Fe(CN)_6]$ solution and cyclic voltammetry to form a cobalt hexacyanoferrate complex on the foam surface. In order to find optimal modification conditions, various potential scan rates and numbers of cycles were tested as well. Free chlorine sensing capabilities were evaluated using chronoamperometry.

Keywords: cobalt; electrodeposition; metal foams; cobalt hexacyanoferrate; free chlorine detection

1. Introduction

One of the most vital issues for the fast-growing human population is the availability of clean and safe drinking water and sanitation, which was recognized by the United Nations by putting it on their Millennium Development Goals list for the second time [1]. Water disinfection, usually the last step in a water cleaning process, helps to prevent sickness and various diseases [2,3]. Nevertheless, disinfection by-products, that form during the technological process using common disinfectants (ozone, chlorine and chlorine dioxide), can react with leftover organic materials or, bromide and iodide in the water, forming genotoxic and carcinogenic compounds [4,5].

Chlorine being the cheapest option, is usually used for residual disinfection of water and limiting pathogen growth within the water distribution system. Therefore, the monitoring and regulation of chlorine are essential [6–8]. Free chlorine concentration, which is a sum of dissolved chlorine gas, hypochlorous acid and hypochlorite anion, is usually monitored using N,N'-diethyl-p-phenylenediamine and spectrophotometric measurements [9]. In this view, electrochemical methods offer accessible, in situ measurement possibilities, that have good sensitivity and selectivity, and can be reusable and thus cheaper too. There has been quite a lot of interest in the development of diverse electrochemical chlorine sensors and electrochemical techniques [10–16].

Porous metal foams have received a great interest due to their compelling physical and chemical properties, such as high porosity, low density, good electrical, magnetic and mechanical properties, and

make an appealing material for a wide area of applications/devices: catalysis [17–23], fuel cells [24], sensors [25], batteries [26,27] and heat exchangers [28,29]. Recent studies regarding foams based on iron group metals, usually focused on an increase in the surface area of a foam (high surface area catalysts) for hydrogen [19,20,23] or oxygen [21–23] evolution reactions. Commonly, to achieve these aims modified foams are employed. The modified foams have proven to be an attractive alternative for expensive catalysts such as platinum and ruthenium dioxide, allowing to create very active asymmetric electrodes cell for water splitting [23].

Metal foams can be manufactured using different methods including electrochemical ones: either using hard (polymeric or metallic template) or dynamic hydrogen bubble template [18,20,30–32]. Dynamic hydrogen bubble template is based on the use of high current densities, and hydrogen bubbles forming on the substrate surface prevent the deposition of metal, then the metal ions are reduced only in the gaps between gas bubbles, thus leading to the development of the metal foam structure [33]. This method of metal foams production has received much attention, because of the ability to control pore size, deposits density, crystallite size and morphology. Numerous metallic foams have been deposited, however, to the best of our knowledge, no pure cobalt foams have been deposited using a dynamic hydrogen bubble template assisted electrodeposition. Usually galvanostatic, potentiostatic or pulse deposition techniques are used for metal foams production. When the pulse electrodeposition technique is used, one can still form a metallic foam, which offers both micro and nanoscale morphological templating [27,34]. Organic additives and different ions (ammonium ions, BTA, etc.) during metal foams depositions also help to control the porosity and mechanical stability [35–37]. Ligands, which can form weak complexes with cobalt ions and produce hydrogen bubbles during the cathodic reaction, can increase porosity and mechanical stability of cobalt foam's [35].

High surface area and sturdy Co foams could be applied directly or modified creating Prussian blue $Fe_4[Fe(CN)_6]_3$ like complex on the foams surface. Prussian blue and other derivatives with transition metals such as cobalt, nickel, copper etc., have been extensively investigated for many years [10,11,38–43]. Its applications vary from the detection of new molecules [43], ascorbic acid [40], morphine [42], free chlorine in water [10,11], or even used as photoanodes [41].

Thus, the objectives were: To investigate in detail the feasibility of Co foam fabrication, employing a dynamic hydrogen bubble template electrochemical formation method; to reveal the effects of bath chemistry and deposition conditions on the structure and morphology of cobalt foams; to modify foams in $K_3[Fe(CN)_6]_3$ acetate buffer solution and for the first time to apply modified surfaces as sensors for the determination of the concentrations of the free chlorine in the water.

2. Materials and Methods

Composition of electrolytes for cobalt foams deposition are presented in Table 1. All of the reagents used were of analytical grade and were used as received without further purification. All of the solutions were prepared using deionized water (DI). Electrodeposition of Co foams was performed at room temperature.

Table 1. The chemical compositions of solutions used for deposition of cobalt foams; pH 2.

Solution No	$CoCl_2$ (mol/L)	NH_4Cl (mol/L)	$CoSO_4$ (mol/L)	$(NH_4)_2SO_4$ (mol/L)	Isopropyl Alcohol (mol/L)
1	0.2	2	–	–	–
2	0.2	2	–	–	2
3	–	–	0.2	1	–
4	–	–	0.2	1	2

2.1. Surface Preparation and Deposition of Cobalt Foams

Cobalt foams were electrodeposited using a dynamic hydrogen bubble template method on copper substrate, which was used as a working electrode. The geometrical area of copper foil sheets

was 0.8 cm^2. Prior to the electrodeposition, the Cu substrate was mechanically polished, degreased in acetone and then cleaned with DI water in the ultrasonic bath. Before deposition, the native copper oxide layer was removed by dipping the substrate into 2 M H$_2$SO$_4$ solution. In order to improve adhesion of the deposits to the substrate, a Ni seed layer (~10 nm) was deposited from the solution containing 1 M NiCl$_2$ and 2.2 M HCl under galvanostatic mode (j = −12.5 mA/cm^2) for 1 min.

Two electrode cells were used for the deposition of the cobalt foams, where a circular platinized titanium mesh was used as the counter electrode. The distance between electrodes was fixed at 2.5 cm. The cobalt foams were deposited under galvanostatic or pulse deposition mode. The influence of Cl$^-$ and SO$_4{}^{2-}$ based electrolytes, of the cathodic current density (0.6–2.5 A/cm^2), of the deposition time (20–300 s) on porosity, structure and morphology of cobalt foams was evaluated.

As-deposited cobalt foams were thoroughly rinsed with DI water. Afterwards, coatings were immediately transferred into a beaker with ethanol, in order to minimize contact with the atmosphere and thus avoid oxidation of a highly active surface area of cobalt foams. The true surface area was evaluated using electrochemical impedance spectroscopy (EIS). The scans at different potentials were registered in 0.1 M Na$_2$SO$_4$ solution at four decades of frequencies (f = 10^3–0.1 Hz) using a standard three-electrode cell. The saturated Ag/AgCl electrode was used as a reference electrode. The fitting of EIS data was done using ZView software (version 2.8d). EIS measurements were performed at room temperature.

2.2. Modification of Co Foams and Detection of Free Chlorine

Cobalt hexacyanoferrate was formed using cyclic voltammetry (CV) in the same three electrodes that were set-up for EIS measurements. Cobalt foams were immersed into 0.05 M ammonium acetate buffer solution with 0.1 M KNO$_3$ and 1.5 mM of K$_3$[Fe(CN)$_6$]; the pH of the chosen buffer solution was fixed at 5.5, adjustments were made using acetic acid. All solutions were freshly prepared. CV measurements were performed at room temperature. In order to find the best conditions for foams modification (i.e., an enhanced sensitivity and longevity of a free chlorine sensor), the influence of different cycling speeds (25, 50, 100 mV/s) and count of cycles was investigated.

Chronoamperometric measurements were performed in order to determine the amount of free chlorine in water. Ca(OCl)$_2$ was used as a source of chlorine. Various amounts of Ca(OCl)$_2$ were dissolved in 0.05 M ammonium acetate buffer, containing 0.1 M KNO$_3$ as a background electrolyte. All the solutions used for chlorine detection were prepared just prior to chronoamperometric measurements. A standard three-electrode system was used during chronoamperometric measurement, with a modified cobalt foam as the working electrode. All of the measurements were performed at room temperature.

2.3. Instrumentation

The electrodeposition of Co foams coatings and other electrochemical measurements (cyclic voltammetry, chronoamperometry, EIS etc.) were performed using programmable potentiostat/galvanostat AUTOLAB PGSTAT302N (Methohm, Ultrech, The Netherlands), controlled using Nova 1.10 software. Cobalt foams morphology was characterized using scanning electron microscopes (Hitachi's Tabletop Microscope TM3000, and Hitachi's SU-70, Tokyo, Japan). Energy-dispersive X-ray Spectroscopy was used to determine the elemental surface composition of as-deposited and modified Co foams. X-ray diffractometry (XRD, Rigaku Miniflex II, Tokyo, Japan, λ = 1.5418 Å/Cu Kα, 2θ = 20°→100°, 10°/min) was used to evaluate the phase composition of obtained cobalt foams. Porosity of cobalt deposits were calculated using SEM images and Fiji image processing software (version 1.52n), considering the pores as voids and subtracting their area from the total surface area of a SEM image.

3. Results and Discussion

3.1. The Influence of Electrolyte Composition and Operating Conditions on Co Coatings Deposition

As it was shown by DoHwan Nam et al. [37] the ammonium ions played an important role in copper foams deposition, whilst using a dynamic hydrogen bubble template method. The ammonium ions in water-based solutions were in the equilibrium with NH_3:

$$NH_3 + H^+ \Leftrightarrow NH_4^+ \tag{1}$$

In our case, the solution used for depositions was acidic (pH 2), thus the equilibrium shifted towards NH_4^+. Ammonium ions can act as a ligand forming complexes with cobalt ions, but may also adsorb onto the surface of a substrate during deposition. Reduction of the adsorbed ammonium ions on the cathode leads to a decrease of the cathodic current efficiency, but also acts as an additional hydrogen source (Equation (2)), which in turn influences the porosity of the obtained coatings [44]:

$$NH_4^+ + e^- \rightarrow 0.5H_2 + NH_3 \tag{2}$$

In order to reveal the importance of ammonium ions, whilst depositing cobalt foams coatings, the ammonium-free electrolytes that contained only 0.2 M $CoCl_2$ or 0.2 M $CoSO_4$ were used. The galvanostatic deposition at various cathodic current densities (0.6–4.8 A/cm^2) and deposition times (10–180 s) were studied, but a foam-like structure was not obtained (Figure 1). The coatings were extremely uneven using both sulfate- and chloride-based electrolytes, and the jet of formed hydrogen bubbles removed most of the reduced metal from the substrate surface. Nevertheless, as it is depicted in SEM images the coatings obtained from chloride-based electrolyte had a better coverage (Figure 1a) than coatings obtained from the sulfate bath (Figure 1b) that were uneven and had micro-agglomerates on the surface. Both time and current density did not positively affect the formation of cobalt foams from the electrolytic baths.
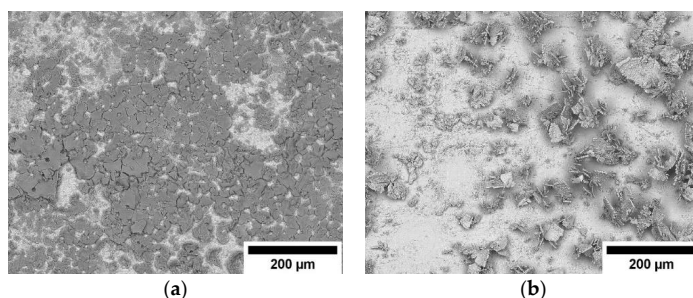

Figure 1. SEM images of Co coatings deposited under galvanostatic conditions, at cathodic current density j = 2.5 A/cm^2, deposition time t = 60 s. The composition of solutions: (**a**) 0.2 M $CoCl_2$; (**b**) 0.2 M $CoSO_4$.

The addition of ammonium ions (Figure 2) to the solutions resulted in the deposition of Co coatings riddled with cylindrically shaped pores of various sizes, but often displaying numerous defects, caused by hydrogen evolution. Coatings electrodeposited from the chloride-based solution (solution 1) had larger and irregular pores (diameter of pores was varied from 5 to 100 μm) in comparison to the sulfate-based solution, where pores size were much more uniform (diameter 5–20 μm solution 3). This fact can be explained by the higher capability of the ammonium sulfate in the suppression of hydrogen bubble coalescence compared to the ammonium chloride solutions [45].
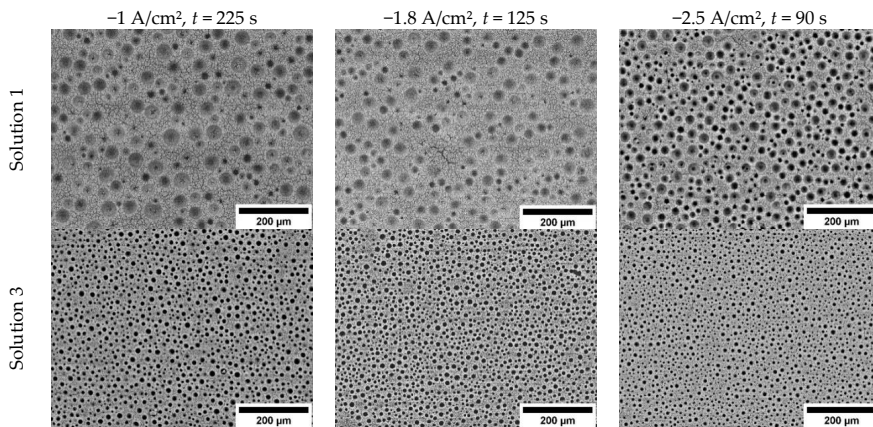
Figure 2. Scanning Electron Microscopy images of cobalt coatings obtained under a galvanostatic mode at various deposition conditions, but the same value of charge passed (q = 180 C).

The influence of the cathodic current density on the foam's formation revealed the following aspects: From the chloride-based solution, the foam-like structure was obtained only at cathodic current densities >1.8 A/cm^2 (Figure 2). The porosity of coatings obtained from solution 1 alternated dependently on the cathodic current density (q = 360 C), namely: 19% at 1 A/cm^2, 23.3% at 1.8 A/cm^2 and 21.7% at 2.5 A/cm^2. The increase in porosity from the chloride-based solution at higher cathodic current densities could be explained by the increase in the rate of a secondary reaction–hydrogen evolution reaction. As it was mentioned above, the ammonium sulfate was approximately three times better at suppressing hydrogen bubbles coalescence, and thus, the diameter of pores usually does not exceed 15 μm for foams obtained from a sulfate-based solution. Hence, the overall porosity of such foams is much lower than the ones obtained from a chloride-based solution: At −2.5 A/cm^2 porosity is ca 8.2%.

In order to evaluate the role of a surfactant on the formation of Co foams, the isopropyl alcohol was added (solutions 2 and 4), and the porosity and morphology of the growing coatings was evaluated. The isopropanol was chosen as an efficient agent to reduce the surface tension. Thus, the hydrogen bubbles formed during deposition, were able to easily detach from the surface. As it is apparent from the SEM pictures (Figure 3), the porosity of the deposits increased substantially even at comparatively low current densities of 1 A/cm^2. However, the radius of pores did not seem to be affected by the reduction of the solutions surface tension. This could be linked to the fact, that the influence of ammonium ions on hydrogen bubbles is much higher than that of isopropyl alcohol on the reduction of surface tension. The porosity of the foams obtained from the sulfate-based solutions also increased substantially with the addition of isopropyl alcohol. Thus, at a cathodic current density of 2.5 A/cm^2 the development of tridimensional cobalt foam structure can be noticed, and it is formed from interconnected cylindrical pores (Figure 3). It this case the estimation of the porosity using SEM images was rather difficult due to many interconnected pores.
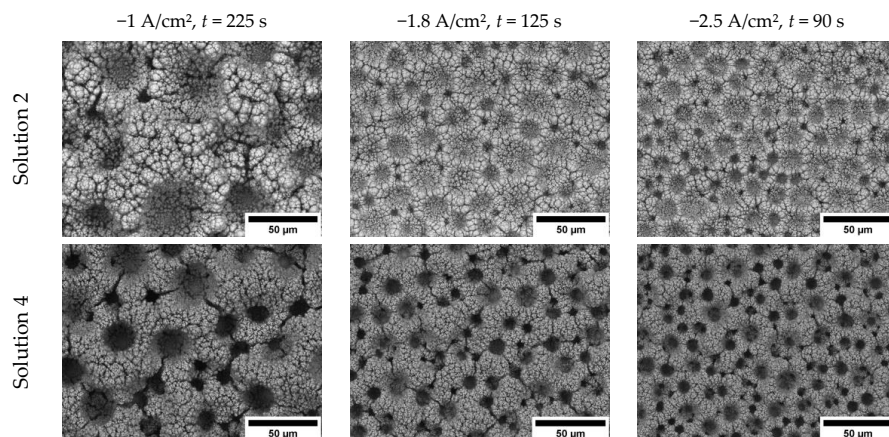
Figure 3. Scanning Electron Microscopy images of cobalt coatings obtained under a galvanostatic mode at various deposition conditions, but the same value of charge passed (q = 180 C), from solutions containing isopropyl alcohol.

The two main reactions occurring during depositions using such high current densities were reduction of cobalt ions, and reduction of water. The use of a dynamic hydrogen bubble template takes advantage of hydrogen evolution, forcing the metal ions to be reduced only in-between the hydrogen bubbles. The decrease in surface tension and easier detachment of formed bubbles resulted in an increase in the area for metal ions reduction, however cobalt is a very good catalyst for water reduction reaction, and isopropanol addition makes the water reduction reaction the dominant reaction by a huge margin. This was evident from current efficiency (CE) data (Figure 4), which was calculated using Faraday's law. The hollow figures display solutions with the isopropanol.
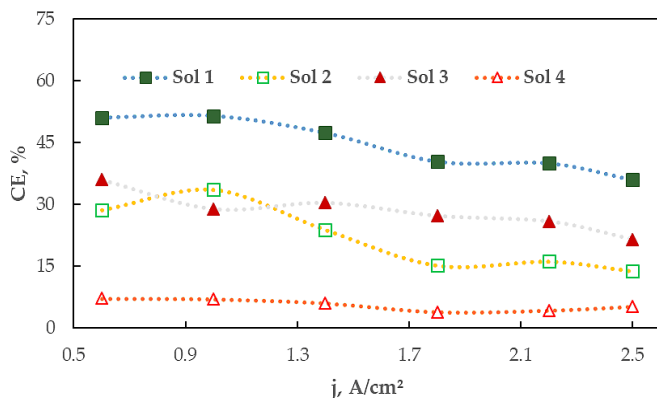

Figure 4. Influence of the cathodic current density on the current efficiency (CE) of Co coatings obtained under a galvanostatic mode and q = 180 C.

There were three clear trends for CE dependence on applied current density which were seen: (1) Increasing cathodic current density decreased the amount of deposited metal; (2) the use of sulfate based electrolytes (solutions 3 and 4) led to less deposited metal compared to chloride-based electrolytes (solutions 1 and 2); (3) the isopropyl alcohol significantly lowered CE. The first phenomenon can be explained by an increased overpotential, which in turn increased the rates of both reactions (Co and

water reduction). The cobalt ions reduction was controlled by the diffusion rate, which affected the quantity of deposited metal with increased current density. The second trend can be explained by the significantly different capabilities of hydrogen bubbles coalescence suppression. The smaller bubbles cover the surface, encumbering the diffusion of metal ions around them. The third phenomenon is caused by significant reduction of surface tension, when using isopropyl alcohol. With reduced surface tension, hydrogen bubbles detach faster, and since the reduction reaction is diffusion controlled, so HER dominates even more, hence the increase in porosity and the formation of cobalt foams.

The use of such high current densities could affect also the preferred crystallographic orientation of Co. XRD spectra (Figure 5) recorded for cobalt foams electrodeposited from solution 4 by applying various current densities showed a clear face centered cubic (fcc) structure. Usually for electrodeposited cobalt coatings the hexagonal close packing (hcp) structure is indexed [46]. The fcc structure of Co with two most intense peaks (1 1 1) and (2 0 0) are commonly obtained applying other methods [47]. Nevertheless, electrodeposited Co using high current densities formed crystalline deposits with most preferred plains (2 0 0) and (2 2 0), while the intensity of (1 1 1) was comparable to that of the (3 1 1) plane, or even less for higher cathodic current densities. That outcome could be linked to the distortion created by the evolution of hydrogen bubbles.
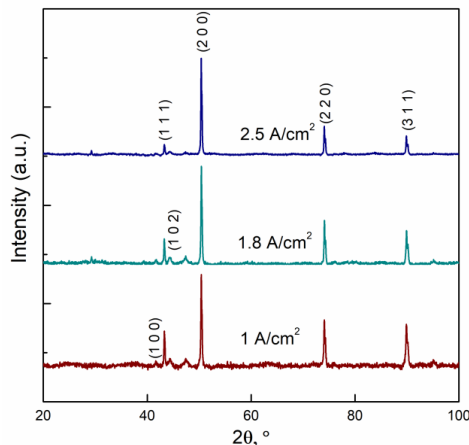

Figure 5. XRD pattern of Co foams electrodeposited from solution 4. Peaks were analyzed according to JCPDS cards No. 01-071-4238 and 01-077-7453.

3.2. The Mechanism of Co Foams Depositon and Determination of True Surface Area

As it was mentioned earlier when using the dynamic hydrogen bubble template, high current densities were applied, and deposition occurred in-between hydrogen bubbles, whilst being diffusion controlled. SEM top (Figure 3) and cross-sectional (Figure 6) images of cobalt foams, coupled with EDS data of the surface, revealed that after the initial formation of crystallization centers, intensive growth of fern-like cobalt agglomerates occurred, in such a way forming cobalt foam, leaving cylindrically-shaped pores. In the course of deposition, the radius (size) of the pores increased. Such an increase can be explained by the increase in the HER rate, caused by the exposed high surface area of the cobalt deposits, since it is well-known that cobalt is a good catalyst for the HER reaction [48–50].
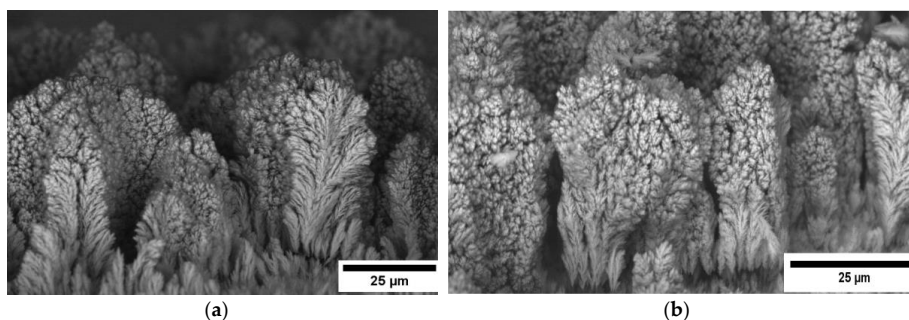
(a)   (b)

Figure 6. SEM images of cobalt foams cross-sections deposited under galvanostatic mode, from solution 4: (**a**) *j* = 1 A/cm^2, *t* = 225 s; (**b**) *j* = 2.5 A/cm^2, *t* = 90 s.

With huge differences in porosities and CE, the true surface area was estimated by electrochemical impedance spectroscopy under the assumption that the capacitance of the double electric layer of the same metal depended on the real surface area. To ensure the reliable characterization, the EIS measurements were performed across a wide range of frequencies (10 kHz to 0.1 Hz), at selected cathodic potentials– −0.8, −1 and −1.2 V (vs Ag/AgCl). An example of EIS spectra is presented in Figure 7 recorded using cobalt foams obtained from Solution 4 at different current densities. Fitting of impedance data was done using an equivalent scheme containing two pairs of constant phase elements in parallel with resistances (inset in Figure 7). We could see only one clear capacitive behavior, however since the electrodes were very porous and EIS was measured during HER, the physical meaning had to have an equivalent electric circuit (EEC) containing at least two capacitors. In our case, the EEC shown in Figure 7 showed a best fit for the obtained EIS spectra (minimal Chi-squared and elements values errors). First capacitance could be attributed to: (1) Porosity of the electrode, (2) double layer formation, or (3) diffusion limitations. According to Mulder et al., at highly contorted surfaces (3D) one can expect to obtain CPE n values of around 0.5 [51]. It was shown that when the first (high frequency) semicircles radius was potential independent, it was related to porosity and the shape of pores [52,53]. However, in our case the high frequency semicircle capacitance changed, hence it could not be purely porosity related. Also, during measurement evolving hydrogen bubbles might have blocked up pores and restricted further hydrogen evolution, then in impedance spectra it would seem like diffusion limitation.

Moreover, Łosiewicz et al. [54] showed that charge-up of the double layer of porous electrodes usually occurred not uniformly (there was frequency dependence). Hence the second semicircle (low frequency) could then be attributed to modeling of a charge transfer resistance process and differential charge-up of the double-layer. It was also shown [54] that double layer capacitance reduced with an increase in the overpotential in HER, which showed similar behavior to the low-frequency semicircle values like in our case. Nevertheless, the first semicircle probably was related to the combination of double layer partial charge-up process, porosity of electrode and maybe even diffusion processes, but separation of given processes in our case was quite difficult.

The second semicircle, located in the low frequencies region that also changed with potential was attributed to double layer capacitance and adsorption of hydrogen on the surface of cobalt foams. Both of these processes were potential dependent. All our efforts to separate the two processes were fruitless.

All the calculations and comparisons were made from the data obtained at −1.0 V vs Ag/AgCl. The equivalent circuit model (Figure 7) represented our best efforts, as it can be seen that it fit quite well with the measured data. The Chi-squared values were usually in the range from 10^{-4} to 10^{-5}, which was acceptable for porous electrodes. Some examples are shown in Table 2. The second constant phase element value was recalculated into true capacitance values using Mansfeld's procedure. The calculated capacitances were much higher than the ones obtained for flat metallic cobalt, which did

not exceed 100–200 µF/cm². It indicated that the obtained porous electrodes had 100–300 times larger actual surface area than the flat surface.
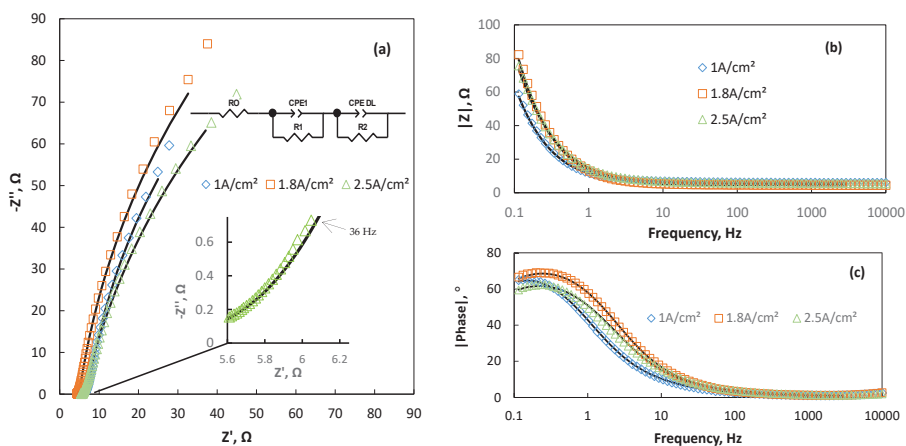

Figure 7. EIS data of cobalt foams measured in 0.1 M Na$_2$SO$_4$ at −1.0 V vs Ag/AgCl, foams deposited from solution 4, *q* = 180 C, EIS data represented in: (**a**) Nyquist's coordinates, (**b**) Bode modulus, and (**c**) Bode phase modulus coordinates. The equivalent electric circuit used for fitting is presented in the insert; points–experimental data, solid lines–results of fitting to the shown equivalent electric circuit.

Table 2. Values of elements of the equivalent electric circuit fitted EIS data obtained in 0.1 M Na$_2$SO$_4$ at −1.0V vs Ag/AgCl of cobalt foams deposited at *j* = 2.5 A/cm², *t* = 90 s.

Solution Used for Co-Foam Deposition	R_0, Ω	CPE$_1$, Fs^{n-1}	*n*	R_1, Ω	CPE$_{DL}$, Fs^{n-1}	*n*	R_2, Ω
1	3.668 ± 0.50%	0.1131 ± 1.7%		0.7317 ± 3.5%	0.0342 ± 0.91%	0.9321 ± 0.54%	133.7 ± 5.5%
2	4.081 ± 0.27%	0.0499 ± 1.6%	0.5	0.7652 ± 1.4%	0.0112 ± 0.37%	0.8844 ± 0.17%	349.7 ± 1.8%
3	4.872 ± 0.43%	0.0468 ± 1.9%		0.878 ± 2.1%	0.028 ± 0.82%	0.8313 ± 0.48%	508.8 ± 10.7%
4	5.427 ± 0.53%	0.046681 ± 2.9%		0.80871 ± 2.3%	0.01736 ± 0.94%	0.85157 ± 0.45%	311.9 ± 9.1%
Pure Co	8.442 ± 0.17%	–	–	–	0.000181 ± 0.402%	0.905 ± 0.0868%	1458 ± 0.79%

As it might seem, the second CPE element values (double layer and hydrogen adsorption capacitance), obtained using chloride-based solutions got the highest double layer capacitance, thus the highest surface area of cobalt foam. Nevertheless, after recalculations of CPE to true capacitance and further calculations of capacitance per gram of cobalt foam (Figure 8), the results changed completely–the highest surface area to mass ratio was obtained for foam electrodeposited from solution 4. This could be explained by higher efficiency of ammonium sulfate in hydrogen coalescence suppression, and lowered surface tension using isopropyl alcohol. These factors allowed the growing coating to form a tridimensional porous structure, with interconnected pores. All of the other foams were quite similar in surface area exposed per unit of mass; however, the ones obtained from solution 4, were three or more times superior.
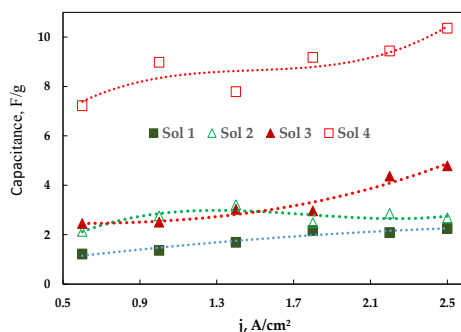
Figure 8. Influence of cathodic current density on the capacitance per gram of cobalt foams in the investigated solutions.

Cobalt foams obtained using pulse deposition, showed better CEs across the board, sometimes reaching up to 50% in efficiency, hence the obtained foams were thicker. Nevertheless EIS analysis of these foams showed that surface area to mass ratio was in all cases lower, than the one obtained using galvanostatic deposition conditions. Further research was done using only cobalt foams obtained at 2.5 A/cm^2 using solution 4 ($q = 180$ C).

3.3. Modification of Cobalt Foams and Detection of Free Chlorine

As mentioned earlier, modification of cobalt foams was with ferrocyanide, which was done using cyclic voltammetry. The measurements were performed in acetic acid buffer solution. Such a buffer was chosen because of highly active and substantial cobalt foams surface area. Other buffer solutions such as phosphate or citrate were tested, however either the foam reacted with the anions in the buffer (phosphate), or formed complexes at the surface (citrate case), diminishing the modification capabilities. The potassium nitrate used as background electrolyte, was shown to have second best ion permeability in various metal HCFs structures, ensuring good conductivity and electrons exchange [10,38]. The chosen potential window for modification was −0.8–0 V vs Ag/AgCl.

The potential in CV scans was first moved to the anodic side, in order to dissolve some of the foam, and afterwards to cathodic, to form cobalt ferrocyanide complex on the surface of the foams. Comparatively high scan rates were used to form cobalt ferrocyanide, so the damage to high surface area cobalt foams would be minimized. Additionally, no clear peaks could be seen on the voltammetric curve, since the scan speed used was quite high, the Co foams surface was very porous, and the response might have been too slow to be detected in such a system. A high scan rate was selected in order to minimize the damage of the cobalt foams surface, trying to keep the highest possible surface area intact, but still covering the whole surface of foam with Co HCF complex. With no clear oxidation or reduction peaks obtained during CV scans, a formation of cobalt ferrocyanide on the surface of cobalt foams had to be done externally. For that reason, EDS measurements were performed to ensure successful formation of cobalt ferrocyanide complex (Figure 9). The EDS picture represents a typical modified cobalt foam. It can be seen that the whole surface was quite uniformly covered with Fe and C compound, proving successful formation of Co HCF complex on the surface of the Co foam.
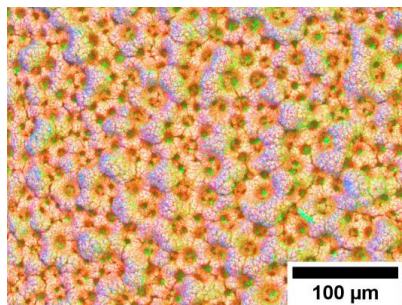
Figure 9. Image of EDS mapping of modified Co foam, using CV at 100 mV/s scan rate and after 100 cycles. Red color represents cobalt, green–iron, blue–carbon.

Free chlorine concentration, which is a sum of dissolved chlorine gas, hypochlorous acid and hypochlorite anion, was detected using acetic acid buffer solution whilst measuring the amperometric response of our system. Prior to the testing the purity of $Ca(OCl)_2$, which was used as a source of free chlorine and checked using the standard DPD method. Determined purity of calcium hypochlorite was 64%. The chosen pH value for chlorine detection measurements was −5.5 and was done so for two reasons: (1) Trying to simulate real tap water pH range, which was usually 5 < pH < 8, (2) all of the compounds of free chlorine exist in the solution at such pH values. However, most of the chlorine exists in the form of HClO, since the pK_a of reaction (3) was 7.48 at 25 °C.

$$HClO \rightarrow ClO^- + H^+ \qquad (3)$$

Hypochlorous acid reduction occurs in two steps (reaction 4 and 5), which according to Cheng et al. If the pH is above 3 is irreversible [55], making it possible to fully reduce and hydrolyze free chlorine in water to chloride anions.

$$HClO + H^+ + e^- \rightarrow 0.5Cl_2 + H_2O \qquad (4)$$

$$Cl_2 + 0.5H_2O \rightarrow HClO + H^+ + Cl^- \qquad (5)$$
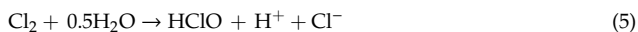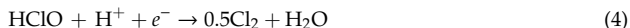
All of the free chlorine-containing compounds were reduced electrochemically very easily, so in order to minimize the damage of high surface area cobalt foams, ensuring longevity of the sensor, a plethora of potentials were tested. The best results were obtained using −0.45 V vs Ag/AgCl potential with the cobalt foams modified for 40 cycles at 100 mV/s speed. A calibration curve and typical chronoamperometric measurements are shown in Figure 10. The linearity of the curve was slightly distorted probably by oxygen reduction that was dissolved in testing solutions. Nevertheless, the increase of cathodic current with the addition of very small amounts of chlorine into water, proved very high sensitivity for our prepared sensor. The standard deviation of the blank solution was calculated using data from 10 chronoamperometric measurements. The calculated limit of blank (LOB = 1.65σ) was 3.06 ppb. The obtained limit of detection (LOD = 3σ) was 5.57 ppb and limit of quantification (LOQ = 10σ) was 18.86 ppb. Such results were acceptable, since the usual concentration of residual chlorine in tap water was somewhere between 0.2 and 1 ppm.
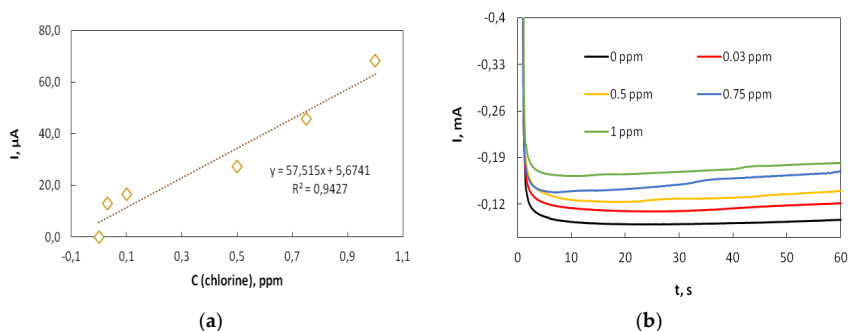
Figure 10. Calibration curve for sensors (**a**) and typical chronoamperometric curves for free chlorine detection in acetic acid buffer (**b**).

4. Conclusions

In the present work, cobalt metal foams were successfully deposited using a dynamic hydrogen bubble template method on the copper substrate. The true surface area of cobalt foams was estimated using the EIS technique. It was determined that the highest surface area cobalt foams were electrodeposited using a solution containing 0.2 M $CoSO_4$, 1 M $(NH_4)_2SO_4$ and 2 M isopropyl alcohol at a cathodic current density of 2.5 A/cm^2. In this case, there was synergy between the ammonium sulfate bubble suppression effect, and solutions surface tensions reduction, which allowed for the formation of highly porous 3D structured cobalt foams. The cobalt foams surface was modified with Co hexacyanoferrate, and such modified foams have been tested as sensors for the detection of free chlorine in water. A linear range from 5.6 ppb to 1 ppm was shown. It was demonstrated that such a sensor can be good and a cheaper alternative to noble metal sensors currently used for the detection of the concentration of residual chlorine in water.

References

1. United Nations sustainable development. Available online: https://www.un.org/sustainabledevelopment/blog/2015/12/sustainable-development-goals-kick-off-with-start-of-new-year (accessed on 23 February 2019).
2. Prüss, A.; Kay, D.; Fewtrell, L.; Bartram, J. Estimating the burden of disease from water sanitation and hygiene at a global level. *Environ. Health Perspect.* **2002**, *110*, 537–542. [CrossRef]
3. Bridle, H. *Waterborne Pathogens: Detection Methods and Applications*; Elsevier: Amsterdam, The Netherlands, 2013; ISBN 9780444595430.
4. Richardson, S.D.; Plewa, M.J.; Wagner, E.D.; Schoeny, R.; DeMarini, D.M. Occurrence, genotoxicity, and carcinogenicity of regulated and emerging disinfection by-products in drinking water: A review and roadmap for research. *Mutat. Res. Rev. Mutat. Res.* **2007**, *636*, 178–242. [CrossRef]
5. Richardson, S.D.; Postigo, C. Drinking water disinfection by-products. In *Emerging Organic Contaminants and Human Health*; Barceló, D., Ed.; Springer: Berlin/Heidelberg, Germany, 2012; pp. 93–137. ISBN 978-3-642-28132-7.
6. Wolfe, T.D. Water monitoring system. U.S. Patent 9,015,003B2, 17 December 1998.
7. Berry, D.; Xi, C.; Raskin, L. Microbial ecology of drinking water distribution systems. *Curr. Opin. Biotechnol.* **2006**, *17*, 297–302. [CrossRef]
8. Clark, R.M.; Skov, K.; Goodrich, J.A.; Deininger, R.A.; Grayman, W.M. Measuring and modeling chlorine propagation in water distribution systems. *J. Water Resour. Plan. Manag.* **2006**, *120*, 871–887. [CrossRef]

9.   Moberg, L.; Karlberg, B. An improved N,N′-diethyl-p-phenylenediamine (DPD) method for the determination of free chlorine based on multiple wavelength detection. *Anal. Chim. Acta* **2000**, *407*, 127–133. [CrossRef]

10. Salazar, P.; Martín, M.; García-García, F.J.; González-Mora, J.L.; González-Elipe, A.R. A novel and improved surfactant-modified Prussian Blue electrode for amperometric detection of free chlorine in water. *Sens. Actuators B Chem.* **2015**, *213*, 116–123. [CrossRef]

11. Salazar, P.; Martín, M.; González-Mora, J.L.; González-Elipe, A.R. Application of prussian blue electrodes for amperometric detection of free chlorine in water samples using flow injection analysis. *Talanta* **2016**, *146*, 410–416. [CrossRef]

12. Del Campo, F.J.; Ordeig, O.; Muñoz, F.J. Improved free chlorine amperometric sensor chip for drinking water applications. *Anal. Chim. Acta* **2005**, *554*, 98–104. [CrossRef]

13. Kodera, F.; Umeda, M.; Yamada, A. Determination of free chlorine based on anodic voltammetry using platinum, gold, and glassy carbon electrodes. *Anal. Chim. Acta* **2005**, *537*, 293–298. [CrossRef]

14. Okumura, A.; Hirabayashi, A.; Sasaki, Y.; Miyake, R. Simple miniaturized amperometric flow cell for monitoring residual chlorine in tap water. *Anal. Sci.* **2005**, *17*, 1113–1115. [CrossRef]

15. Kishioka, S.Y.; Kosugi, T.; Yamada, A. Electrochemical determination of a free chlorine residual using cathodic potential-step chronocoulometry. *Electroanalysis* **2005**, *17*, 724–726. [CrossRef]

16. Jin, J.; Suzuki, Y.; Ishikawa, N.; Takeuchi, T. A miniaturized FIA system for the determination of residual chlorine in environmental water samples. *Anal. Sci.* **2004**, *20*, 205–207. [CrossRef]

17. Yu, H.; Chen, H.; Pan, M.; Tang, Y.; Zeng, K.; Peng, F.; Wang, H. Effect of the metal foam materials on the performance of methanol steam micro-reformer for fuel cells. *Appl. Catal. A Gen.* **2007**, *327*, 106–113. [CrossRef]

18. Shahbazi, P.; Kiani, A. Fabricated Cu_2O porous foam using electrodeposition and thermal oxidation as a photocatalyst under visible light toward hydrogen evolution from water. *Int. J. Hydrog. Energy* **2016**, *41*, 2–11. [CrossRef]

19. Liu, H.; Zeng, S.; He, P.; Dong, F.; He, M.; Zhang, Y.; Wang, S.; Li, C.; Liu, M.; Jia, L. Samarium oxide modified Ni-Co nanosheets based three-dimensional honeycomb film on nickel foam: A highly efficient electrocatalyst for hydrogen evolution reaction. *Electrochim. Acta* **2019**, *299*, 405–414. [CrossRef]

20. Siwek, K.I.; Eugénio, S.; Santos, D.M.F.; Silva, M.T.; Montemor, M.F. 3D nickel foams with controlled morphologies for hydrogen evolution reaction in highly alkaline media. *Int. J. Hydrog. Energy* **2019**, *44*, 1701–1709. [CrossRef]

21. Dong, Y.; Sun, F.; Li, X.; Chu, M.; Li, N.; Li, X.; Wang, L.; Qu, D.; Dong, Y.; Xie, Z.; et al. A porous FeCuNi-based electrocatalyst supported by nickel foam for oxygen evolution reaction in alkaline conditions. *J. Electrochem. Soc.* **2018**, *165*, F1127–F1132. [CrossRef]

22. Jin, J.; Xia, J.; Qian, X.; Wu, T.; Ling, H.; Hu, A.; Li, M.; Hang, T. Exceptional electrocatalytic oxygen evolution efficiency and stability from electrodeposited NiFe alloy on Ni foam. *Electrochim. Acta* **2019**, *299*, 567–574. [CrossRef]

23. Pei, Y.; Ge, Y.; Chu, H.; Smith, W.; Dong, P.; Ajayan, P.M.; Ye, M.; Shen, J. Controlled synthesis of 3D porous structured cobalt-iron based nanosheets by electrodeposition as asymmetric electrodes for ultra-efficient water splitting. *Appl. Catal. B Environ.* **2019**, *244*, 583–593. [CrossRef]

24. Ma, Y.; Wang, H.; Feng, H.; Ji, S.; Mao, X.; Wang, R. Three-dimensional iron, nitrogen-doped carbon foams as efficient electrocatalysts for oxygen reduction reaction in alkaline solution. *Electrochim. Acta* **2014**, *142*, 317–323. [CrossRef]

25. Sanzó, G.; Taurino, I.; Antiochia, R.; Gorton, L.; Favero, G.; Mazzei, F.; De Micheli, G.; Carrara, S. Bubble electrodeposition of gold porous nanocorals for the enzymatic and non-enzymatic detection of glucose. *Bioelectrochemistry* **2016**, *112*, 125–131. [CrossRef]

26. Nam, D.-H.; Kim, R.-H.; Lee, C.-L.; Kwon, H.-S. Highly reversible Sn-Co alloy anode using porous Cu foam substrate for Li-Ion batteries. *J. Electrochem. Soc.* **2012**, *159*, A1822–A1826. [CrossRef]

27. Trahey, L.; Vaughey, J.T.; Kung, H.H.; Thackeray, M.M. High-capacity, microporous Cu_6Sn_5–Sn anodes for Li-ion batteries. *J. Electrochem. Soc.* **2009**, *156*, A385. [CrossRef]

28. Xu, J.; Ji, X.; Zhang, W.; Liu, G. Pool boiling heat transfer of ultra-light copper foam with open cells. *Int. J. Multiph. Flow* **2008**, *34*, 1008–1022. [CrossRef]

29. Hong, S.T.; Herling, D.R. Open-cell aluminum foams filled with phase change materials as compact heat sinks. *Scr. Mater.* **2006**, *55*, 887–890. [CrossRef]

30. Shin, H.C.; Dong, J.; Liu, M. Nanoporous structures prepared by an electrochemical deposition process. *Adv. Mater.* **2003**, *15*, 1610–1614. [CrossRef]

31. Raoof, J.B.; Ojani, R.; Kiani, A.; Rashid-Nadimi, S. Fabrication of highly porous Pt coated nanostructured Cu-foam modified copper electrode and its enhanced catalytic ability for hydrogen evolution reaction. *Int. J. Hydrog. Energy* **2010**, *35*, 452–458. [CrossRef]

32. Lange, G.A.; Eugénio, S.; Duarte, R.G.; Silva, T.M.; Carmezim, M.J.; Montemor, M.F. Characterisation and electrochemical behaviour of electrodeposited Cu-Fe foams applied as pseudocapacitor electrodes. *J. Electroanal. Chem.* **2015**, *737*, 85–92. [CrossRef]

33. Eugénio, S.; Silva, T.M.; Carmezim, M.J.; Duarte, R.G.; Montemor, M.F. Electrodeposition and characterization of nickel-copper metallic foams for application as electrodes for supercapacitors. *J. Appl. Electrochem.* **2014**, *44*, 455–465. [CrossRef]

34. Niu, J.; Liu, X.; Xia, K.; Xu, L.; Xu, Y.; Fang, X.; Lu, W. Effect of electrodeposition parameters on the morphology of three-dimensional porous copper foams. *Int. J. Electrochem. Sci.* **2015**, *10*, 7331–7340.

35. Marozzi, C.A.; Chialvo, A.C. Development of electrode morphologies of interest in electrocatalysis. Part 1: Electrodeposited porous nickel electrodes. *Electrochim. Acta* **2000**, *45*, 2111–2120. [CrossRef]

36. Kim, J.H.; Kim, R.H.; Kwon, H.S. Preparation of copper foam with 3-dimensionally interconnected spherical pore network by electrodeposition. *Electrochem. commun.* **2008**, *10*, 1148–1151. [CrossRef]

37. Nam, D.; Kim, R.; Han, D.; Kim, J.; Kwon, H. Effects of $(NH4)_2SO_4$ and BTA on the nanostructure of copper foam prepared by electrodeposition. *Electrochim. Acta* **2011**, *56*, 9397–9405. [CrossRef]

38. De Tacconi, N.R.; Rajeshwar, K.; Lezna, R.O. Metal hexacyanoferrates: electrosynthesis, in situ characterization, and applications. *Chem. Mater.* **2003**, *15*, 3046–3062. [CrossRef]

39. Kumar, A.; Kanagare, A.; Banerjee, S.; Kumar, P.; Kumar, M.; Sudarsan, V. Synthesis of cobalt hexacyanoferrate nanoparticles and its hydrogen storage properties. *Int. J. Hydrog. Energy* **2018**, *43*, 7998–8006. [CrossRef]

40. Cai, C.-X.; Xue, K.-H.; Xu, S.-M. Electrocatalytic activity of a cobalt hexacyanoferrate modified glassy carbon electrode toward ascorbic acid oxidation. *J. Electroanal. Chem.* **2000**, *486*, 111–118. [CrossRef]

41. Hegner, F.S.; Herraiz-Cardona, I.; Cardenas-Morcoso, D.; López, N.; Galán-Mascarós, J.R.; Gimenez, S. Cobalt hexacyanoferrate on $BiVO_4$ photoanodes for robust water splitting. *ACS Appl. Mater. Interfaces* **2017**, *9*, 37671–37681. [CrossRef]

42. Ho, K.C.; Chen, C.Y.; Hsu, H.C.; Chen, L.C.; Shiesh, S.C.; Lin, X.Z. Amperometric detection of morphine at a Prussian blue-modified indium tin oxide electrode. *Biosens. Bioelectron.* **2004**, *20*, 3–8. [CrossRef]

43. Ricci, F.; Palleschi, G. Sensor and biosensor preparation, optimisation and applications of Prussian Blue modified electrodes. *Biosens. Bioelectron.* **2005**, *21*, 389–407. [CrossRef]

44. Berkh, O.; Shacham-Diamand, Y.; Gileadi, E. Reduction of ammonium ion on Pt electrodes. *J. Electrochem. Soc.* **2008**, *155*, F223. [CrossRef]

45. Ribeiro, C.P.; Mewes, D. The effect of electrolytes on the critical velocity for bubble coalescence. *Chem. Eng. J.* **1993**, *97*, 10192–10197. [CrossRef]

46. Tsyntsaru, N.; Cesiulis, H.; Pellicer, E.; Celis, J.P.; Sort, J. Structural, magnetic, and mechanical properties of electrodeposited cobalt-tungsten alloys: Intrinsic and extrinsic interdependencies. *Electrochim. Acta* **2013**, *104*, 94–103. [CrossRef]

47. Liu, X.; Wu, N.; Zhou, P.; Bi, N.; Or, S.W.; Cui, C.; Sun, Y. Large scale synthesis of superparamagnetic face-centered cubic Co/C nanocapsules by a facile hydrothermal method and their microwave absorbing properties. *Mater. Res.* **2015**, *18*, 756–762. [CrossRef]

48. Liu, B.H.; Li, Z.P.; Suda, S. Nickel- and cobalt-based catalysts for hydrogen generation by hydrolysis of borohydride. *J. Alloy. Compd.* **2006**, *415*, 288–293. [CrossRef]

49. Staszak-Jirkovský, J.; Malliakas, C.D.; Lopes, P.P.; Danilovic, N.; Kota, S.S.; Chang, K.-C.; Genorio, B.; Strmcnik, D.; Stamenkovic, V.R.; Kanatzidis, M.G.; et al. Design of active and stable Co–Mo–S_x chalcogels as pH-universal catalysts for the hydrogen evolution reaction. *Nat. Mater.* **2015**, *15*, 197–203.

50. Lupi, C.; Dell'Era, A.; Pasquali, M. Nickel-cobalt electrodeposited alloys for hydrogen evolution in alkaline media. *Int. J. Hydrog. Energy* **2009**, *34*, 2101–2106. [CrossRef]

51. Mulder, W.; Sluyters, J.; Pajkossy, T.; Nyikos, L. Tafel current at fractal electrodes: Connection with admittance spectra. *J. Electroanal. Chem. Interfacial Electrochem.* **1990**, *285*, 103–115. [CrossRef]

52. Łosiewicz, B.; Budniok, A.; Rówiński, E.; Łagiewka, E.; Lasia, A. Effect of heat-treatment on the mechanism and kinetics of the hydrogen evolution reaction on Ni-P + TiO$_2$ + Ti electrodes. *J. Appl. Electrochem.* **2004**, *34*, 507–516. [CrossRef]

53. Damian, A.; Omanovic, S. Ni and nimo hydrogen evolution electrocatalysts electrodeposited in a polyaniline matrix. *J. Power Sources* **2006**, *158*, 464–476. [CrossRef]

54. Łosiewicz, B.; Budniok, A.; Rówiński, E.; Łagiewka, E.; Lasia, A. The structure, morphology and electrochemical impedance study of the hydrogen evolution reaction on the modified nickel electrodes. *Int. J. Hydrog. Energy* **2004**, *29*, 145–157. [CrossRef]

55. Cheng, C.Y.; Kelsall, G.H. Models of hypochlorite production in electrochemical reactors with plate and porous anodes. *J. Appl. Electrochem.* **2007**, *37*, 1203–1217. [CrossRef]

ARTICLE 2

Metal Foam Electrode as a Cathode for Copper Electrowinning

M. Vainoris, H. Cesiulis and N. Tsytsaru

![coatings logo]

MDPI

Article

Metal Foam Electrode as a Cathode for Copper Electrowinning

Modestas Vainoris [1] , **Henrikas Cesiulis** [2,*] **and Natalia Tsyntsaru** [1]

1   Department of Physical Chemistry, Vilnius University, LT-01513 Vilnius, Lithuania;
    m.vainoris@gmail.com (M.V.); ashra_nt@yahoo.com (N.T.)
2   JSC Elektronikos Perdirbimo Technologijos, LT-06140 Vilnius, Lithuania
*   Correspondence: henrikas.cesiulis@chf.vu.lt; Tel.: +370-(5)-2193178

check for updates

Abstract: The geometry of porous materials is complex, and the determination of the true surface area is important because it affects current density, how certain reactions will progress, their rates, etc. In this work, we have investigated the dependence of the electrochemical deposition of copper coatings on the geometry of the copper substrate (flat plates or 3D foams). Chronoamperometric measurements show that copper deposition occurs 3 times faster on copper foams than on a flat electrode with the same geometric area in the same potential range, making metal foams great electrodes for electrowinning. Using electrochemical impedance spectroscopy (EIS), the mechanism of copper deposition was determined at various concentrations and potentials, and the capacities of the double electric layer (DL) for both types of electrodes were calculated. The DL capacity on the foam electrodes is up to 14 times higher than that on the plates. From EIS data, it was determined that the charge transfer resistance on the Cu foam electrode is 1.5–1.7 times lower than that on the Cu plate electrode. Therefore, metal foam electrodes are great candidates to be used for processes that are controlled by activation polarization or by the adsorption of intermediate compounds (heterogeneous catalysis) and processes occurring on the entire surface of the electrode.

1. Introduction

The ever-increasing need for electronics, especially, handheld and portable electronics, and the need to reduce their size and increase their efficiency, generates a lot of various electronics waste all over the globe [1–3]. There are many ways to reclaim used metals in electronic waste; however, electrowinning is a very efficient and quite selective process allowing the recovery of high amounts of various pure metals [4–6]. Metallic foams and porous electrodes have an outstanding potential to be used as a cathode to collect deposited metals because of the functionality of their combined material properties resulting from their specific morphology. There already is great interest in the synthesis of various porous materials such as metal foams, nanowires, porous coatings, thin porous films, etc. [7–15]. Depending on the materials, type of pores (open or closed cells), the porosity and size of pores, such materials have broad application capabilities, from simple ones such as heat transfer or electrodes to more complicated cases of various redox reactions, catalysis, sensing, supercapacitors, or even gas storage because of the high surface area and low density available [9,16–29].

Any solid metal surface that acts as a substrate for electrochemical reactions possesses a certain roughness that can affect in different ways the values of the limiting diffusion current and the exchange current density. On the other hand, if the surface coarseness is relatively small, the limiting diffusion current density does not depend on the surface roughness, and it can be only correlated to the apparent

surface of the electrodes. If the surface roughness of electrodes increases, the effective values of the exchange current density are also increased for the process under consideration, which is standardized to the apparent electrode surface area. At the same time, the limiting diffusion current density depends on the surface coarseness due to the decrease of the effective value of the diffusion layer thickness. If the level of the electrode surface coarseness remains low, the change of the limiting diffusion current density can be neglected [30]. In addition, it has been shown that when the metal deposition is controlled by diffusion (particularly silver), the surface with the highest surface roughness had a lower number of active sites but higher deposition efficiency and a higher efficiency of charge transfer [31]. The dependence between surface roughness and deposition efficiency is non-linear; the surface roughness needs to be quite high to affect the deposition efficiency [31,32]. It was proven that when the deposition reaction is controlled by the diffusion, the geometry of the electrode has no significant influence on the reaction [33]. Using very porous or surfaces with high roughness, one can eliminate activation and diffusion overpotentials, making the reaction process controlled by Ohmic effects and thus making the reaction much faster [30,31]. All these effects make porous metal electrodes with pore diameters higher than 50 μm high-performance cathodes for deposition reactions under diffusion control.

The estimation of the active surface area of highly porous conducting materials is also very important. Thus, various in situ or ex situ techniques can be used for these purposes. In situ techniques are preferred, since drying the sample can cause changes in the surface area and/or oxidation of the surface, changing its characteristics. Depending on the material and its porosity, one can use techniques for double electric layer estimations (cyclic voltammetry, initial charge-up dependencies, electrochemical impedance spectroscopy (EIS)), or adapt various adsorption/redox reactions that occur on the surface (underpotential depositions, adsorption measurements, reduction of various dyes, etc.) [29,34–39]. The classical techniques for surface area estimation—liquid permeability, gas adsorption (Brunauer–Emmett–Teller technique)—in some cases can also be used [34,35,39]. However, these techniques require higher amounts of materials and can have quite large error margins, depending on the geometry of the pores and the sample itself. For porous materials that are quite level, and with ordered pores, more sophisticated techniques could be used for porosity estimation such as atomic force microscopy (AFM) or spectroscopic ellipsometry; the latter requires a rather complex modeling [40–42].

EIS is a very powerful and versatile in situ technique that allows not only estimating the true surface area of conducting materials but also investigating the surface and the processes happening at the surface [9,20,23,27,29]. Using the EIS technique, one can investigate both Faradaic and non-Faradaic processes on the surface simultaneously [27,29,34,35,43–47]. Even the size and distribution of the pores can be characterized by employing the EIS technique [45,46]. However, the surface area determined by EIS or any other electrochemical method is not the true surface area, but rather the electrochemically active surface area, which can be much more useful when trying to determine the activity of porous materials for a hydrogen evolution reaction (HER) or other electrochemical reaction [39–47].

In this work, we investigated the deposition of copper on the plate (2D) and foam (3D) copper substrates using voltammetry and EIS. The comparison of 2D and 3D electrodes has been carried out to determine differences in double electric layer formation, charge transfer, diffusion, and deposition rates. These results are important for trying to enhance the potential application of foam electrodes in industry, and particularly for the electrowinning of copper from electronics waste.

2. Materials and Methods

2.1. Materials and Sample Preparation

All of the chemicals used for analysis were of analytical grade (Carl Roth, Karlsruhe, Germany). Solutions have been prepared using deionized water (DI). Solution compositions used for electrochemical experiments are shown in Table 1. The pH of solutions was adjusted using sulfuric acid and controlled by a benchtop pH-meter ProLine Plus (Prosence B.V., Oosterhout, The Netherlands).

Cu plates and Cu foam electrodes served as working electrodes. The Cu foam sheets used to fabricate electrodes were purchased from Alfa Aesar. To characterize commercially available copper foams, we have done some experiments trying to determine the basic characteristics of this foam. Foam density has been determined as gravimetrically being equal to 0.748 g/cm^3, making the porosity of the foam to be around 90.5%. The copper foam has a 3D interconnected porous structure, which can be observed in SEM images (Figure 1). The pore size varies from 1 to 0.1 mm. The surface of the foam is very uneven, making the true surface area of the already porous copper foam even larger.
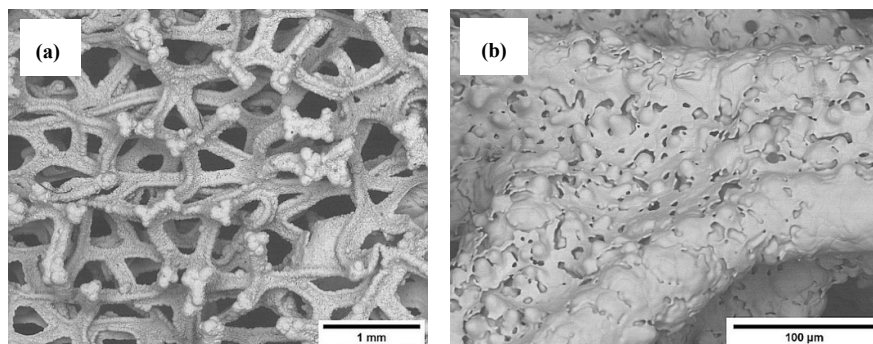

Figure 1. SEM images at low (**a**) and high (**b**) magnification of 3D copper foam.

Working electrodes (copper plates and copper foams) have been washed and degreased using acetone, ethanol, and water in succession and in combination with ultrasonic bath. Both flat and porous samples were 1 cm × 1 cm in geometrical size with both sides conducting. To ensure that the working surface was that of the desired size, other parts of the samples were isolated using insulating plastic spray (PRF 202, Taerosol Oy, Kangasala, Finland). Just before measurements, the native copper oxide layer has been removed by dipping copper samples into 2 M H_2SO_4 solution for 2 s and afterward rinsing with DI water.

Table 1. Composition of solutions used for electrochemical measurements.

$c(CuSO_4)$, M	$c(Na_2SO_4)$, M	pH
0.01	0.49	3.6
0.05	0.45	3.6
0.1	0.4	3.7
0.2	0.3	4.1

2.2. Instrumentation and Methodology

Morphology: The morphology of copper foams has been investigated using a scanning electron microscope (SEM, Hitachi's Tabletop Microscope TM-3000, Tokyo, Japan).

Electrochemical Measurements: Electrochemical measurements (voltammetry, EIS, chronoamperometry, etc.) have been performed using programmable potentiostat/galvanostat AUTOLAB PGSTAT 302N (Metrohm, Utrecht, The Netherlands). The software used for controlling the hardware was Nova 1.11.2.

Conditions of Electrochemical Measurements: A three-electrode system was used for all the electrochemical experiments, where Cu plates or Cu foams were used as working electrodes, circular platinized titanium mesh (Alfa Aesar, Ward Hill, MA, USA) was used as a counter electrode, and Ag/AgCl filled with saturated KCl solution (Sigma-Aldrich, St. Louis, MO, USA) was used as a reference electrode. The distance between the counter and working electrode was fixed at 2.5 cm. All

electrochemical experiments have been performed at room temperature. Voltammetry measurements were done using the potential sweep voltammetry technique on Cu plates and Cu foams as working electrodes, starting at open circuit potential and going up to −1.2 V versus Ag/AgCl at a 2 mV/s scan rate. Voltammetry measurements have been performed using all the solutions shown in Table 1. Chronoamperometry experiments were performed at 4 distinct potentials (−0.1, −0.2, −0.4 and −0.6 V versus Ag/AgCl) using different substrates as working electrodes (Cu plates or foams) in 0.1 M $CuSO_4$ and 0.4 M Na_2SO_4 solution. The same amount of electric charge was used to deposit coatings, i.e., 30 C. The current efficiency was calculated using chronoamperometry data and change in substrate mass after deposition.

Electrochemical Impedance Spectroscopy (EIS): Electrochemical impedance spectroscopy (EIS) measurements have been done using a standard three-electrode system, carried out in a frequency range of 10 kHz to 0.1 Hz, using perturbation amplitude of 10 mV. Obtained data were fitted to the equivalent electric circuit model (EEC) using ZView 2.8d software.

3. Results and Discussion

3.1. Copper Foam Characterization

In order to determine how the behavior of copper foams differs from flat surfaces in solutions, voltammetry experiments with different copper sulfate concentrations were carried out; the compositions of the solutions are shown in Table 1. The concentration of the sulfate anion was kept at 0.5 M to maintain the same buffering power in all of the solutions. The obtained polarization curves for the plate and foam electrode are shown in Figure 2, where the ordinate axis is displayed in a logarithmic scale because of a big difference in the current values between tested concentrations. To estimate the influence of porosity on the copper deposition, the geometrical sample size was the same for both Cu plates and Cu foams (1 cm × 1 cm). As can be seen from Figure 2, Cu deposition starts somewhere around −0.075 V versus Ag/AgCl and did not depend on the substrate used. After the peak representing the Cu^{2+} reduction to Cu^0, the current on both surfaces and all the concentrations turns into an almost constant one. The reason for this could be the mass transport limitations because the leveling off of the current depends on the concentration of Cu(II) in the solution. This is also supported by the slight increase of the current with the rise of polarization at higher concentrations (50 mM to 0.2 M), showing that with higher potential, the positive ions are attracted from further away, and the deposition rate increases.

In addition, voltammetry tests also showed that independently of the substrate used, the hydrogen evolution reaction (HER) started in the range of −1.0 to −1.1 V versus Ag/AgCl in the solutions containing 10 and 50 mM of $CuSO_4$. This fact could be attributed to the governing role of pH change in the pre-electrode layer during electrodeposition, and this change seems to be similar for both solutions. However, in the solution containing 0.2 M $CuSO_4$, the HER started around −0.75 V versus Ag/AgCl on both surfaces. It can be linked to the higher rate of copper electrodeposition, and in turn, the pH decrease near the working electrode. Thus, the major difference between the two surfaces can be noted from voltammetry experiments: there was an approximately 3 times higher current on the foam substrate at all potentials in comparison to the flat surface. This difference can be explained by the better hydrodynamic conditions of copper foams substrate: the porous surface allows for faster mass transport and exchange.

For further investigation, the solution containing a similar amount of Cu(II) as in solutions used for the metals recovery from the electronic waste was chosen. Regarding the influence of the surface type on the Cu electrochemical deposition, chronoamperometric measurements have been done in 0.1 M $CuSO_4$ and 0.4 M Na_2SO_4 solution at four fixed potentials: −0.1, −0.2, −0.4, and −0.6 V versus, Ag/AgCl, and at a fixed amount of charge passed through the cell (30 C). The results have been summarized and are shown in Table 2.
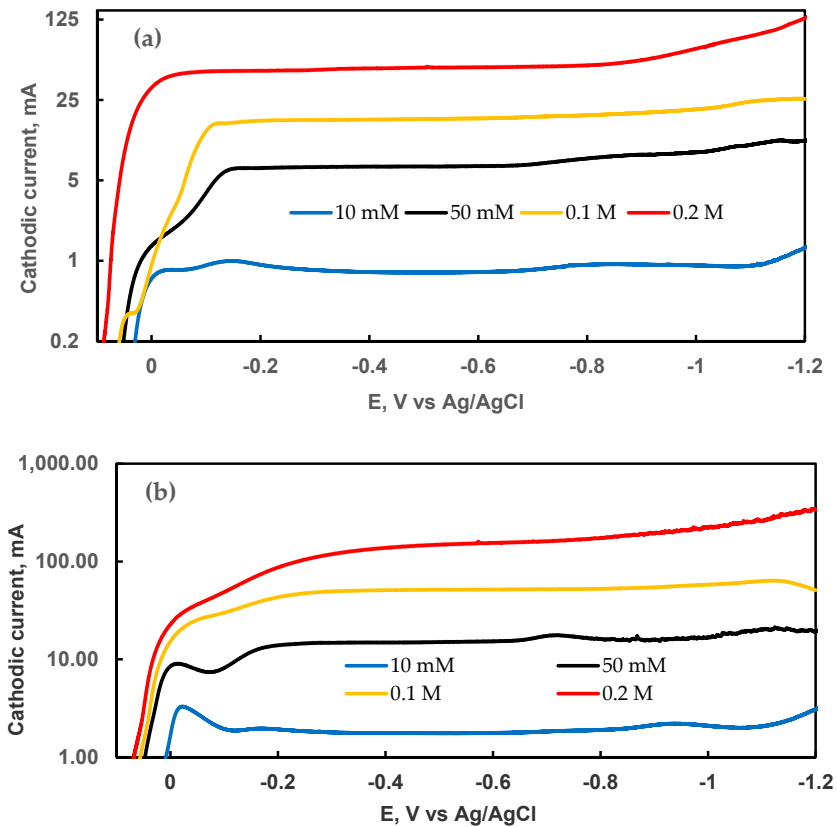
Figure 2. Cathodic voltammograms on Cu plate (**a**) and foam (**b**) obtained in the electrolytes with various concentrations of CuSO$_4$ (the compositions of solutions are shown in Table 1), potential scan rate 2 mV/s.

Table 2. Cu deposition rates on 2D and 3D electrodes in the solution containing 0.1 M CuSO$_4$ and 0.4 M Na$_2$SO$_4$.

Cu Plate			Cu Foam		
E, V versus Ag/AgCl	Deposition Time (s)	Cu Deposition Rate (mg/min)	E, V versus Ag/AgCl	Deposition Time (s)	Cu Deposition Rate (mg/min)
−0.1	1763	0.33	−0.1	643	0.94
−0.2	1681	0.35	−0.2	574	1.1
−0.4	1603	0.36	−0.4	593	1.0
−0.6	1571	0.37	−0.6	518	1.2

Chronoamperometric measurements (Table 2) clearly show an approximately 3 times faster copper deposition rate on the foam at all tested potentials. In this case, there was no hydrogen evolution, and the deposition efficiency was almost 100% on both substrates. A considerably higher deposition rate on the cooper foam substrate supports the idea that the deposition is controlled by diffusion to the electrode having a higher specific surface area. In addition, a higher metal deposition rate on the foam electrodes makes them an attractive substrate for the electrowinning of metals compared to other

materials having a similar geometric area. The morphology of deposits is influenced by the potential and type of substrate, as it is shown in the SEM images in Figure 3.
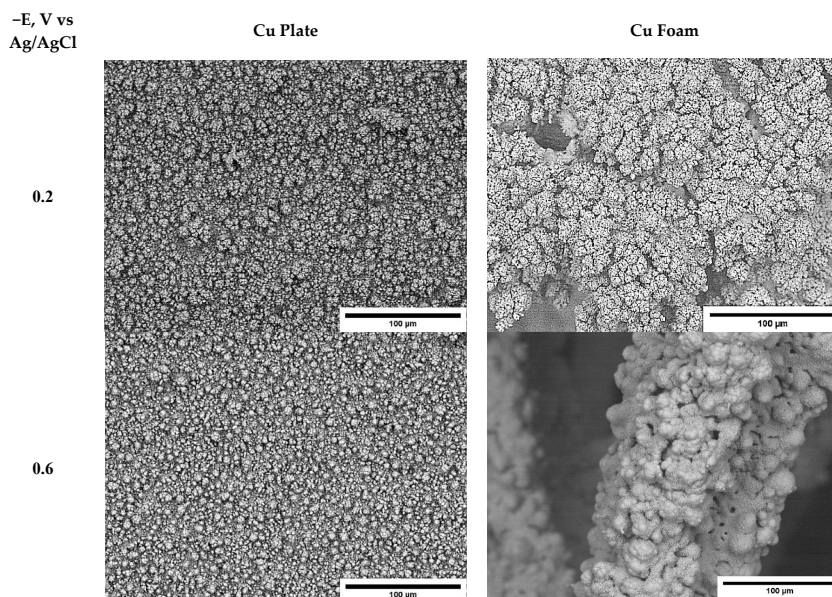

Figure 3. SEM images of potentiostatically electrodeposited Cu coatings at different cathodic potentials on flat and foam copper substrates after 30 C passed charge. The bath was 0.1 M CuSO$_4$ and 0.4 M Na$_2$SO$_4$.

The copper deposits have globules shapes on the flat electrodes, and the morphology did not differ at these two potentials. This is related to the very similar electrochemical deposition rates at these potentials, and as it can be seen from the voltammetry data (Figure 2) and efficiency of deposition, there were no side reactions, and the current was similar at these two potentials. Another case is the deposition on the porous substrate. At −0.2 V versus Ag/AgCl, copper forms cauliflower-like crystalline agglomerates with well-defined edges. At higher potential, the copper forms smoother surfaces that are still cauliflower-like structures. The coverage of both surface geometries was good even without external agitation, even at low potentials.

3.2. Surface Area and Diffusion Rate Estimations

To characterize copper foams and estimate the active surface areas for the charge and mass transfer processes that occur during the electrochemical deposition of copper, we utilized the EIS technique. EIS measurements have been done for all the solutions listed in Table 1. EIS measurements were performed at cathodic potentials of −0.125, −0.15, −0.175, and −0.2 V versus Ag/AgCl on flat and porous copper substrates. These potentials were chosen based on chronoamperometric data. At such low potentials, the change of surface morphology during deposition is still minimal and can be ignored in this case. Typical EIS scans on the copper plate at various potentials are shown in Figure 4. From the EIS data plots, we can see that at investigated potentials, the data plot can be divided into two zones: the high-frequency semicircle and the low-frequency (starting around 75–100 Hz) 45° angle line. The high-frequency semicircle can be attributed to charge up of the double layer and charge transfer to the copper ions, whilst the low-frequency line is attributed to the formation of the concentration gradient of the copper ions. To better evaluate ongoing processes, EIS data were fitted to the equivalent electric

circuit (EEC) that is shown as an inset in Figure 4 of the Nyquist plot (a). The elements of applied EEC have the following physical meaning: R0 is resistance at the electrode/electrolyte interface, CPE(DL) is a double-layer capacitance modeled via the constant phase element (CPE), R(CT) is a charge transfer resistance, CPE(W) stands for the capacitance caused by the concentration gradient, and R(Diff) is a resistance caused by the concentration gradient. The element CPE(W) is attributed to the diffusion because of the signature 45° angle seen in the Nyquist plots at low frequencies (Figure 4), and the value n in this CPE element was very close to 0.5 in all the experiments. This constant phase element acting only in the low-frequency region represents diffusion, and it can be used as a Warburg element when $n = 0.5$ [48,49]. The values of the constant phase element CPE(DL) have been recalculated into true capacitance using Hsu and Mansfeld's equation [50]. All values of components of the fitted EEC are indicated in Table 3.
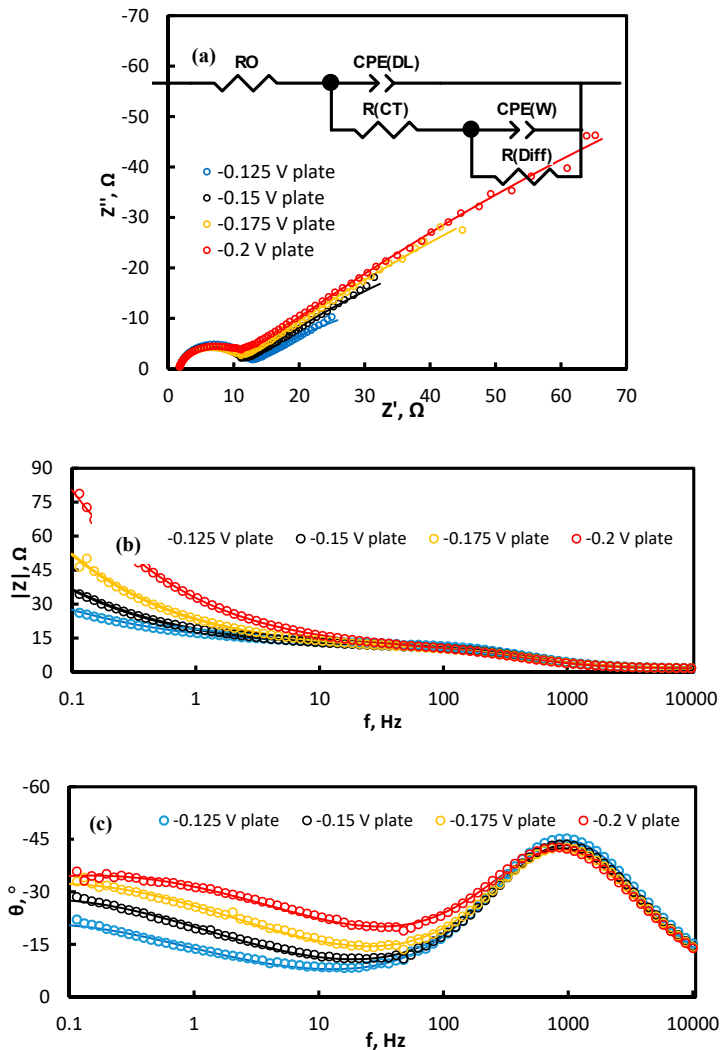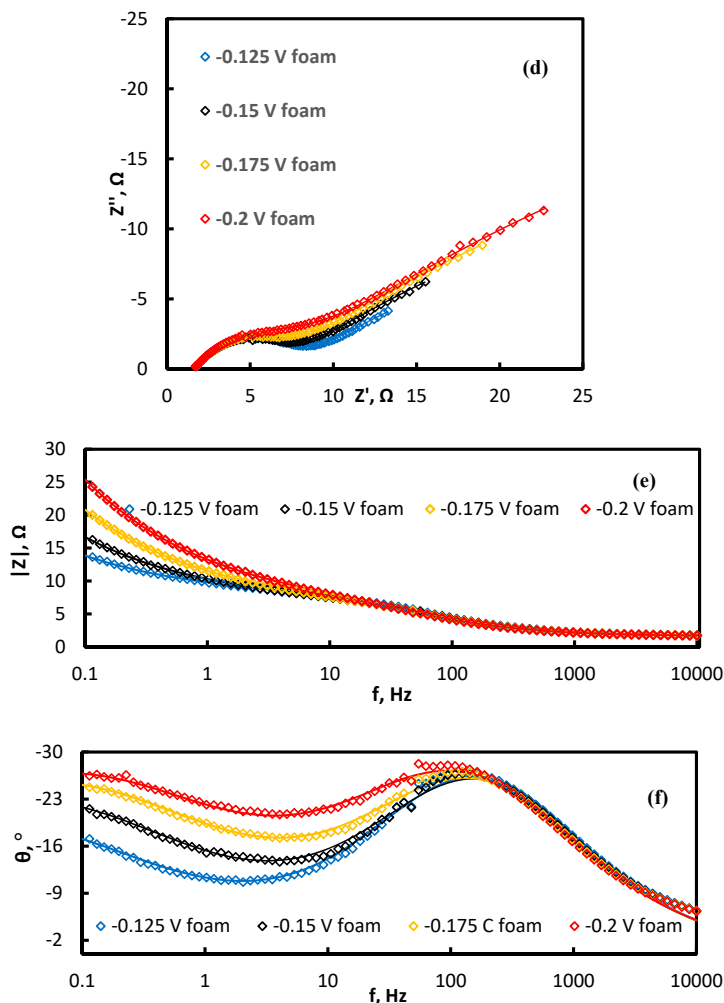

Figure 4. *Cont.*

127

Figure 4. Nyquist (**a**,**d**) and Bode plots (**b**–**c**,**e**–**f**) on Cu plate (**a**–**c**) and foam (**d**–**f**) registered at various potentials (indicated on graphs) in 0.1 M CuSO$_4$ + 0.4 M Na$_2$SO$_4$ solution at 20 °C. Points—experimental data, solid lines—results of fitting to equivalent electric circuit (EEC) shown in the inset (**a**).

As it is seen, the proposed EEC describes well experimental EIS data on both substrates in a whole investigated potential range. The values of the capacitance of the double electric layer on both substrates might be used to estimate differences in real areas between the plate and foam electrodes, i.e., to estimate the roughness factor as a ratio of C(DL) on foam and plates that have the same geometric area (1 cm × 1 cm). Notably, the double-layer capacitance (C(DL)) extracted from the EIS data is 50 μF (see Figure 5), and it is in good agreement with the theoretical values assigned to 1 cm^2 of copper [49]. The capacitance of the double layer of a commercial foam, that has the same geometric area as a plate, is 7 to 14 times higher in comparison with a plate electrode. The thickness of the double electric layer is very small and is in tens of nanometers; therefore, this layer replicates the surface morphology on the nano-level, and the ratio with the value obtained on the plate electrode can represent the roughness

factor, and it matches the ratio of C(DL) of both surfaces –(C(DLfoam); C(DL plate) is 7–14:1). However, the increase of double-layer capacitances with the increase of applied cathodic potential on both flat and porous surfaces is different. On the porous electrode, the C(DL) increase is much higher when compared to the change in capacitances of the flat electrode. This increase is related to the much higher surface area, and the distribution of current on the surface of the foam. With higher potential, the current distributes more evenly on the whole foam surface, and the edge effect is less apparent, which also influences the surface area estimations [51,52].

When looking at the effect that the concentration of copper ions has on the EIS parameters (Table 3), we can divide the results into three sections: high concentration (0.2 M), mid-level concentrations (0.1 and 0.05 M), and low concentrations (0.01 M). The double electric layer (DL) capacitance values do not differ that much with the change of the concentration on both surface geometries. However, when looking at charge transfer resistance, the differences between concentrations are significant. At low concentrations, the charge transfer resistance is very high; this is caused by the lack of copper ions. In contrast, this resistance at mid-level concentrations is around 6–9 Ω, which depends on the surface geometry as well as applied potential (Figure 5). At high concentrations (0.2 M and higher), the charge transfer resistance values decrease approximately 3 times on both surfaces, because of an abundance of conducting particles. Nevertheless, this charge transfer resistance is lower at all investigated potentials and all concentrations on the foam electrode, showing that the reduction reaction occurs faster on the copper foams.

When taking a look at the charge transfer resistance dependence on potential (Figure 5) with both types of electrodes, it is clear that the 3D electrode displays approximately 1.5–1.7 times lower charge transfer resistance than the 2D electrode, agreeing with the results of voltammetry (see Figure 2). The differences in the charge transfer resistance on plate and foam electrodes are lower than the differences in the capacitances of DL, because the reaction layer is thicker than the DL, and in some areas of the foam electrode, it overlaps. As it can be seen from Figure 5, the difference between 2D and 3D electrodes in charge transfer resistance is higher at low potentials; thus, the charge transfer reaction on the foam occurs easier, and it partially explains the higher Cu deposition rate (see Table 2). However, lowering the charge transfer resistance, or in turn, the increase of the rate of the charge transfer reaction by approximately 2 times, does not result in increases in the Cu deposition rate by approximately 3 times.
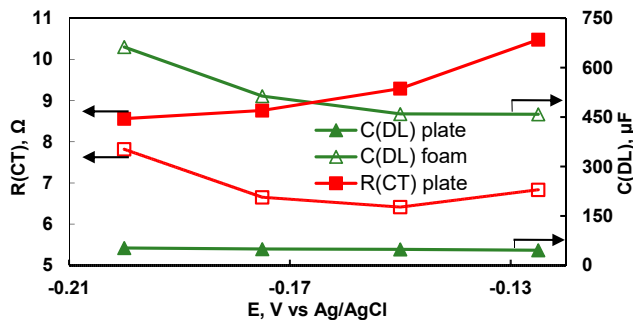

Figure 5. Dependence of double-layer capacitance (ordinate at the right) and charge transfer resistance (ordinate at the left) on potential applied for Cu plate and foam electrodes in 0.1 M CuSO$_4$ + 0.4 M Na$_2$SO$_4$ solution.

To further characterize the difference in copper deposition reactions on flat and porous copper surfaces, the components of EEC related to diffusion have been investigated in detail (Figure 6). The foam has lower charge transfer resistance, meaning faster reactions and better hydrodynamic qualities,

allowing for faster diffusion and in turn the much faster deposition, even with a larger surface and in turn, lower current density.
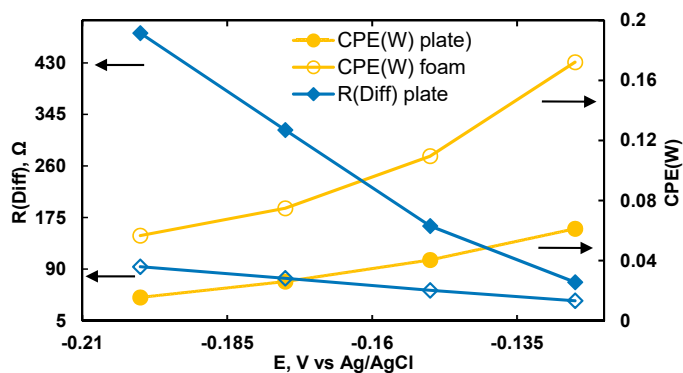

Figure 6. Dependence of diffusion-related elements of EEC on the potential applied. Measurements performed using a copper plate and copper foam as working electrodes in 0.1 M $CuSO_4$ + 0.4 M Na_2SO_4 solution.

Table 3. Values of electrochemical impedance spectroscopy (EIS) parameters obtained by fitting data obtained on copper foam and copper plates at −0.175 V versus Ag/AgCl at different copper concentrations. EC used for modeling shown in Figure 3 inset. CPE(DL): a double-layer (DL) capacitance modeled via the constant phase element (CPE), CPE(W): the capacitance caused by the concentration gradient, R(CT): charge transfer resistance, R(Diff): resistance caused by the concentration gradient.

Cu Plate	0.2 M $CuSO_4$ + 0.3 M Na_2SO_4	0.1 M $CuSO_4$ + 0.4 M Na_2SO_4	0.05 M $CuSO_4$ + 0.45 M Na_2SO_4	0.01 M $CuSO_4$ + 0.49 M Na_2SO_4
C(DL), μF	40.5	49.3	41.9	56.4
R(CT), Ω	2.98	8.76	7.44	54.66
CPE(W)	0.0696	0.0260	0.0285	0.00247
R(Diff), Ω	233.4	319.3	199.6	663.7
Cu Foam		−		
C(DL), μF	299.2	513.5	456.6	754.1
R(CT), Ω	2.39	6.65	6.74	122.20
CPE(W)	0.2033	0.0748	0.0668	0.0039
R(Diff), Ω	14.9	74.9	83.3	1551.0

The parameter related to diffusion CPE(W) at low concentrations is almost equal on both surface geometries, showing that the diffusion effect is similar, but the resistance at low concentration is about 2.5 times higher. It means that the diffusion layer is much thicker on the copper foams surface because of the porosity effect. Therefore, it causes a higher rate of copper electrodeposition. The overall trend in mid-level and high concentrations is that with the increase of Cu^{2+} concentration, the CPE(W) value increases, and the R(Diff) decreases. As it is seen from Table 3, the difference between R(Diff) values at 0.2 and 0.05 M concentrations on the flat surface is only around 14%, whereas on the foam electrode, the values of R(Diff) are lower, but all values are sensitive to the concentration of Cu(II) in the solution. The highest value of R(Diff) is obtained on the foam electrode at a relatively low concentration of Cu(II), i.e., 0.01 M, which is probably due to the faster depletion of copper ion concentration in the 3D diffusion layer and the necessity of a longer time to supply Cu(II) ions into the pores. Since the deposition rate on the foam electrode at a higher concentration of Cu(II) is 3 times faster than on the

flat electrode, this is mirrored by the behavior of CPE(W), showing that the diffusion occurs 3 times faster on the foam. The efficiency of charge transfer on the porous surfaces is higher as well, which is in good agreement with other studies of metal depositions on porous surfaces [31].

To even better understand the diffusion peculiarities on 2D and 3D electrodes, the diffusion impedance using extracted values from total impedance data (presented in Table 4) was calculated. As it is shown in Figure 4, the copper deposition occurs under diffusion control at low frequencies (below 100 Hz) on both foam and plate electrodes, and diffusion is modeled by a parallel connection of CPE(W) and R(Diff) elements (see Figure 4). In this case, diffusion impedance, Z_{diff}, as a function of frequency is calculated by the equation:

$$Z_{diff}(\omega) = \frac{R_{Diff}}{1 + (j\omega)^{\alpha} Q R_{Diff}} \tag{1}$$

where Q and α are parameters of CPE(W), R(Diff) is resistance caused by diffusion, and ω is the phase angle ($\omega = 2\pi f$). However, when $\alpha = 1 - Q$ is pure capacitance, in our case, $\alpha = 0.5$, and the CPE represents diffusion [53].

The calculated diffusion impedance data are presented in Figure 7. As it is seen, the diffusion impedance on the plate Cu electrode is 2–4 times higher than that on the foam Cu electrodes, which is dependent on the frequency and potential applied.
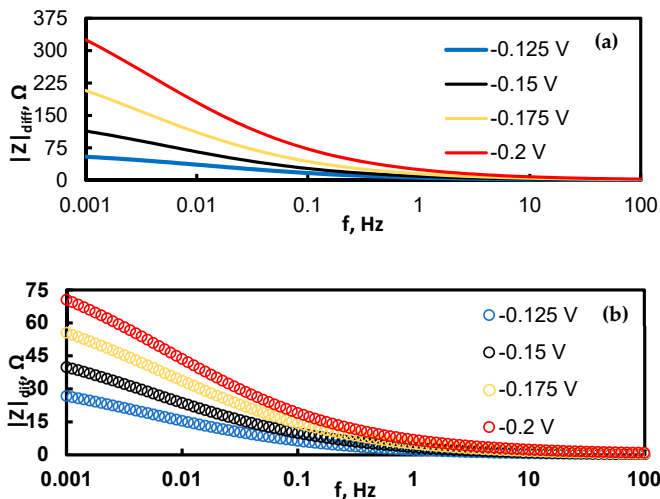

Figure 7. Bode plots of extracted diffusion impedance at various potentials on flat Cu substrate (**a**); and Cu foam substrate (**b**).

These results once again confirm the chronopotentiometric data obtained on both 2D and 3D Cu electrodes. For chronopotentiometry experiments, current values have been chosen higher than the limiting current values seen in Figure 8. In this case, the transition time at which the concentration of metal ions on the electrode becomes equal to zero is visual on the chronopotentiograms, and the effective diffusion coefficient can be calculated by the Sand equation:

$$i\sqrt{\tau} = \frac{nFAC_0 \sqrt{\pi D_{eff}}}{2} \tag{2}$$

where τ is a transition time (s), i is a current (A), C_0 is the concentration of Cu(II) ions (mol/cm³), D_{eff} is the effective diffusion coefficient (cm²·s⁻¹), F is Faraday's constant, n is the number of electrons participating in the electrochemical reaction; and A is a geometrical surface area.
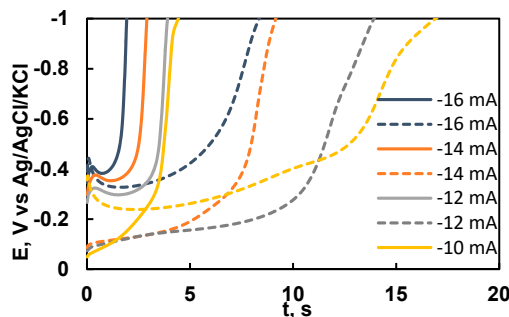

Figure 8. Chronopotentiograms on flat (continuous lines) and porous (dashed lines) electrodes at various current densities in 50 mM CuSO₄ and 0.45 M Na₂SO₄ solution. All the densities have been calculated for the geometrical area of the substrate of 1 cm².

In our case $i \sqrt{\tau} \sim const$, so the maximal deposition rate is controlled by the mass transfer. The values of the effective diffusion coefficient of Cu²⁺ ions on both plate and foam Cu electrodes were calculated by Equation (2), and the data are shown in Table 4. The effective diffusion coefficient on the plate electrode is almost three times lower than on the foam electrode, and it is in good agreement with EIS data.

Table 4. Effects of electrode geometry on effective Cu(II) ions diffusion coefficient.

Applied Current	Effective Diffusion Coefficient	
	Plate	Foam
I, mA	10^6 D, cm²·s⁻¹	10^6 D, cm²·s⁻¹
−10	6.79	18.06
−12	6.72	19.70
−14	6.73	20.16
−16	6.62	20.77
Average D_{eff}	**6.72**	**19.67**

So, copper foams are great substrates for reactions that are either limited by the mass transfer (electrochemical depositions, etc.) or the ones that are restricted by adsorption or activation (HER and similar), making them great candidates to reduce the size of electrodes, but not to lose out on the efficiency and activity of electrodes.

4. Conclusions

A comprehensive investigation of the electrochemical deposition of copper onto 2D (plate) and 3D (foam) Cu substrates has been done. Using various electrochemical methods, it was determined that the rate-determining step in a copper deposition is diffusion. The main processes occurring on the electrode are the charge-up of double electric layer, charge transfer, and diffusion. The specific electrochemically active area of Cu foam was estimated from EIS data, and based on the values of the double electric layer, it was determined to be 7–14 times higher than that for the plate electrode. Based on the EIS data, it was determined that the charge transfer resistance on the Cu foam electrode is 1.5–1.7 times lower than that on the Cu plate electrode, which results in an increase in a charge transfer rate of

approximately 2 times. Based on the analysis of the diffusion impedance and chronopotentiometry data, it was found that Cu^{2+} mass transfer and the copper deposition rate is up to 3 times faster on the foam surface in comparison with a flat surface having the same geometric area in the same potential range. In addition, effective diffusion coefficients have been calculated from chronopotentiometry data using Sand's equation. These findings make Cu foam an attractive material for metal electrowinning processes as well as for processes controlled by adsorption (e.g., hydrogen evolution reaction).

Author Contributions: Investigation, M.V. and N.T.; methodology, M.V. and H.C.; supervision, H.C. and N.T.; visualization, M.V.; writing—original draft preparation, M.V.; writing—review and editing, M.V., H.C. and N.T. All authors have read and agreed to the published version of the manuscript.

Conflicts of Interest: The authors declare no conflict of interest.

References

1. Liu, X.; Tanaka, M.; Matsui, Y. Generation amount prediction and material flow analysis of electronic waste: A case study in Beijing, China. *Waste Manag. Res.* **2006**, *24*, 434–445. [CrossRef] [PubMed]

2. Jain, A.; Sareen, R. E-waste assessment methodology and validation in India. *J. Mater. Cycles Waste Manag.* **2006**, *8*, 40–45. [CrossRef]

3. Eurostat, Statistics Explained. Available online: https://ec.europa.eu/eurostat/statistics-explained/index.php/Waste_statistics_-_electrical_and_electronic_equipment (accessed on 7 August 2020).

4. Vegliò, F.; Quaresima, R.; Fornari, P.; Ubaldini, S. Recovery of valuable metals from electronic and galvanic industrial wastes by leaching and electrowinning. *Waste Manag.* **2003**, *23*, 245–252. [CrossRef]

5. Grimshaw, P.; Calo, J.M.; Hradil, G. Cyclic electrowinning/precipitation (CEP) system for the removal of heavy metal mixtures from aqueous solutions. *Chem. Eng. J.* **2011**, *175*, 103–109. [CrossRef] [PubMed]

6. Bertuol, D.A.; Amado, F.D.R.; Veit, H.; Ferreira, J.Z.; Bernardes, A.M. Recovery of nickel and cobalt from spent nimh batteries by electrowinning. *Chem. Eng. Technol.* **2012**, *35*, 2084–2092. [CrossRef]

7. Kim, J.H.; Kim, R.H.; Kwon, H.S. Preparation of copper foam with 3-dimensionally interconnected spherical pore network by electrodeposition. *Electrochem. Commun.* **2008**, *10*, 1148–1151. [CrossRef]

8. Niu, J.; Liu, X.; Xia, K.; Xu, L.; Xu, Y.; Fang, X.; Lu, W. Effect of electrodeposition parameters on the morphology of three-dimensional porous copper foams. *Int. J. Electrochem. Sci.* **2015**, *10*, 7331–7340.

9. Shahbazi, P.; Kiani, A. Fabricated Cu_2O porous foam using electrodeposition and thermal oxidation as a photocatalyst under visible light toward hydrogen evolution from water. *Int. J. Hydrogen Energy* **2016**, *41*, 17247–17256. [CrossRef]

10. Shin, H.C.; Dong, J.; Liu, M. Nanoporous structures prepared by an electrochemical deposition process. *Adv. Mater.* **2003**, *15*, 1610–1614. [CrossRef]

11. Zhang, W.; Ding, C.; Wang, A.; Zeng, Y. 3-D Network pore structures in copper foams by electrodeposition and hydrogen bubble templating mechanism. *J. Electrochem. Soc.* **2015**, *162*, D365–D370. [CrossRef]

12. Nam, D.; Kim, R.; Han, D.; Kim, J.; Kwon, H. Effects of $(NH_4)_2SO_4$ and BTA on the nanostructure of copper foam prepared by electrodeposition. *Electrochim. Acta* **2011**, *56*, 9397–9405. [CrossRef]

13. Li, D.; Podlaha, E.J. Template-assisted electrodeposition of porous Fe–Ni–Co nanowires with vigorous hydrogen evolution. *Nano Lett.* **2019**, *19*, 3569–3574. [CrossRef] [PubMed]

14. Raoof, J.B.; Ojani, R.; Kiani, A.; Rashid-Nadimi, S. Fabrication of highly porous Pt coated nanostructured Cu-foam modified copper electrode and its enhanced catalytic ability for hydrogen evolution reaction. *Int. J. Hydrogen Energy* **2010**, *35*, 452–458. [CrossRef]

15. Luo, Z.-H.; Feng, M.; Lu, H.; Kong, X.-X.; Cao, G.-P. Nitrile butadiene rubber hydrogenation over a monolithic Pd/CNTs@Nickel foam catalysts: Tunable CNTs morphology effect on catalytic performance. *Ind. Eng. Chem. Res.* **2019**, *58*, 1812–1822. [CrossRef]

16. Ashby, M.F.; Evans, A.; Fleck, N.A.; Gibson, L.J.; Hutchinson, J.W.; Wadley, H.N. Metal foams: A design guide. *Mater. Des.* **2002**, *23*, 119. [CrossRef]

17. Abdel-karim, R.; El-raghy, S. Electrochemical Deposition of Nanoporous Metallic Foams for Energy Applications. pp. 69–91. Available online: http://www.onecentralpress.com/wp-content/uploads/2017/08/Chapter-4-AMA-.pdf (accessed on 22 August 2020).

18. Eugénio, S.; Demirci, U.B.; Silva, T.M.; Carmezim, M.J.; Montemor, M.F. Copper-cobalt foams as active and stable catalysts for hydrogen release by hydrolysis of sodium borohydride. *Int. J. Hydrogen Energy* **2016**, *41*, 8438–8448. [CrossRef]

19. Liu, W.; Hu, E.; Jiang, H.; Xiang, Y.; Weng, Z.; Li, M.; Fan, Q.; Yu, X.; Altman, E.I.; Wang, H. A highly active and stable hydrogen evolution catalyst based on pyrite-structured cobalt phosphosulfide. *Nat. Commun.* **2016**, *7*, 10771. [CrossRef]

20. Lange, G.A.; Eugénio, S.; Duarte, R.G.; Silva, T.M.; Carmezim, M.J.; Montemor, M.F. Characterisation and electrochemical behaviour of electrodeposited Cu–Fe foams applied as pseudocapacitor electrodes. *J. Electroanal. Chem.* **2015**, *737*, 85–92. [CrossRef]

21. Murakami, T.; Akagi, T.; Kasai, E. Development of porous iron based material by slag foaming and its reduction. *Procedia Mater. Sci.* **2014**, *4*, 30–35. [CrossRef]

22. Kelpšaite, I.; Baltrušaitis, J.; Valatka, E. Electrochemical deposition of porous cobalt oxide films on AISI 304 type steel. *Medziagotyra* **2011**, *17*, 236–243.

23. Mattarozzi, L.; Cattarin, S.; Comisso, N.; Gerbasi, R.; Guerriero, P.; Musiani, M.; Vazquez-Gomez, L.; Verlato, E. Electrodeposition of Cu-Ni alloy electrodes with bimodal porosity and their use for nitrate reduction. *ECS Electrochem. Lett.* **2013**, *2*, D58–D60. [CrossRef]

24. Rehman, T.U.; Ali, H.M.; Saieed, A.; Pao, W.; Ali, M. Copper foam/PCMs based heat sinks: An experimental study for electronic cooling systems. *Int. J. Heat Mass Transf.* **2018**, *127*, 381–393. [CrossRef]

25. Zhao, J.; Zou, X.; Sun, P.; Cui, G. Three-dimensional Bi-continuous nanoporous Gold/Nickel foam supported MnO_2 for high performance supercapacitors. *Sci. Rep.* **2017**, *7*, 1–8. [CrossRef] [PubMed]

26. Liu, Y.; Hangarter, C.M.; Garcia, D.; Moffat, T.P. Self-terminating electrodeposition of ultrathin Pt films on Ni: An active, low-cost electrode for H2 production. *Surf. Sci.* **2015**, *631*, 141–154. [CrossRef]

27. Vainoris, M.; Tsyntsaru, N.; Cesiulis, H. Modified electrodeposited cobalt foam coatings as sensors for detection of free chlorine in water. *Coatings* **2019**, *9*, 306. [CrossRef]

28. Ma, S.; Zhou, H.C. Gas storage in porous metal-organic frameworks for clean energy applications. *Chem. Commun.* **2010**, *46*, 44–53. [CrossRef] [PubMed]

29. Karimi Shervedani, R.; Lasia, A. Evaluation of the surface roughness of microporous Ni–Zn–P electrodes by in situ methods. *J. Appl. Electrochem.* **1999**, *29*, 979–986. [CrossRef]

30. Popov, K.I.; Nikolić, N.D.; Živković, P.M.; Branković, G. The effect of the electrode surface roughness at low level of coarseness on the polarization characteristics of electrochemical processes. *Electrochim. Acta* **2010**, *55*, 1919–1925. [CrossRef]

31. Miranda-Hernández, M.; González, I.; Batina, N. Silver electrocrystallization onto carbon electrodes with different surface morphology: Active sites vs surface features. *J. Phys. Chem. B* **2001**, *105*, 4214–4223. [CrossRef]

32. Menshykau, D.; Streeter, I.; Compton, R.G. Influence of electrode roughness on cyclic voltammetry. *J. Phys. Chem. C* **2008**, *112*, 14428–14438. [CrossRef]

33. Kostevšek, N.; Rožman, K.Ž.; Pečko, D.; Pihlar, B.; Kobe, S. 33NN A comparative study of the electrochemical deposition kinetics of iron-palladium alloys on a flat electrode and in a porous alumina template. *Electrochim. Acta* **2014**, *125*, 320–329. [CrossRef]

34. Gira, M.J.; Tkacz, K.P.; Hampton, J.R. Physical and electrochemical area determination of electrodeposited Ni, Co, and NiCo thin films. *Nano Converg.* **2015**, *3*, 6. [CrossRef] [PubMed]

35. Zankowski, S.P.; Vereecken, P.M. Electrochemical determination of porosity and surface area of thin films of interconnected nickel nanowires. *J. Electrochem. Soc.* **2019**, *166*, D227–D235. [CrossRef]

36. Tadros, T.F.; Lyklema, J. Adsorption of potential—determining ions at the silica—aqueous electrolyte interface and the role of some cations. *J. Electroanal. Chem. Interf. Electrochem.* **1968**, *17*, 267–275. [CrossRef]

37. Schneider, I.A.; Kramer, D.; Wokaun, A.; Scherer, G.G. Effect of inert gas flow on hydrogen underpotential deposition measurements in polymer electrolyte fuel cells. *Electrochem. Commun.* **2007**, *9*, 1607–1612. [CrossRef]

38. Green, C.L.; Kucernak, A. Determination of the platinum and ruthenium surface areas in platinum-ruthenium alloy electrocatalysts by underpotential deposition of Copper. I. Unsupported catalysts. *J. Phys. Chem. B* **2002**, *106*, 1036–1047. [CrossRef]

39. Yamaguchi, R.; Kurosu, S.; Suzuki, M. Hydroxyl radical generation by zero-valent iron/Cu (ZVI/Cu) bimetallic catalyst in wastewater treatment: Heterogeneous Fenton/Fenton-like reactions by Fenton reagents formed in-situ under oxic conditions. *Chem. Eng. J.* **2018**, *334*, 1537–1549. [CrossRef]

40. Macht, F.; Eusterhues, K.; Pronk, G.J.; Totsche, K.U. Specific surface area of clay minerals: Comparison between atomic force microscopy measurements and bulk-gas (N_2) and -liquid (EGME) adsorption methods. *Appl. Clay Sci.* **2011**, *53*, 20–26. [CrossRef]

41. Sharifi-Viand, A.; Mahjani, M.G.; Jafarian, M. Determination of fractal rough surface of polypyrrole film: AFM and electrochemical analysis. *Synth. Met.* **2014**, *191*, 104–112. [CrossRef]

42. Wongmanerod, C.; Zangooie, S.; Arwin, H. Determination of pore size distribution and surface area of thin porous silicon layers by spectroscopic ellipsometry. *Appl. Surf. Sci.* **2001**, *172*, 117–125. [CrossRef]

43. Damian, A.; Omanovic, S. Ni and Ni{single bond}Mo hydrogen evolution electrocatalysts electrodeposited in a polyaniline matrix. *J. Power Sources* **2006**, *158*, 464–476. [CrossRef]

44. Kandalkar, S.G.; Lee, H.M.; Chae, H.; Kim, C.K. Structural, morphological, and electrical characteristics of the electrodeposited cobalt oxide electrode for supercapacitor applications. *Mater. Res. Bull.* **2011**, *46*, 48–51. [CrossRef]

45. Song, H.; Song, H.; Jung, Y.; Jung, Y.; Lee, K.; Lee, K.; Dao, L.H.; Dao, L.H. Electrochemical impedance spectroscopy of porous electrodes: The effect of pore size distribution. *Electrochim. Acta* **1999**, *44*, 3513–3519. [CrossRef]

46. Ogihara, N.; Itou, Y.; Sasaki, T.; Takeuchi, Y. Impedance spectroscopy characterization of porous electrodes under different electrode thickness using a symmetric cell for high-performance lithium-ion batteries. *J. Phys. Chem. C* **2015**, *119*, 4612–4619. [CrossRef]

47. Yan, B.; Li, M.; Li, X.; Bai, Z.; Dong, L.; Li, D. Electrochemical impedance spectroscopy illuminating performance evolution of porous core-shell structured nickel/nickel oxide anode materials. *Electrochim. Acta* **2015**, *164*, 55–61. [CrossRef]

48. Kaufmann, B.Y.K. Transfer function simulation for electrochemical impedance spectroscopy (EIS). *Rev. Colomb. Fis.* **2005**, *37*, 25–27.

49. Mahato, N.; Singh, M.M. Investigation of passive film properties and pitting resistance of AISI 316 in aqueous ethanoic acid containing chloride ions using electrochemical impedance spectroscopy(EIS). *Port. Electrochim. Acta* **2011**, *29*, 233–251. [CrossRef]

50. Hsu, C.H.; Mansfeld, F. concerning the conversion of the constant phase element parameter Y_0 into a capacitance. *Corrosion* **2001**, *57*, 747–748. [CrossRef]

51. Krzewska, S. Impedance investigation of the mechanism of copper electrodeposition from acidic perchlorate electrolyte. *Electrochim. Acta* **1997**, *42*, 3531–3540. [CrossRef]

52. Halsey, T.C. Frequency dependence of the double-layer impedance at a rough surface. *Phys. Rev. A* **1987**, *35*, 3512–3521. [CrossRef]

53. Hirschorn, B.; Orazem, M.E.; Tribollet, B.; Vivier, V.; Frateur, I.; Musiani, M. Determination of effective capacitance and film thickness from constant-phase-element parameters. *Electrochim. Acta* **2010**, *55*, 6218–6227. [CrossRef]